PNNL-13347

Letter Report

Noble Metals and Spinel Settling in High Level Waste Glass Melters

Tanks Focus Area
RL3-7-WT-31 (Task A)

S. K. Sundaram and J. M. Perez, Jr.
Pacific Northwest National Laboratory[a], Richland, WA 99352

September 2000

Prepared for the U. S. Department of Energy
under Contract DE-AC06-76RL0 1830 F

[a] Operated for the U.S. Department of Energy by Battelle under Contract DE-AC06-76RL0 1830

Disclaimer

PACIFIC NORTHWEST NATIONAL LABORATORY
operated by
BATTELLE MEMORIAL INSTITUTE
for the
UNITED STATES DEPARTMENT OF ENERGY
under Contract DE-AC06-76RL0 1830

Summary

In the continuing effort to support the Defense Waste Processing Facility (DWPF), the noble metals issue is addressed. There is an additional concern about the amount of noble metals expected to be present in the future batches that will be considered for vitrification in the DWPF. Several laboratory- as well as melter-scale studies have been completed by various organizations (mainly Pacific Northwest National Laboratory (PNNL), Savannah River Technology Center (SRTC), and West Valley Demonstration Project (WVDP) in the US). This letter report presents the status the noble metals issue and focuses on the settling of noble metals and spinels in melters.

Following the introduction, chapter 2 presents the results of physical modeling performed at PNNL in the early 1990's. The data analysis indicated that if noble metals had a density of about 12 g/cm^3 (Pd/Rh) and if their sizes were less than 40 μm, only about 1 percent of the incoming noble metals would settle under steady-state melter operating conditions. In the size range of 40-60 μm, 10 percent would settle in the melter and for sizes up to 100 μm, 50 percent would settle. Chapter 3 summarizes melter studies performed to address the noble metals issue in the US and other countries (Germany, Japan, and United Kingdom). The melter studies raised more issues in the process. Chapter 4 outlines recent efforts at PNNL to understanding the settling of spinel in the melter under the Environmental Management Science Program (EMSP). This chapter is followed by remarks on future work and recommendations. Table S.1 presents a summary of the estimated settling rates of noble metals or spinels.

Table S.1. Summary of Settling of Noble Metals and Spinels

Determined using SRTC IDMS Data:

Element	Poured/Total Time (lb/day)	Poured/Idling Time (lb/day)
Ru	0.027	0.034
Rh	0.006	0.008
Pd	0.014	0.018
Te	0.008	0.010
Se	0.0005	0.0006
Ag	0.006	0.007

Predicted using Kernforschungszentrum Karlsruhe (KfK) Engineering Scale Melter (ESM) Data:

Element	Noble Metals on the Floor (lb/day)	Sludge Layer Buildup (cm/day)
RuO_2	0.076	0.013
RuO_2 (3X feed rate)	0.294	0.038
Pd	0.019	---
Rh	0.016	---

PNNL Studies: The effect of crystal size on the growth of the spinel sludge layer and on spinel retention in glass (preliminary estimate)

Crystal Size (μm)	Sludge Growth Rate (mm/Y)	Spinel Removed with Glass (percent)
1	0.27	99.99
10	27	99.39
100	2700	39.04

Acronyms and Abbreviations

AERE	Atomic Energy Research Establishment
AES	Atomic Emission Spectroscopy
BDL	Below Detection Limit
CETL	Clemson Environmental Technology Laboratory
CPU	Central Processing Unit
DWPF	Defense Waste Processing Facility
EDX	Electron Dispersive X-ray spectrometer
EMSL	Environmental Molecular Science Laboratory
EMSP	Environmental Management Science Program
ESM	Engineering Scale Melter (testing)
FY	Fiscal Year
GFT	Gradient Furnace Testing
HAW	High Activity Waste
HEWC	High Enrichment Waste Concentrate
HLLW	High Level Liquid Waste
HLW	High Level Waste
HM	TBS
HNM	High Noble Metals
HWVP	Hanford Waste Vitrification Plant
ICP	Inductively Coupled Plasma
IDMS	Integrated DWPF Melter System
INEEL	Idaho National Engineering and Environmental Laboratory
JAEC	Japan Atomic Energy Commission
JHCM	Joule-Heated Ceramic Melter
KfK	Kernforschungszentrum Karlsruhe
LEWC	Low Enrichment Waste Concentrate
LFCM	Liquid-Fed Ceramic Melter
LFMM	Liquid-Fed Mini Melter
LNM	Low Noble Metals
LP	Lumped Parameter
MS	Mass Spectrometer
N/A	Not Applicable
NCAW	Neutralized Current Acid Waste
NM	Noble Metals
PNC	Power Reactor and Nuclear Fuel Development Corporation
PNNL	Pacific Northwest National Laboratory
PUREX	TBS
RSM	Research Scale Melter (testing)
SEM	Scanning Electron Microscopy
SFCM	Slurry-Fed Ceramic Melter
SRS	Savannah River Site
SRTC	Savannah River Technology Center
SSC	Swanson Service Corporation
TBS	To Be Supplied
TEM	Transmission Electron Microscopy
TFA	Tanks Focus Area
TIM	Technology Integration Manager

TRP	Tokai Reprocessing Plant
TTP	Technical Task Plan
TVF	Tokai Vitrification Facility
WAK	Waste Stored at Karlsruhe Reprocessing Plant
WSRC	Westinghouse Savannah River Company
WVDP	West Valley Demonstration Project
XRD	X-ray Diffraction
XRF	X-Ray Fluorescence
YMP	Yucca Mountain Project

Acknowledgments

The authors would like to thank Bill Holtzscheiter, Technology Integration Manager (TIM) of Tanks Focus Area (TFA) for management and guidance. We also would like to acknowledge Dennis Bickford for his suggestions and technical input. The authors also acknowledge Ron Goles for technical review, Nancy Foote for editorial review, and Pavel Hrma for technical review of Chapter 4. This study was funded by the Department of Energy Office of Science and Technology through the Tanks Focus Area. Pacific Northwest National Laboratory is operated for the U.S. Department of Energy by Battelle under Contract DE-AC06-76RLO 1830.

Contents

List of Figures

List of Tables

1.0 Introduction

Generally, the noble metals are defined as silver, gold, platinum and the platinum group metals. These metals are characterized by the common property of general chemical inertness. The platinum group is comprised of ruthenium, osmium, rhodium, iridium, palladium, and platinum, as shown in Figure 1.1.

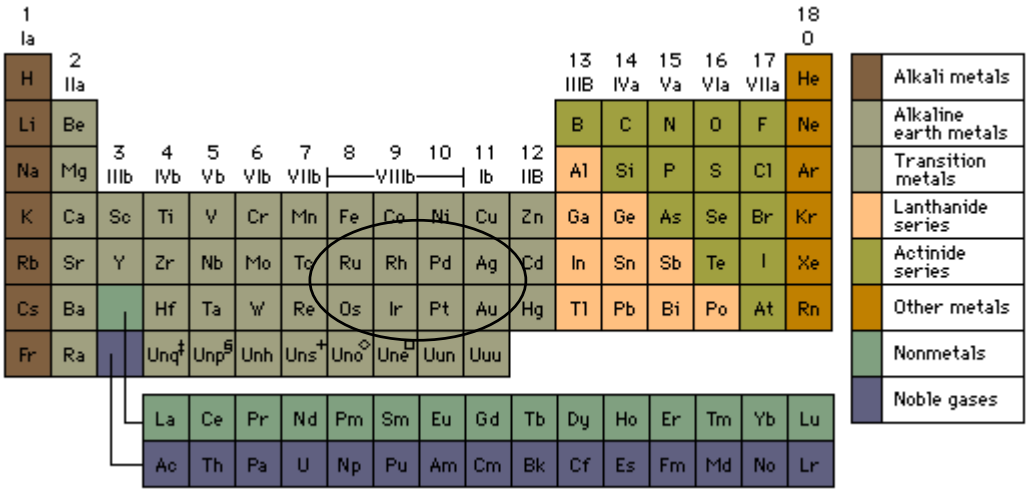

Figure 1.1. Periodic Table (Microsoft Illustration)

Of these, Ru, Rh, and Pd originate from the fission of ^{235}U and are present U. S. defense high-level radioactive waste (HLW) as a product from the reprocessing of irradiated fuel. As an example, Hanford neutralized current acid waste (NCAW) contains the radioactive noble metal isotopes listed in Table 1.1:

Table 1.1. Radioactive Noble Metals in NCAW

Isotope	Half Life	Stable Decay Product
^{103}Ru	39.3 days	^{103}Rh
^{106}Ru	372.6 days	^{106}Pd
^{102}Rh	2.9 years	^{102}Ru
^{103m}Rh	56.1 min	^{103}Rh
^{107}Pd	$6.5 \times 10^{+6}$ years	^{107}Ag

Ruthenium-103 and ^{103m}Rh decay to stable ^{103}Rh within one year. Rhodium-102 decays to stable ^{102}Ru after approximately 30 years. This increase in stable Ru is largely offset by the decay of ^{106}Ru that becomes stable ^{106}Pd after 10 to 20 years. No appreciable decay of ^{107}Pd occurs in 10^3 years. Fuel discharged from the reactor also contains small quantities of shorter half-life isopotes of Ru and Rh. These isotopes decay quickly. The amount of these isotopes is small ($<10^{-1}$ g/MTU) compared to the stable Ru isotopes that are present. Thus, the isotopic distribution of noble metals is nearly constant over time. Ruthenium remains by far the most predominant noble metal. The NCAW contains several times as much Ru as Rh or Pd, and therefore the chemistry of Ru is of most interest to the vitrification of Hanford wastes. The chemistry of Ru is complex, in part because it has eight possible valence states.

Metallic Ru has a melting point of 2310ºC and a boiling point of 3900ºC, both of which are higher than temperatures reached in the joule-heated ceramic melters currently in use at the Defense Waste Processing Facility (DWPF) at the Savannah River Site (SRS) and the West Valley Demonstration Plant (WVDP) or planned to be at the Hanford Site Waste Treatment Plant (WTP). At approximately 800ºC, Ru oxidizes in air to form RuO_2. The reprocessing of nuclear fuel yields wastes that contain many different species of Ru. Nitro and nitrato complexes of nitrosylruthenium are the most common and are mainly Ru (III) nitrosyl derivatives (Fletcher and Martin 1955), such as trinitrato nitrosylruthenium $[RuNO(NO_3)_3(H_2O)_2]$ or sodium tetranitro nitrosylruthenium, $Na_2[RuNO(NO_2)_4OH]$. It is difficult to predict the distribution of Ru among the numerous possible complexes in high-level wastes. In addition, silver is also a concern due to its reducibility. Silver present in HLW originated from reprocessing equipment and was not a fission product or a process chemical additive, e.g., most of the silver present in SRS defense waste came from the silver saddles used in iodine strippers.

Generally, noble metals are easily reducible and are dense and electrically conductive. The major concern is settling of noble metals to the bottom of melters and causing disruption of normal melter electrical currents. Besides significant capital investment of a melter, an inoperable melter will result in major additional cost in terms of replacement, facility downtime, decommissioning, storage, and melter disposal. Besides the U. S. facilities described above, vitrification facilities operated in Belgium and Japan (the German/Belgium PAMELA facility in Mol, Belgium and the Tokai Vitrification Facility (TVF) in Tokai, Japan) employed similar vitrification technology and have had to address the issues of noble metals accumulations and reduced melter life. The PAMELA facility began operation in 1985. The TVF began radioactive operations in 1995. The high-level wastes in these countries are from the reprocessing of commercial nuclear fuel used in power reactors. Table 1.2 shows a comparison of concentration of noble metals in selected German, Japanese, and American wastes. The commercial wastes have considerably higher noble metal content than that of the defense wastes from SRS and Hanford. Almost all major vitrification facilities (research or production) have experienced different levels of operational problems that can be traced to the presence of noble melters in the melter.

Table 1.2. Comparison of Noble Metals Content (ppm) in Different Waste Glasses

Component	PAMELA LEWC/WAK*	TVF GLASS	SRS/DWPF HM/BLEND	HWVP NCAW'91	WVDP (Dempster 1998)
Ru	1000/5100	5530	830/350	870	608
Pd	?/3000	2960	310/160	300	261
Rh	?/1400	1290	150/68	240	162
Ag	Trace	93	20/77	320	---
Total	?/9500	9873	1310/655	1730	1031

* LEWC = Low Enrichment Waste Concentrate
WAK = waste stored at the Karlsruhe Reprocessing Plant

The probability of significant noble metals settling in HLW melters was only fully appreciated after the design of the DWPF melter had been completed and construction had started on the first two melters. The WVDP melter was designed with the potential for noble metal settling and accumulation taken into account. However, the limited scope of the WVDP permitted a melter design that is not directly applicable to the DWPF or Hanford Site plant requirements. To date, the DWPF melter has been operated non-radioactively for 2 years and radioactively for 3 years. The HLW batches to be vitrified during the first five years of DWPF operation contain essentially no noble metals. As a result the facility has already exceeded the minimum two-year melter design operating life. This has allowed DOE the opportunity to identify and pursue several areas for improvement in melter design were identified. A

major task was initiated to address performance limitations and deficiencies identified by the user, DWPF, under the Tank Focus Area (TFA) program. This work is being performed in collaboration with Task Technical Plans (TTP) SR16WT31-C, RL37WT31-A and C (FY 1999-2000 TTP), and ID77WT31-B.

In support of this effort, it is important to acquire, review, and become reacquainted with previous noble metals and spinels settling research and melter testing. Since the late 1980's research was conducted by the DOE and internationally. This report summarizes the previous work and discusses its relevance to the current effort.

2.0 Physical Modeling

Physical modeling of melters has long been used to study phenomena and predict operating parameters in commercial glass production furnaces (Bansal 1978). This tool has also been used to support the development of HLW melters. Physical modeling involves building and operating a scaled-down melter using a simulated liquid to represent molten glass. Measurements made in the physical model can be extrapolated to the full-scale melter. The extrapolation is done through physically significant dimensionless groups. Data generated by physical modeling includes temperature profiles in the melt cavity and characterization of liquid flow patterns and velocities. Several DOE sponsored studies have been conducted in support of basic melter design and noble metal investigations. The major work is summarized in this section.

During the early stages of DOE melter development and design, Quigley and Kried (1979) performed early studies on a flat bottom tank design and side electrodes. The authors found that the upper potions of the cavity were well-mixed and had significant stirring. However, the lowest fluid velocities and poorest mixing occurred in the bottom quarter of the model. This resulted in recommendations to increase floor insulation to reduce heat losses and also to be able to independently control the current directed to the lower tank area, i.e., separate electrode pairs. Skarda et al. (1985) evaluated two tank configurations; one with a flat bottom and one with a 5º sloped bottom; both using side electrodes. Forced mixing through the use of bubblers was also studied and found to significantly enhance glass circulation by inducing two counter-rotating eddies symmetric about the model's vertical center. Such bubbling was necessary to prevent temperature stratification in the two-electrode melter design.

Routt (1983) performed physical modeling using a cylindrical melter cavity with four symmetrically spaced bayonet-type electrodes, an early design for the DWPF melter. Voltage gradients were measured thus providing an indication of power density. Highest power densities occurred on a diagonal path between opposing electrodes. However, the bottom part of the cavity was found to be poorly heated. This was consistent with the observation that model liquid velocities at the bottom were slow relative to higher-up locations. Asano et al (1986) reported physical modeling of three different cavity geometries, which had bottom slopes of 0º, 30º, and 45º. All had a three-electrode design, with two mounted on sidewalls and one on the bottom. The distribution of heating between electrode pairs was controlled sequentially by time-sharing. When only the upper two electrodes were fired, temperature stratification occurred, with the lowest temperatures at the bottom. This situation was remedied by firing from the bottom electrode in the two models with sloped bottoms. In the flat bottom model, temperature stratification remained even while firing from all three electrodes. Flow cells in the sloped-bottom models were sufficient to maintain a simulated insoluble phase (powdered copper) in suspension. In the case of the flat bottom model, copper tended to accumulate on the bottom of the cavity even when all three electrodes were being fired.

As part of the HWVP project's noble metals studies Peters (1990) compared the flat bottomed with side electrodes design (DWPF melter design) to the slope-bottomed with bottom electrodes design. The models were 1:4.65 scale (based on linear dimensions) of melters designed for 100 kg/h glass production rate. The liquid used to simulate molten glass was glycerin with 7.5 wt percent LiCl. The nominal operating temperature of the HWVP planned was 1150ºC and the corresponding model liquid temperature was 62ºC. Noble metal particles were represented by nickel and silica. The slope-bottomed model exhibited enhanced convection currents due to the bottom electrode. However, both models performed about the same with regard to maintaining particles in suspension. The data indicated that if noble metals had a density of about 12 g/cm^3 (Pd/Rh) and if their sizes were less than 40 μm, then only about 1 percent of the incoming noble metals would settle under steady-state melter operating conditions.

In the size range of 40-60 μm, 10 percent would settle and for sizes up to 100 μm, 50 percent would settle in the melter. Experiments simulating melter idling indicated that noble metal particles up to 40 μm would completely settle in about 30 days. German investigators found noble metal particles in simulated waste glass to be in the size range of 10-50 μm. The noble metal particle scaling analysis is presented in Appendix A.

The study also suggested that a bubbler operating in the full-scale melter at 8 scfh would be ineffective at either re-suspending noble metals in the size range of 40-100 μm, or keeping them in suspension. For smaller particle sizes, the bubbler was effective at re-suspension (and thus presumably at maintaining suspension) but the results were not consistent. A more profound suspension/re-suspension effect from a bubbler was expected since it greatly increased the degree of convection throughout the model melter cavity, as revealed by streak photography. A possible explanation by the investigator was that settled particles tended to form a settled layer (sludge) that made them difficult to resuspend. During experiments, it was observed that the bubbler's area of influence was very small, i.e., only the area in immediate proximity to the bubbler. The bubbler flow scaling analysis is presented in Appendix A. Under actual processing conditions particle or sludge resuspension is complicated by additional factors. Glass viscosity and resistive heating are strongly dependent on temperature. Heat losses through the floor refractory lead to decreasing glass temperatures in the floor region. As a result, glass viscosity can rise be a factor of three or more and electrical conductivity will drop 20 percent to 30 percent. The effect of reduced conductivity is that joule-heating of this glass will decrease with time; further exacerbating the local conditions. The end result is a cooler more viscous layer of material that promotes spinel formation (leading to yet higher viscosities and retention of any settled noble metals). As a result, resuspension efforts through bubbling or other mechanical means would be even difficult.

3.0 Melter Studies

Several organizations in the U.S.A, as well as in other countries, have studied the noble metals issue, using different melter sizes and designs. In this section, a brief summary of the international results is first presented. This material is followed by an extensive survey of studies conducted in the U.S.A.

3.1. International Experience

3.1.1. Germany

Germany began a vitrification development program for treating radioactive wastes in 1976. Much of the initial work centered around treating radioactive waste generated from reprocessing fuel elements at the Eurochemic plant in Mol, Belgium. Two wastes were produced and subsequently vitrified at the Mol plant, 50 m^3 of LEWC and 760 m^3 of high enriched waste concentrate (HEWC). The LEWC had a high concentration of noble metals, some of which settled in the melter to form a conductive layer on the melter floor. This ultimately led to processing difficulties in the melter and contributed to its eventual shutdown and replacement. Realizing the problems caused by noble metals in melters, Germany developed a program to evaluate the glass chemistry of noble metals and the effect of noble metals on glass melter performance.

Table 3.1 summarizes data obtained from melter development studies in Germany. Test results showed that the accumulation of noble metals could be greatly decreased by increasing the slope of the melter floor. When using a flat-bottom melter with a bottom drain, approximately 65 percent of the noble metals fed were retained in the melter. However, with a 75º/60º sloped melter floor, net deposits of noble metals were not detected by measuring changes in electrical resistance at the end of each pour through the bottom drain. After comparing two systems for glass pouring, the bottom drain was found to be more efficient than the overflow system in discharging noble metals. For Ru, retention was 10.3 percent using the bottom drain and 41.4 percent with the overflow system. Air sparging was also tested to determine its effects on noble metals accumulation. With a melter having 45º-sloped floor, agitating the molten glass resulted in a decrease of Ru retention from 38 percent to 24 percent, and a decrease of Pd retention from 45 percent to 3 percent. However, in tests with a 75º/60º sloped floor, it was found that air sparging was not effective enough at suspending noble metal particles to allow discharge through the overflow system. A thorough investigation of the behavior of noble metal deposits and a complete analysis of the individual particles was also performed. It was concluded that the removal of Rh from the simulant waste stream had no effect on the size and sedimentation of other noble metals. Also, general relationships were found between noble metal content and electrical, rheological, and morphological behavior of the accumulated sludge layer.

3.1.2. Japan

The first Japanese nuclear fuel reprocessing plant, Tokai Reprocessing Plant (TRP), has been in operation since 1977. TRP had produced about 300 m^3 of high-level liquid waste (HLLW) as of 1988, storing the waste in tanks onsite. In 1980, the Japan Atomic Energy Commission (JAEC) issued a policy for the treatment and disposal of HLLW, stating that the HLLW should be vitrified to form a borosilicate glass using a joule-heated LFCM. After storage for 30 to 50 years, the glass will be disposed of in a deep geological formation. As a result of this and other policies, Power Reactor and Nuclear Fuel Development Corporation (PNC) has been actively developing technology for use in Japan's first vitrification plant, the Tokai Vitrification Facility (TVF) (Tsuboya and Tsunoda 1988).

Table 3.1. Summary of Germany's Melter Data

Melter	Characteristics	Campaign/Run	Dates	Noble Metals Retention
K-1/VA-1	0.36 m^2 area, bottom drain, flat bottom	18 m^3 glass	1977-1979	Data not available
K-2/VA-2	0.64 m^2 area, bottom drain, flat bottom	2.5 tons glass	1980-	67 percent for Ru 63 percent for Pd
K-3/VA-3	0.72 m^2 area, bottom and overflow drain flat bottom	22 campaigns 37 tons glass	1983-1985	Data not available
K-4/ PAMELA	0.72 m^2 area, bottom and overflow drain 4º sloped bottom	LEWC campaign 77.8 tons glass	1/85-12/86	67 percent total
K-4/ PAMELA	0.72 m^2 area, bottom and overflow drain 4º sloped bottom	HEWC campaign 248.3 tons glass	1/86-1/89	Data not available
K-5/ PAMELA	Assumed to be the same as the K-4 design		1987-	Data not available
K-W1/V-W1	1.4 m^2 area, bottom drain, overflow vacuum suction, flat bottom		1986-	Data not available
K-W2	1.4 m^2 area, bottom drain, overflow vacuum suction, 45º sloped floor	Campaign W4 13.2 tons glass	4/88-5/88	38 percent for Ru 45 percent for Pd 41 percent for Rh
K-W2	1.4 m^2 area, bottom drain, overflow vacuum suction, 45º sloped floor, air bubbling	Campaign W5 12.8 tons glass	1/89-3/89	24 percent for Ru 3 percent for Pd
K-6´	0.88 m^2 area, bottom drain 75º/60º sloped floor	8.5 tons glass	6/90-present	10.3 percent for Ru
K-6´	0.88 m^2 area, overflow system 75º/60º sloped floor, air sparging	5.5 tons glass	6/90- present	41.4 percent for Ru

Table 3.2 provides a summary of data on melter development in Japan. Overflow and as well as bottom drains were used. In general, the accumulation of noble metals decreased as the slope of the melter floor increased. With a 30º sloped floor, retention of RuO_2 and of PdO were approximately 80 percent and 65 percent, respectively. Increasing the slope to 45º decreased the retention of noble metals, from 43 percent to 12.5 percent for RuO_2 and from 39 percent to 0 percent for PdO. In addition to increasing the slope of the melter floor, a method of glass cooling near the melter floor proved successful in limiting deposition of noble metals. The cold, viscous glass near the bottom acted as a settling barrier. The noble metals therefore remained in the molten glass above the layer of cold glass. A decrease in the bottom electrode temperature to 800ºC resulted in a decrease of noble metals retention from 43 percent to 17 percent for RuO_2, and from 39 percent to 3 percent for PdO. Several tests were completed in a large-scale melter to determine the effects of temperature and Na_2O content on the length of RuO_2 crystals. Changing the melting temperature from 1000ºC to 1200ºC resulted in an increase of RuO_2 crystal length from 0 to 8 ⎕m. Increasing Na_2O content from 5 percent to 15 wt percent increased the RuO_2 crystal length from 0 to 6 ⎕m (Igarashi 1991, 1992). It was recommended that mechanical stirring or air sparging be incorporated into future designs.

3.1.3. England

In the late 1970s, the Atomic Energy Research Establishment (AERE)-Harwell in Oxfordshire, England, began to evaluate the joule-heated ceramic melter (JHCM) process. Harwell developed a final design after studying various concepts developed from observation of U.S. melter designs. A company that specialized in glass-making furnace design and construction built a full-scale JHCM melter and delivered it to Harwell in March 1982. Because of its unique design, it was expected that this melter would remain in operation more than five years (Morris 1985; Morris et al. 1986a; Morris et al. 1986b). During installation of the full-scale JHCM in August 1982, financial difficulties canceled the project. Harwell then designed a one-third scale JHCM, which was similar to the full-scale JHCM except for its smaller size. It had a melting cavity of 0.2 m x 0.2 m compared to the full-scale melter cavity of 0.6 m x 0.6 m. A vertical pipe was installed to withdraw the glass product using suction through the top of the melter into small 10-L canisters. Construction of the new melter was completed in October 1982. During 10 months, the one-third scale JHCM operated approximately 6000 hours, but was idling at 1000ºC most of that time. During operation, 7 canisters were filled in 64 hours of pouring, with an average glass quantity of 16.7 kg/canister.

After 7 months of operation, the electrical resistance between the electrodes had dropped noticeably. The melter power supply became current limited about a month later, causing the idling temperature to fall below 1000ºC. When the cold, viscous melt could no longer be poured (at 850ºC), the melter was shut down and cooled; it was dismantled in February and March 1984 (Morris et al. 1986a; Morris et al. 1986b). Examination of the melter electrodes showed localized corrosion in the lower sections, with material weight losses of 14.6 percent and 4.2 percent from the two electrodes. In two places corrosion had penetrated completely through the electrodes. Samples of the electrodes from areas of minimal corrosion showed evidence of slow corrosion due to oxidation of Cr to Cr_2O_3. However, a large quantity of Ru (average concentration 15.8 wt percent) was found near areas of high corrosion. The glass target composition was only 0.6 wt percent Ru. A layer (estimated at <10 mm thick) on the melter floor contained a high concentration of Ru. Further examination of the bottom of the electrodes showed signs of melting, indicating localized, excessive heating of the glass, which accelerated the rate of electrode corrosion. Separate tests showed that the high Ru concentrations did not directly affect the electrode corrosion. It was concluded that, because deposition of Ru could not be prevented, a new melter capable of removing the sediments as they formed needed to be designed (Morris et al. 1986a; Morris et al. 1986b).

Table 3.2. Summary of Japan's Melter Data

Melter	Characteristics	Campaign/Run	Dates	Noble Metals Retention
ETF - A	0.3 m^2 area, overflow drain, flat bottom		1978-1984	N/A
ETF - B	0.59 m^2 area, overflow drain, flat bottom		1980-1983	N/A
ETF - C	0.3 m^2 area, bottom drain, flat bottom		1978-1984	N/A
MTF Mock-up	160 L volume, overflow & bottom drain flat bottom	5 Campaigns Total	1982-1983	First detected noble metals Data not available
Advanced-B	45º floor, 0.53 m^2 area, bottom drain	Campaign #1	11/85-12/85	12.5 percent for RuO_2 0 percent for PdO
Advanced-B	45º floor, 0.53 m^2 area, bottom drain	Campaign #2	5/86-6/86	27.5 percent for RuO_2 0 percent for PdO
Advanced-B	45º floor, 0.53 m^2 area, bottom drain	Campaign #3	7/86-8/86	13.9 percent for RuO_2 0 percent for PdO
CPF	bottom drain	11 Runs Total	12/82-1987	Data not available
Small-Scale	30º floor, 0.054 m^2 area, bottom drain	8 Batches Total	Estimated 1983-1984	80 percent for RuO_2 65 percent for Pd
Small-Scale	45º floor, 0.054 m^2 area, bottom drain	13 Batches Total	Estimated 1983-1984	30 percent for RuO_2 10 percent for Pd
Pilot-Scale IHI	0.25 m^2 area, 45º/53º floor, bottom drain	5 Campaigns 2.3 tons glass	1987	Data not available
Mock-up II	Data not available		1984-1986	Data not available
Mock-up III	0.66 m^2 area, 45º floor, bottom drain	Campaign 16 2.6 tons glass	2/88-3/88	Reported no accumulation
Mock-up III	0.66 m^2 area, 45º floor, bottom drain	Campaign 17 1.1 tons glass	6/88	Reported no accumulation
Mock-up III	0.66 m^2 area, 45º floor, bottom drain	Campaign 18 1.8 tons glass	7/88	Reported no accumulation
Mock-up III	0.66 m^2 area, 45º floor, bottom drain	Campaign 19 2.5 tons glass	1/89	43 percent for RuO_2 39 percent for PdO
Mock-up III	0.66 m^2 area, 45º floor, bottom drain 800ºC bottom electrodes	Campaign 20 5.6 tons glass		17 percent for RuO_2 3 percent for PdO
Mock-up III	0.66 m^2 area, 45º floor, bottom drain 800ºC bottom electrodes	Campaign 21		< 1 percent
Large-Scale	2.2 m^2 area, 49.6º/53.3º sloped floor bottom drain	30.3 tons glass	1991 -	0.08 percent for RuO_2 0.09 percent for PdO

3.2. Savannah River Site Studies

The Integrated DWPF Melter System (IDMS) was designed as a pilot-scale test facility for the DWPF. Before testing with the IDMS, two short-term noble metals campaigns with a 1/100th scale mini-melter revealed a need for extended noble metals testing. Numerous test runs with the IDMS melter addressed the designs of the DWPF feed preparation system, offgas system, and the melter itself. The IDMS engineering-scale melter is prototypic of the DWPF melter. It was designed with a melt surface area of 0.29 m^2 (approximately 1/9th of the DWPF surface area), and a melt volume of 0.20 m^3. The decrease in melt surface area was achieved by adding a second 12-inch layer of K-3 refractory to the lower inside walls of the melt tank of a DWPF melter, reducing the inner diameter from 48 inches to 24 inches. The design production rate of this smaller melter is therefore about 1/9 that of the DWPF melter, or 11 kg/h. Two pairs of electrodes maintain the melt temperature at around 1150ºC by providing

35-kW power. All other design features of the IDMS melter, such as materials of construction, drain systems, and cooling and heating systems, are essentially the same as the DWPF melter design (Hutson et al. 1991; Hutson 1992).

The IDMS has conducted a total of 16 noble metal-related runs with four different types of wastes sludges (Blend, HM, PUREX, and NCAW) containing various amounts of noble metals. Some of the sludge compositions were modified in order to judge the effects of components such as mercury and nitrite. Noble metals were added in different forms in these runs, as shown in Table 3.3. A brief overview of the runs is presented in this section.

Table 3.3. Additives Used for Noble Metals and Concentrations

Element	Additive From and Formula	Blend (Wt %)	HM (Wt %)	PUREX (Wt %)	TANK 51 (Wt%)	NCAW (Wt %)
Ru	Nitrosy lruthenium Hydroxide; $RuNO(OH)_3$ Ruthenium Chloride; $RuCl_3$ (in PX6)	0.100	0.217	0.028	0.007	0.231
Rh	Rhodium Nitrate; $Rh(NO_3)_3 \cdot xH_2O$	0.018	0.038	0.008	0.001	0.064
Pd	Palladium Nitrate; $Rh(NO_3)_3 \cdot xH_2O$	0.045	0.073	0.026	0.006	0.080
Ag	Silver Nitrate; $AgNO_3$	0.014	0.014	0.014	0.014	0.084
Hg	Mercuric Nitrate; $Hg(NO_3)_2$	1.583	3.263	0.102	0.192	0.000
Se	Selenium Oxide; SeO_2	0.022	0.048	0.006	0.00009	0.060
Te	Tellurium Oxide; TeO_2	0.002	0.004	0.001	0.0007	0.009

Before testing was initiated with the IDMS melter, two campaigns were done with a 1/100th scale mini-melter between March and June 1989. The two main objectives were to determine a) the impact of noble metals on the behavior of the vitrification system and b) the need for further testing. In the first low noble metals (LNM) campaign, feed was processed with the expected low concentrations of noble metals, producing 215 pounds of glass in approximately 2 weeks. The second high noble metals (HNM) campaign used feed with high noble metals concentrations, representing the worst case; 310 pounds of glass were produced in about 3 weeks. The noble metals concentrations are presented in Table 3.4 as a weight percent of the dry sludge in the feed. During operation of the mini-melter, no decline in electrical resistance due to noble metals was detected, and the electrodes displayed no adverse effects from noble metals. The glass product contained noble-metal particles of approximately 5 Tm, and no problems were experienced with the glass pouring system. When the melter was dismantled after the campaigns, metal nuggets containing Ru, Rh, Pd, Te, and Se were found on the melter floor.[1] Unlike the experience of Germany, Japan, and PNNL (presented in section 3.3), needle-like crystals of Ru were not present in the glass product or on the melter floor. An overall noble metals mass balance indicated that 15 percent to 20 percent of the noble metals in the feed accumulated in the melter during each campaign. The observations during these two runs led to the decision to perform additional campaigns with the IDMS melter to further investigate the behavior of noble metals (Allen 1989; Nakaoka and Strachan 1990).

[1] Information on the form or oxidation state of noble metal particles was not provided.

Table 3.4. Metals Concentrations (Allen 1989) (Wt percent dry sludge solids)

Noble Metal	LNM Campaign	HNM Campaign
PdO	0.046	0.046
RhO_2	0.025	0.025
RuO_2	0.135	0.458
Total	0.206	0.529

Nine IDMS campaigns were proposed to investigate the effects of mercury and noble metals on melter operation. A total of 15 runs were completed. Table 3.5 shows the target compositions of the three simulated sludges used in these campaigns. The sludges are referred to as Blend, PUREX (high iron, low viscosity), and HM (high aluminum, high viscosity). Three campaigns were completed with the Blend sludge, four campaigns with the HM sludge, and five with the PUREX sludge. (Two additional runs for the HWVP are discussed later in this section.) As shown in Table 3.5, the PUREX and HM sludges contained the same amounts of noble metals. The original PUREX sludge formulation had a much lower noble metals content, but additional noble metal compounds were added to the feed in all PUREX campaigns to match the concentrations in the HM sludge (Hutson, et al. 1991; Hutson 1993).

The first two IDMS noble metals campaigns were conducted between June 1990 and March 1991. Their main purpose was to verify that hydrogen would evolve as a result of the noble metal-catalyzed destruction of formic acid during feed preparation. The Blend sludge simulant was used in these runs, referred to as Blend 1 (BL1) and Blend 2 (BL2). A glass frit (Frit-202) was also added to the feed; its composition is shown in Table 3.6. Addition of noble metal compounds to achieve the desired concentrations in sludge preceded frit addition; these quantities are shown in Table 3.7. Campaigns BL1 and BL2 produced, respectively, 2809 and 4368 pounds of glass (Hutson et al. 1991). The BL1 and BL2 runs were preceded by an IDMS campaign that did not include noble metals in the feed. Data from that run indicated that the glass pool resistances between the upper electrodes and lower electrodes remained relatively constant. When noble metals were introduced during BL1 and BL2, a slight change in the ratio of upper electrode resistance to lower electrode resistance suggested that any accumulation of noble metals had little effect on the electrical characteristics of the glass (Hutson et al. 1991).

Approximately 2 months after BL1 was initiated, a glass sample that was taken 1 to 2 inches above the melter floor showed no signs of noble metals accumulation. After completion of the BL2 run, a second glass sample was taken from approximately the same location. Although Pd and Rh were not detected in this sample, Ru needles of 5 to 15 μm in length were found in 20 to 40 μm clusters. Samples of the BL1 glass product contained RuO_2 needles, usually less than 5 microns long and frequently associated with Fe/Mn/Cr/Ni spinels. BL2 glass product samples contained RuO_2 needles up to 5 μm, 20-μm Ru/spinel clusters, and 2-micron spherical aggregates of Pd/Rh and Pd/Ru (Hutson et al. 1991).

The next two campaigns (Blend 3 and HM1) were performed to investigate hydrogen generation during non-noble metal cold testing and did not include noble metals or mercury; they produced about 4751 pounds of glass using Frit-202 as the glass former. The next four runs used high levels of noble metals to determine maximum amounts of hydrogen generation expected during actual radioactive operation of the DWPF. These four runs included two with the PUREX simulant (PX1 and PX2), and two with the HM simulant (HM2 and HM3). They produced about 14,160 pounds of glass, using Frit 202. An accumulation of noble metal deposits was first detected on the melter floor near the completion of these runs, when the melter began showing the first signs of changes in electrical behavior. Specific information about noble metals retention and glass product composition for the first six runs is currently not available (Hutson 1993). Because of similarities between the DWPF and proposed HWVP melter designs, the IDMS facility was then used to process and characterize a waste sludge simulant known as the Hanford neutralized current acid waste (NCAW '91). Two noble metals campaigns completed between November 1991 and February 1992 are referred to as HWVP1 and HWVP2.

Table 3.5. Target Compositions of Simulated Sludges (Wt percent elemental dry basis)

Element	Blend	PUREX	HM
Ag	0.014	0.014	0.014
Al	6.860	3.936	8.966
Ba	0.302	0.271	0.129
Ca	1.540	2.133	0.839
Cr	0.042	0.256	0.150
Cs	0.006	0.002	0.019
Cu	0.161	0.133	0.043
Fe	20.600	24.486	13.611
Group B (Nd)	0.170	0.231	2.342
Hg	1.588	0.102	3.263
K	0.284	0.260	0.163
Mg	0.141	0.147	0.277
Mn	4.800	4.226	4.202
Na	4.190	6.376	5.552
Ni	1.880	2.607	0.828
P	0.071	0.048	0.027
Pd	0.045	0.079	0.079
Pb	0.440	0.315	0.151
Rh	0.018	0.038	0.038
Ru	0.100	0.217	0.217
Se	0.002	0.002	0.002
Si	3.900	1.033	4.318
Sr	0.000	0.021	0.242
Te	0.022	0.022	0.022
Zn	0.332	0.250	0.035
Zr	0.127	2.589	1.363

Table 3.6. Frit-202 Composition (Hutson et al. 1991)

Component	Specified (Wt percent)	Actual (Wt percent)
SiO_2	77.0 ± 1.0	76.6
Na_2O	6.0 ± 0.5	6.1
B_2O_3	8.0 ± 0.5	6.7
Li_2O	7.0 ± 0.5	7.7
MgO	2.0 ± 0.25	1.9
Al_2O_3	< 1.89	0.45
Fe_2O_3	< 0.29	0.04
Mn	< 0.2	n/a
Ni	< 0.2	n/a
Cr	< 0.1	n/a
Pb	< 0.1	n/a
TiO_2	< 0.15	0.09
F	< 0.05	0.01
Cl	< 0.05	0.01

Table 3.7. Noble Metals Quantities Added in Campaigns BL1 and BL2 (Hutson et al. 1991)

		Compound (grams)		Element (grams)	
Element	Compound Added	BL1	BL2	BL1	BL2
Ru	$RuCl_3$, 42 wt percent Ru	1617.4	1617.0	679.3	679.1
Rh	$Rh(NO_3)_3$ solution 4.933 wt percent Rh	2871.5	2871.9	141.7	141.7
Pd	$Pd(NO_3)_2$ solution 8.769 wt percent Pd	4040.5	4037.0	354.3	354.0

The melter feed for the HWVP campaigns was prepared by first combining mixed hydroxide slurry with primary trim chemicals to obtain a waste simulant that was deficient in noble metals. Noble metal compounds were then added in the amounts shown in Table 3.8. Frit, formic acid, and other chemicals were then added to the feed mixture to produce a simulant nearly identical to NCAW '91. The frit used in the runs was specified by PNL; its composition is shown in Table 3.9. The final compositions of the waste simulant feeds used in the HWVP campaigns are shown in Tables 3.10 and 11 (Hutson 1992).

Table 3.8. Noble Metals Quantities (Hutson 1992)

		Compound (grams)		Element (grams)	
Element	Compound Added	HWVP1	HWVP2	HWVP1	HWVP2
Ru	$RuCl_3$, 42 wt percent Ru	4445.0	4445.0	1866.9	1866.9
Rh	$Rh(NO_3)_3$ solution 4.933 wt percent Rh	10482.5	10482.3	517.1	517.1
Pd	$Pd(NO_3)_2$ solution 8.769 wt percent Pd	7334.0	7334.0	643.1	643.1

Table 3.9. Frit Composition (Hutson 1992)

Component	Specified (Wt %)	Actual (Wt %)
SiO_2	72.26	73.135
B_2O_3	20.45	18.902
Li_2O	7.29	6.972
Na_2O	--	0.359
CaO	--	0.088
Fe_2O_3	--	0.039
TiO_2	--	0.103
ZrO_2	--	0.039
Al_2O_3	--	0.189
BaO	--	0.016
K_2O	--	0.031
ZnO	--	0.078

Table 3.10. HWVP1 Waste Simulant Feed Composition (Hutson 1992)

Component	Oxide	Elemental (Wt percent)	Measured Oxide (Wt percent)	Corroded Oxide (Wt percent)	NCAW'91 Oxide (Wt percent)
Potassium	K_2O	0.14	0.18	0.18	0.07
Cesium	Cs_2O	0.73	0.84	0.17	0.17
Aluminum	Al_2O	1.33	2.74	2.74	2.75
Barium	BaO	0.05	0.05	0.05	0.05
Boron	B_2O_3	3.98	13.94	12.98	13.91
Cadmium	CdO	0.79	0.98	0.98	1.00
Calcium	CaO	0.23	0.36	0.36	0.24
Cerium	CeO_2	0.21	0.27	0.27	0.18
Chromium	Cr_2O_3	0.06	0.09	0.12	0.08
Copper	Cuo	0.07	0.09	0.08	0.07
Germanium	GeO_2	BDL	BDL	BDL	<0.01
Iron	Fe_2O_3	4.88	7.59	7.11	8.12
Lanthanum	La_2O_3	0.20	0.26	0.26	0.19
Lead	PbO	0.13	0.15	0.15	0.18
Lithium	Li_2O	2.31	5.41	4.81	4.96
Magnesium	MgO	0.08	0.15	0.15	0.12
Manganese	MnO	0.43	0.60	0.60	0.65
Molybdenum	MoO_3	0.11	0.18	0.19	0.16
Neodymium	Nd_2O_3	1.81	2.30	2.30	1.00
Nickel	NiO	0.43	0.59	0.59	0.66
Niobium	Nb_2O_5	BDL	BDL	BDL	<0.01
Palladium	PdO	0.07	0.09	0.09	0.03
Phosphorus	P_2O_5	0.06	0.16	0.16	0.38
Praseodymium	Pr_2O_3	0.15	0.19	0.19	0.04
Rhodium	Rh_2O_3	0.04	0.05	0.05	0.03
Rubidiium	Rh_2O_3	BDL	BDL	BDL	0.02
Ruthenium	Ru_2O_3	0.13	0.17	0.17	0.11
Samarium	Sm_2O_3	0.10	0.12	0.02	0.02
Selenium	SeO_2	0.03	0.05	0.05	<0.01
Silicon	SiO_2	21.23	49.45	49.45	52.04
Silver	Ag_2O	0.04	0.04	0.04	0.03
Sodium	Na_2O	4.97	8.77	7.90	7.83
Strontium	SrO	0.02	0.02	0.02	0.03
Tantalum	Ta_2O_5	BDL	BDL	BDL	<0.01
Tellurium	TeO_2	ND	ND	ND	0.03
Tin	SnO	0.02	0.02	0.02	<0.01
Titanium	TiO_2	0.09	0.15	0.15	0.19
Yttrium	Y_2O_3	0.02	0.03	0.03	0.02
Zinc	ZnO	0.11	0.16	0.15	0.10
Zirconium	ZrO_2	2.55	3.75	3.75	4.31

Table 3.11. HWVP2 Waste Simulant Feed Composition (Hutson 1992)

Component	Oxide	Elemental (Wt percent)	Oxide (Wt percent)	NCAW '91 Oxide (Wt percent)
Potassium	K_2O	0.08	0.09	0.07
Cesium	Cs_2O	0.10	0.11	0.17
Aluminum	Al_2O_3	1.36	2.68	2.75
Barium	BaO	0.05	0.06	0.05
Boron	B_2O_3	3.99	13.43	13.91
Cadmium	CdO	0.80	0.95	1.00
Calcium	CaO	0.27	0.39	0.24
Cerium	CeO_2	0.11	0.14	0.18
Chromium	Cr_2O_3	0.05	0.08	0.08
Copper	CuO	0.07	0.09	0.07
Germanium	GeO_2	0.02	0.03	<0.01
Iron	Fe_2O_3	5.08	7.59	8.12
Lanthanum	La_2O_3	0.12	0.15	0.19
Lead	PbO	0.18	0.20	0.18
Lithium	Li_2O	2.29	5.15	4.96
Magnesium	MgO	0.10	0.18	0.12
Manganese	MnO_2	0.41	0.55	0.65
Molybdenum	MoO_3	0.11	0.17	0.16
Neodymium	Nd_2O_3	0.88	1.08	1.00
Nickel	NiO	0.45	0.60	0.66
Niobium	Nb_2O_5	BDL	BDL	<0.01
Palladium	PdO	0.01	0.01	0.03
Phosphorus	P_2O_5	0.03	0.07	0.38
Praseodymium	Pr_2O_3	0.04	0.05	0.04
Rhodium	Rh_2O_3	0.01	0.01	0.03
Rubidium	Rb_2O_3	BDL	BDL	0.02
Ruthenium	Ru_2O_3	0.04	0.05	0.11
Samarium	Sm_2O_3	0.02	0.02	0.02
Selenium	SeO_2	BDL	BDL	<0.01
Silicon	SiO_2	24.00	53.63	52.04
Silver	Ag_2O	0.04	0.05	0.03
Sodium (ICP)	Na_2O	5.79	8.16	7.83
Strontium	SrO	0.03	0.04	0.03
Tantalum	Ta_2O_5	0.01	0.02	<0.01
Tellurium	TeO_2	NA	NA	0.03
Tin	SnO	0.01	0.02	<0.01
Titanium	TiO_2	0.09	0.16	0.19
Yttrium	Y_2O_3	0.02	0.02	0.02
Zinc	ZnO	0.10	0.13	0.10
Zirconium	ZrO_2	2.66	3.75	4.31

Melter operation began with the transfer of approximately 490 gallons of HWVP1 simulant feed to the melter feed tank. However, approximately 300 gallons of residual waste simulant (containing noble metals) from a previous melter run remained in the feed tank. The first batch of HWVP1 simulant was therefore mixed with the residual simulant in the melter feed tank before pumping to the melter. The HWVP1 campaign produced approximately 3390 pounds of glass, and some residual waste simulant remained in the melter feed tank following the run. The HWVP2 campaign was initiated by transferring approximately 550 gallons of simulant to the melter feed tank, where it was mixed with the residual HWVP1 simulant. During this campaign, the average feed rate was about 25.4 lb oxides/h, producing a total of 4561 pounds of glass. As before, approximately 300 gallons of waste remained in the melter feed tank at the completion of the run (Hutson 1992).

Samples of the feed material and the glass product for both campaigns were obtained and analyzed for noble metals content by Monarch Analytical Laboratories, an independent laboratory. Analysis results of samples obtained at steady state (after 2 to 3 melter turnovers) during each campaign were used to calculate steady state noble metals retentions; all noble metals not accounted for in the product were assumed to have remained on the melter floor. The steady state retention values were then used in calculating overall retentions for each campaign. Table 3.12 shows the results of these calculations. As noted in the table, negative retention values for Pd during the HWVP2 campaign suggest that more Pd was discharged than was fed. The actual reason is not known. Possible explanations are:

1) Tables 3.10 and 3.11 show that the HWVP1 feed had a greater Pd content than the HWVP2 feed (0.09 wt percent versus 0.01 wt percent). Since a significant amount of the HWVP1 feed remained in the melter feed tank at the end of the first campaign and was then combined with the first batch of HWVP2 feed, it was possible that more Pd was fed than was reported. That would have occurred if the HWVP2 feed were analyzed before it was mixed with the residual waste in the tank.
2) A significant amount of Pd from the HWVP1 campaign remained in the melter cavity at the end of the run, was removed with the HWVP2 glass product, and was included in the material balance for the HWVP2 campaign.
3) Analytical error in measuring noble metals the glass and feed samples.

Table 3.12. Noble Metals Retentions in HWVP Campaigns (Hutson 1992)

	Steady State Retention (percent)		Overall Campaign Retention (percent)	
Element	HWVP1	HWVP2	HWVP1	HWVP2
Ru	13.1	12.7	17.7	17.5
Rh	15.1	9.2	20.6	9.7
Pd	3.4	-8.1	1.9	-7.6

Periodically during and after the HWVP campaigns, glass samples were taken about 3 to 5 cm above the melter floor, analyzed for noble metal content, and examined with a scanning electron microscope (SEM). Table 3.13 shows the analysis results for those samples. Before feeding of the HWVP1 simulant, a sample taken above the melter floor showed evidence of mainly RuO_2 crystals and Ni/Mn Fe/Cr spinels accumulated on the melter floor in previous runs. A sample taking during the campaign contained the same noble metal and spinel compounds, as well as individual Pd particles. Finally, a sample taken after completion of the run contained the same types of deposits plus some Rh. All HWVP1 glass samples were obtained through the feed tube port at the center of the melter floor. During the HWVP2 campaign, glass samples were obtained from both the center feed tube port and the borescope

port located near the face of one electrode. A comparison of the analysis results of samples taken from the two locations shows that an uneven layer of noble metals had accumulated on the melter floor, with a higher concentration of Ru in the samples taken from the borescope port, which was near the outside edge of the melter cavity. Therefore, convective currents may act to move the RuO_2 from the melter center toward the outside edges. Also, the presence of RuS_2 in samples taken from the outside edge of the melter floor suggests that the temperature near the edge may be lower than the bulk glass temperature; RuS_2 decomposes at temperatures >1000ºC (Hutson 1992, 1993).

Table 3.13. Analysis of Melter Floor Samples (Wt percent) from HWVP Campaigns (Hutson 1992)

Sample (wt percent) →	Before HWVP1	During HWVP1	After HWVP1	After HWVP2	After HWVP2	After HWVP2	After HWVP2
Location →	Feed Tube	Feed Tube	Feed Tube	Feed Tube	Borescope	Feed Tube	Borescope
Element ↓	Date: 10/15/91	12/4/91	12/18/91	2/18/92	3/6/92	3/27/92	4/20/92
Ru	4.68	0.42	6.20	2.02	9.67	5.53	12.60
Rh	0.41	0.03	0.30	0.02	0.27	--	0.18
Pd	0.07	0.02	0.01	0.33	0.08	--	0.09

Five additional campaigns with the IDMS melter, using Frit-202 as the glass former, were conducted primarily to justify a change in the feed preparation system from formic acid to nitric acid addition. One run used the HM simulant (HM4), and the remaining four used the PUREX simulant (PX3, PX4, PX5, and PX6). During HM4, approximately 3226 pounds of glass was produced. During PX3, PX4, PX5, and PX6, approximately 5108, 4850, 4075, 1693 pounds of glass were produced, respectively.

Feed and glass product samples were analyzed during the first twelve IDMS campaigns to estimate overall retentions of noble metals. Approximately 43,542 pounds of glass produced during these twelve campaigns contained an average of 0.039 wt percent Ru, 0.009 wt percent Rh, and 0.021 wt percent Pd.[2] Table 3.14 shows the overall mass balances and the resulting retentions of noble metals. The negative value for " Percent Retained" of Pd was most likely a result of analytical error.

Table 3.14. Noble Metals Mass Balance (Hutson 1993)

Element	Quantity Fed (lb)	Quantity Poured (lb)	Retained (percent)
Ru	26.05	16.90	35.1
Rh	5.10	4.02	21.2
Pd	8.93	8.95	- 0.2

[2] These values represent the overall glass product compositions, calculated from the total glass and total noble metals poured during the twelve campaigns. Two of the campaigns, however, did not include noble metals in the feed simulant as previously mentioned.

The IDMS melter was shut down on June 30, 1995, after continuous operation since October 1988 (Smith and Bickford 1997). An inspection of the melter refractory, melter components, and off-gas piping, as well as sampling of the material at the bottom of the melter drain. The Inconel 690® drain valve and pipe had extensive corrosion. The Inconel 690® upper electrode was in excellent condition above the normal glass level while the bottom of the electrode exhibited some wears. The Inconel 690® lower electrode that was continuously in contact with the melt had lost about 12 percent of the material from the face of the electrode.

The overall experience of IDMS noble metals melter campaigns was similar to the experience of Germany, Japan, and PNNL (see Section 3.3). Tests performed with a 1/100th scale mini-melter resulted in overall noble metals retention of 15 percent to 20 percent during the production of 525 pounds of glass; changes in electrical resistance of the glass were not detected during the runs. Subsequent campaigns with noble metals were done with the IDMS 1/9th scale melter. During initial operation of that melter, changes in electrical behavior were not detected due to noble metals; however, after the completion of approximately six campaigns, the melter began showing signs of changes in electrical behavior, and an accumulation of noble metals was detected. Two campaigns using an HWVP simulant feed also showed retention of noble metals: 0 percent to 2 percent for Pd, 10 percent to 21 percent for Rh, and 18 percent for Ru. Analysis of samples taken from varying locations on the melter floor suggested an uneven layer of accumulated noble metals. Convective currents within the melter may have been moving the particles toward the outside edges of the melter floor. Overall noble metals retentions for all IDMS campaigns were estimated from analyses of feed and glass product samples during the runs. Several methods, SEM, energy-dispersive x-ray spectrometer (EDX), inductively coupled plasma (ICP)-atomic emission spectroscopy (AES), ICP-mass spectrometer (MS), x-ray florescence (XRF), and transmission electron microscopy (TEM) were used to determine the concentration of noble metals in the IDMS samples.

Feed slurry analyses (SEM/EDX) revealed scattered palladium nuggets of about 1 μm. In melter feeds containing mercury, amalgams of Hg/Ag and Hg/Ag/Pd were found. Although one very small aggregate of Ru/Pd/Ag was seen in the second Hanford NCAW run (HWVP2), no individual or amalgamated Ru or Rh particles were observed in any of the melter feed slurry insoluble solids. In general, in the melter feed slurry, the noble metals were present as either very small finely dispersed particles or as soluble salts. Analyses of cold cap revealed RuO_2 needles of up to 20 μm long present in 20-50 μm clusters. These samples also contained scattered 1 μm AgI salts, RuS_2, Pd tellurides and selenides, and complex mixtures of PD/Ag/Te/I/S/Cu. The SEM results indicated that noble metal compounds (especially the Pd) were preferentially located on the surface of the vitrified “gas bubbles”. This suggested that the forthing, which took place as a result of vitrification offgases, might promote the growth of platinum metal nodules. It was also suggested that palladium oxides might decompose to metallic Pd and oxygen, with the Pd transported to the melt surface within the oxygen bubble. Once at the metal surface, the Pd particles might combine with other free particles to form nodules, which would then settle to the melter floor.

Normally, the melter offgas deposits consisted of alkali-rich chlorides, sulfates, borates, and fluorides with entrained Fe_2O_3, spinels, and frit particles. In addition to these components, the IDMS offgas deposits also contained trace quantities of RuO_2, $(Rh,Rh)O_2$, and Ru/Rh/Te mixtures (and some entrained Cd compounds during the NCAW processing. While the formation of RuO_4, a toxic gas, was possible in very oxidizing conditions, most of the Ru exiting the melter was the result of entrainment rather than volatility as the RuO2 in the melter offgas deposits were most often associated with entrained spinel crystals. Analysis of the soluble fraction of the melter offgas condensate revealed very low concentrations of the noble metals. However, analysis of the insoluble solids present in the offgas condensate showed the solids to contain RuO_2 crystals, spinels, and insoluble silver halides (AgI, AgCl)

salts. However, the amount of the noble metals exiting the melter through the offgas line was small and therefore not expected to significantly affect the overall mass balance of any of the elements.

Ruthenium was the most frequently observed (SEM/EDX) in glass products from several IDMS campaigns. It was present as both individual and clustered acicular (needlelike) RuO_2 crystals which were usually < 10 μm. The RuO_2 was quite often associated with $(Ni,Mn)Fe_2O_4$ and $(Ni,Mn)Cr_2O_4$ spinels. It had been previously shown that RuO_2 would serve as a seed for the heterogeneous nucleation of these spinels (Bickford and Jantzen 1986). The SEM/EDX analysis of the IDMS glass also revealed spinel growth which had been nucleated by aggregates of $(Ru,RH)O_2$, Rh/Rh, Ru/Pd, and Rh/Pd. Further TEM results showed that the Ru and Rh oxides not only acted as nucleating agents for the formation of the spinel structure but also substituted other components in the spinel structure. Additionally, palladium, as Pd and Pd/Te, was also occasionally found in the glass product. The silver was completely dissolved within the glass melt.

Since the introduction of noble metals in the IDMS melter, samples of the melter floor had been taken on a regular basis. The samples were taken using a "grain thief" type-sampling device (Smith and Bickford 1997). The samples were normally taken through the feed tube port but also had also been taken from the borescope port. The observations a re summarized in Table 3.15.

The results suggested a non-uniform layer of noble metals (mainly RuO_2) and Ni/Fe/Cr spinel on the melter floor. A higher concentration of Ru in samples taken from the borescope port was observed as compared to the samples taken from the center of the melter. This suggested that the convective currents in the melter might have pushed the RuO_2, spinels, and other inoslubles from the center of the melter (where they entered) to the outside edges. During idling, the convective currents would be different as the coldcap was absent. The accumulation of RuO_2 and Rh/Pd/Te was consistent with what had been demonstrated in waste vitrification simulations in Germany. However, in melter floor samples taken from a research melter in Karlsruhe, Germany, the RuO_2 needles were much more acicular and perfectly formed. This might be attributed to the difference in the type of glass forming additive (glass beads in Germany vs. finely ground frit in IDMS or WVDP (Smith and Bickford 1997).

Extensive sample characterization was used to determine the concentration of noble metals in order to complete a meaningful material balance. Plots of the cumulative amount of noble metals fed to the melter and the cumulative amount exiting the melter with the glass vs. glass production are shown in Figure 3.1.

The percentages of noble metals retained were: 35 percent Ru, 21 percent Rh, < 10 percent Pd, 15 percent Te, and 0 percent Ag. During the operation, the IDMS melter idled most of the time (+80 percent). In agreement with German observation (Krause and Luckscheiter 1991), the data indicated that most of settling took place during periods of idling. This was attributed to convective currents present during slurry feeding were sufficient to keep the noble metal particles suspended. During periods of idling, the convective currents were relatively minor which might allow the particles to settle to the melter floor. The relationship between the Ru concentration and idling time is shown in Figure 3.2. Initially the relative concentration varied linearly until the critical point was reached, and then the rate of change of concentration decreased rapidly until the ultimate concentration was reached. In the Figure 3.2, the critical settling points seemed to reach between 10 and 20 days of idle time. The data taken before 20 days was used to generate a least-square relationship in the linear region, $[Ru]t/[Ru]0 = 0.9814 - 0.049131t$, where t was the idle time in days. The data indicated that about 25-30 percent of the Ru in the melter was of a size and shape that did not settle easily.

Using the overall materials balance data (Figure 3.1) and timeline of melter floor samples (Table 3.15), the settling and retaining rates can be estimated, assuming a linear relationship between the Ru

concentration (settling) and time. It is also assumed that the noble metals settled is directly proportional to that is poured. The estimates are presented in Table 3.16.

Table 3.15. Melter Floor Samples from IDMS (Smith and Bickford 1997)
(Analysis by ICP-AES/Sodium Peroxide Fusion-HCl Uptake)

Time since Start of Campaigns (Months)	Observations
2	Sample at about 1-2" above the floor No evidence of any noble metals or crystalline material
5	Sample at about 1-2" above the floor Scattered RuO_2 needles (5-15 μm long) and clusters (20-40 μm) No evidence of any deposition of Pd, Rh, Ag, Se, Te or any other components
13	Sample at about ½" off the floor Significant increase in the amount of RuO_2 Evidence of a small amount of Pd deposition No evidence of spinel accumulation
15	Sample just before feeding of the first batch of NCAW A dense layer of melt insolubles, mainly RuO_2 and (Ni,Mn)(Fe,Cr) spinels First evidence of Rh deposition on the melter floor Obvious layer (1-2" thick more viscous than the glass present) on the melter floor
16.5	Sample during feeding HWVP1 Significant RuO_2 and spinel accumulation Individual metallic Pd
17	Sample after completing feeding of the HWVP1 feed Dense RuO_2/spinel accumulation Scattered Rh accumulation
19	Sample after completing feeding of the HWVP2 Chemical analysis - Decrease in Ru, Rh, and spinel components (Cr, Mn, and Fe) Flushing out or rearranging on the melter floor?
19.5	Sample at the face of the bottom electrode that was closest to the riser throat entrance SEM – less accumulation of spinels – flushing out of spinels – RuO_2 moving away from the center Presence of normal RuO_2 clusters, a relatively large mass of metallic palladium, even RuS_2
20	Sample from the center of the melter Large masses of deposited material (mainly RuO_2 and spinels)
21	Sample from the borescope port Dense accumulation of noble metals and spinels; also confirmed the presence of RuS_2

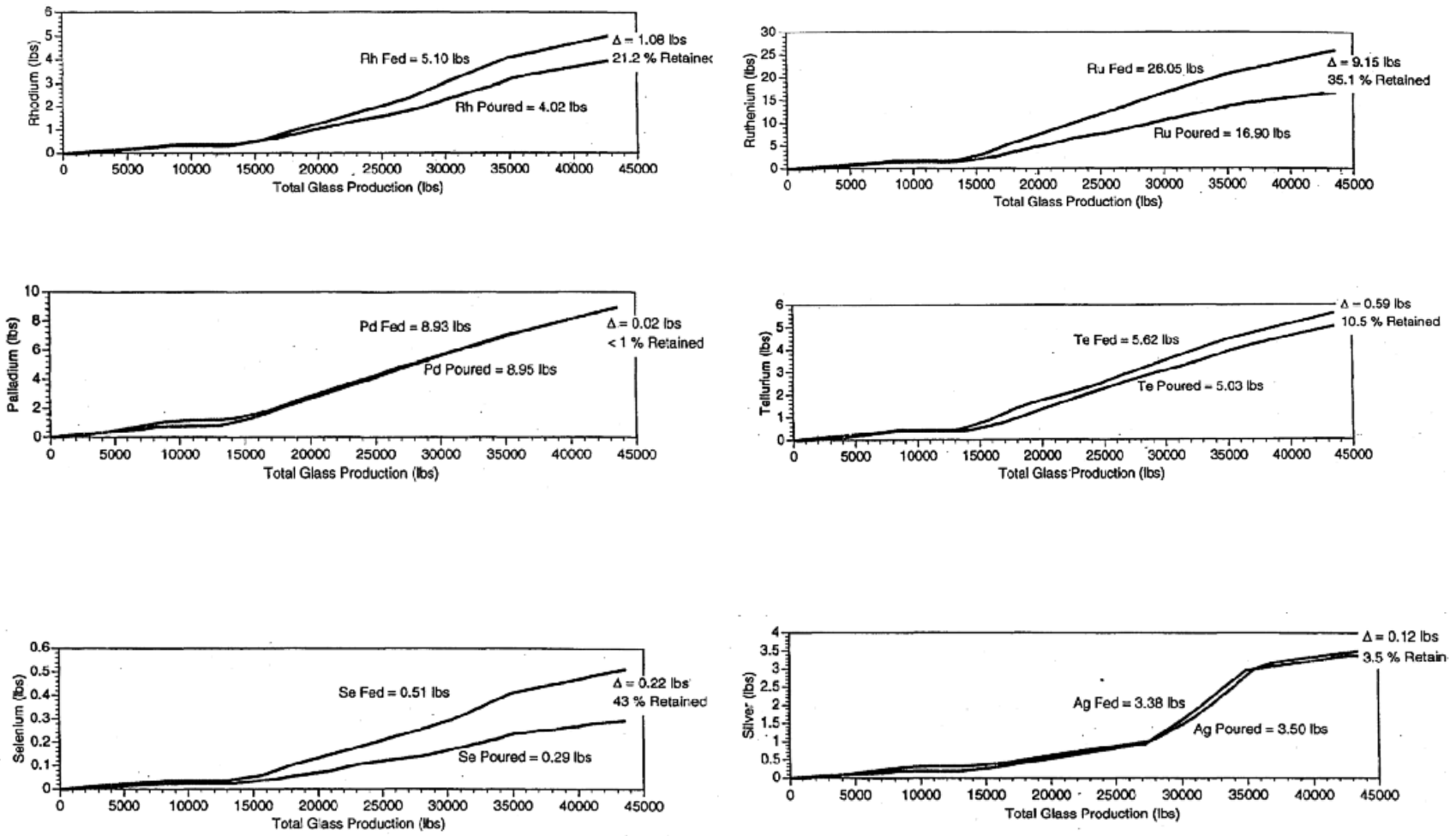

Figure 3.1. Overall Materials Balance for Noble Metals (Smith and Bickford 1997)

Table 3.16. Noble Metals Settling and Retaining Rates Estimated*

Element	Poured/Total Time (lb/day)	Poured/Idling Time (lb/day)	Retained/Total Time (lb/day)	Retained /Processing Time (lb/day)
Ru	0.027	0.034	0.015	0.073
Rh	0.006	0.008	0.002	0.032
Pd	0.014	0.018	0.00003	0.0002
Te	0.008	0.010	0.0009	0.005
Se	0.0005	0.0006	0.0004	0.002
Ag	0.006	0.007	0.0002	0.0009

* Total glass produced ≈ 42000 lb, Total time ≈ 21 months (30 days), Idling time ≈ 16.8 months (80 percent of total time), Processing time ≈ 4. 2 months (20 percent of total time)

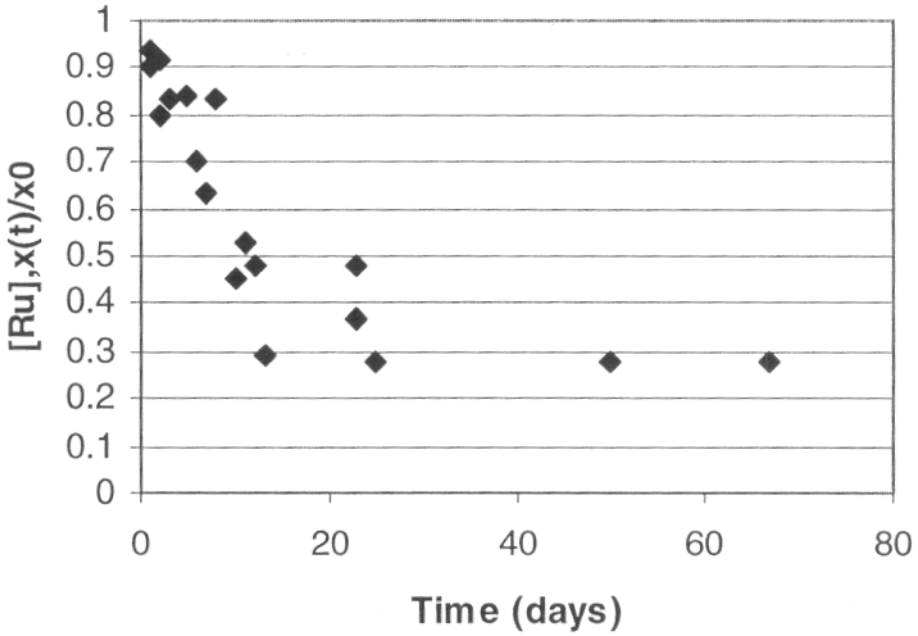

Figure 3.2. Concentration of Ruthenium vs. Idling Time (Smith and Bickford 1997)

3.3. PNNL Studies

Noble metals have been included in glass development studies since some of the earliest waste solidification and vitrification work at PNNL. The insolubility of noble metals in glasses was observed at those early stages and was also known from the literature; however, the effect this insolubility could have on melter operation was not known. Early work focused on waste-form durability and leaching behavior rather than processing concerns. As the processing concerns related to noble metal insolubility in glasses became known, studies became focused on determining particle agglomeration mechanisms, settling behavior, and related subjects. Early work at PNNL (Mendel et al. 1977, Ross et al. 1978) addressing low-melting (<1100ºC) borosilicate waste glasses used several high-level waste simulants and glass-forming frits. Melts were conducted at laboratory-scale (~100g). The simulant preparation and melting procedures are not well described; however, frit and waste compositions are available in the references. X-ray diffraction (XRD) studies identified the Ru species as RuO_2. A detailed analysis was performed for one of the glasses. The XRD analysis showed tetragonal RuO_2 crystals (lattice constants a_o = 4.5 Å, c_o = 3.1 Å) after melting at 1000ºC. These crystals comprised 1.4 wt percent of the glass, but did not exceed approximately 1 µm in size. They were not visibly altered after 1 year at 700ºC. The product glass contained Pd at 1.0 wt percent with a maximum particle size of 10 µm and a 100-µm Rh particle. The observed increase in concentration of Rh toward the top of the sample was presumed to have been caused by particles rising with bubbles.

Recovery of noble metals from fission product wastes was examined, mainly for economic reasons (Jensen et al. 1984). Investigators found that adding a metal oxide and a reducing agent to the waste and glass-formers permitted recovery of most of the noble metals. The reducing agent reduced the metal oxide to pure metal, which then acted as a "scavenger" to collect the noble metals. The metals fell to the bottom of the melter, from where they could be drained, separated, and purified. Investigators proposed that the metal mixture could be drained from the bottom of a melter through a freeze valve. The freeze valve concept had been tested using glass but required evaluation for use in draining molten metals. Laboratory studies were performed to determine the efficiency of this process in noble metal recovery. A mixture of simulated waste, glass-formers, a scavenger oxide, and a reducing agent was melted in a porcelain crucible at 1100ºC for 2 hours. Various metal oxides and reducing agents were evaluated. In general, 70 percent to 100 percent of the palladium, 70 percent to 100 percent of the rhodium, and 30 percent to 70 percent of the ruthenium could be recovered

After it became known that the noble metals had the potential to form a sludge that would interfere with melter operation, laboratory tests were initiated tests to obtain a preliminary characterization of noble metals in simulated HWVP glass (Geldart et al. 1987). These tests included crucible melts and a continuous liquid-fed minimelter (LFMM) run, all using the reference HW-39 waste and frit. The noble metals were added as the oxides RuO_2, PdO, and Rh_2O_3 with average particle sizes of approximately 15 µm, 5 µm, and 2 µm, respectively. The noble metal oxide concentrations (Wt percent) in the glass were RuO_2 = 0.16, PdO = 0.05, and Rh_2O_3 = 0.05.

The crucible melts were performed to determine the effects of redox state, temperature, duration of melt, and noble metal concentration on the behavior of noble metals in the melt. Ferrous/ferric (Fe^{+2}/Fe^{+3}) ratios studied were 0.0, 0.03. 0.27, and 0.65. Temperatures studied were 940ºC, 1100ºC, and 1170ºC. The various melt durations were 2.4, 24, and 240 hours, and total noble metal concentrations used were 0.26, 2, and 11 wt percent of the total glass oxides. An increased Fe^{+2}/Fe^{+3} (redox) ratio caused a decrease in the number of spinel crystals present in the glass product; however, the degree to which this occurred depended on the reducing agent used. For example, no spinels were observed at a Fe^{+2}/Fe^{+3} ratio of 0.27 when formic acid was the reducing agent. However, when sugar was the reducing agent, spinels were present at a Fe^{+2}/Fe^{+3} ratio of 0.65. At higher Fe^{+2}/Fe^{+3} ratios, noble metal particles were of high

purity, with little mixing of elements. Increases in temperature enhanced the settling rate of agglomerated particles and therefore decreased the number and size of particles suspended in the melt. Increases in duration of the melt caused increases in the size of particle observed in the melt and in the amounts of settled particles. The only apparent effect of increasing concentration of noble metals was to increase the total number of particles and agglomerates. Most of the agglomerated particles observed in these crucible melts were <10 μm. Some of the particles were alloys of Ru, Rh, and Pd, with traces of Cu, Fe, Ni, and Cr. Palladium was observed alloyed with Te in some cases. XRD analysis showed particles that were pure RuO_2 and RhO_2. Particles were seen adhering to bubbles, and some noble metals had accumulated at the surface of the melts.

The LFMM test was conducted to create more representative melter conditions than the crucible melts. The LFMM was a laboratory-scale continuously fed melter. It consisted of an Inconel crucible with an overflow tube where glass was discharged. The crucible is located in a furnace. Liquid feed was fed to the LFMM at a rate of between 180 and 300 mL/h. The reference HW-39 feed was used. The glass depth was approximately 10 cm. The temperature at the bottom of the crucible varied from 1095ºC to 1150ºC, and the temperature at the top was 660ºC to 1030ºC. The discharged glass was analyzed by XRF, SEM/EDAX, and ICP. The results showed mostly submicron Ru and Pd particles. A core sample taken upon completion of the LFMM test revealed a 0.5 cm metal nodule at the bottom of the crucible, which was mostly an alloy of all three noble metals. Numerous other metal nodules were found at the bottom of the melt, many of which were under the tip of an Inconel thermowell. The behavior of noble metals in the LFMM might not be representative of their behavior in the HWVP, because the noble metals were added as oxides rather than as soluble nitrates or other complexes. In addition, redox conditions could not be accurately controlled in the LFMM. The expected range of Fe^{+2}/Fe^{+3} ratios (from crucible melts) was 0.0 to 0.3. Actual values obtained in the LFMM were 0.18 to 0.51, again, a likely result of oxidation of the Inconel.

Preliminary calculations assuming that all particles in a typical glass melt are micron-sized RuO_2 particles evenly spaced throughout the melt showed that settling of individual particles cannot account for the sludges formed on melter floors. The proposed mechanism was shear-induced agglomeration at the cold cap-melt interface. A relatively simple model was created to determine if agglomeration rates caused by shear could be significant. Results indicated that shear-induced agglomeration could be significant, especially when combined with other agglomeration mechanisms, such as electric field interaction, hydrodynamic interaction, and bubble phenomena.

Additional crucible studies were performed to examine agglomeration and settling of noble metal particles, particularly RuO_2 (Cobb and Hrma 1990). Glass with a total noble metal oxide concentration of 0.45 wt percent (0.27 wt percent RuO_2, 0.09 wt percent PdO, 0.09 wt percent Rh_2O_3) was mixed as oxide particles <100 μm and was melted at 1150ºC for 95 minutes. The glass was then cooled, crushed, and disc-milled, and a portion was remelted at 1150ºC for 25 minutes. The samples were then heated in alumina crucibles at 1050ºC for 15 minutes, 2 hours, 6 hours, 14 hours, 64 hours, or 140 hours, and the product glasses were examined by optical microscopy. In addition, two samples were heated in platinum crucibles for 16 and 64 hours. The RuO_2 was initially present as particles approximately 1 μm in diameter. Examination of the glasses indicated that much of the agglomeration occurred in the melt meniscus, where velocity gradients would be expected to be the greatest. The 2-hour sample showed agglomerates of up to 50 μm dispersed throughout the melt, although most particles were only 1 to 2 μm. Agglomerates were present mainly in the upper half of the 14-hour melt, whereas at 16 hours agglomerates were again dispersed throughout the melt. In melts conducted for longer than 14 hours, a layer of large agglomerates covered the bottom of the crucible. The 64-hour melt contained a 3.5- x 1.5-mm agglomerate beneath the center of the upper melt surface and smaller particles of metallic Rh and Pd. Calculations using Stoke's law estimated that a spherical RuO_2 particle with a diameter of 1 μm would settle 1 cm in 278 days. Therefore, agglomeration must precede settling. Because the mechanism for

agglomeration was velocity-induced shear, particularly in the crucible meniscus, these results could not be directly correlated to noble metal behavior in a melter. In this section, five major studies, gradient furnace testing (GFT), research scale melter (RSM) testing, engineering scale melter (ESM) testing, modeling, and engineering analysis, completed at PNNL are reviewed.

3.3.1. Gradient Furnace Testing

Gradient furnace testing (GFT) was conducted in FY 1992 to determine the behavior of noble metals in the cold cap region of the melter glass pool (Elliott et al. 1994). The primary objective of this work was to provide particle characteristics for modeling the behavior of noble metals in the HWVP melter. A secondary objective was to establish the relative differences between the nominal NCAW melter feed and Kernforschungszentrum Karlsruhe (KfK) and DWPF feeds, regarding noble metals particle formation and characteristics. Testing provided information on the physical characteristics (size, shape, chemical/alloy composition, particle density, evidence of agglomeration and settling) of the noble metal particles expected to exist during processing of NCAW melter feed. The data collected during the course of the GFT accomplished the following specific goals:

- Determined the behavior of noble metals in the nominal NCAW melter feed simulant as it progressed through the various reaction layers of the melter cold cap.
- Provided data for the development and refinement of numerical models used to predict convective flow patterns, particle formation, accumulation mechanisms, processing conditions, and particle characteristics.
- Postulated particle agglomeration mechanisms.
- Supported understanding of the role of cold cap chemistry on particle formation.

The gradient furnace testing results provided the upper boundary condition for the computer simulation of the melter, i.e. the size, density, and type of particles entering the glass melt through the cold cap. However, the gradient furnace could not completely simulate the cold cap behavior in a melter due to the differing geometries and temperature histories. In an actual melter, the feed in the cold cap would be exposed to an atmosphere produced by the gases evolved. Different gases would be produced in different strata of the cold cap, according to the local temperature and the nature of the gas-generating reactions occurring at that temperature (Schreiber et al. 1990; 1991). Gases evolved at lower layers, where the temperature is higher, left the cold cap through the upper layers, where they mix with gases generated locally. This complex situation could not be easily reproduced in a laboratory crucible or boat.

Four feeds were prepared, subjected to heat treatment in the gradient furnace, and analyzed using optical and scanning electron microscopy (SEM): 1) HWVP-1 Feed (Noble metals precipitated with major constituents), 2) HWVP-2 Feed (Noble metals precipitated with minor constituents), 3) DWPF Feed, and 4) KfK Feed. HWVP-1 feed was prepared with simulated NCAW in which the noble metals had been precipitated with major constituents. HWVP-2 feed was prepared with simulated NCAW in which the noble metals had been precipitated with minor constituents. The target concentrations of noble metals in the product glasses are shown in Table 3.17.

Table 3.17. Concentration of Noble Metals in Glass (Wt percent) (Elliott et al. 1994)

Noble Metal	NCAW (HWVP-1 and HWVP-2)	DWPF	KfK
RuO_2	0.11	0.1	0.655
Rh	0.024	0.02	0
Pd	0.030	0.03	0.298
SUM	0.164	0.15	0.953

For each test, the feed was loaded into a 30.5-cm-long boat-shaped quartz crucible and held at a specified temperature gradient for 1 hour in the gradient furnace. The gradient furnace used in this test produced an adjustable linear temperature gradient. For the HWVP-1 and DWPF samples, the range used was 579°C to 928°C. For the HWVP-2 sample, the range was 593°C to 936°C, and for the KfK sample, it was 698°C to 1046°C. After removal from the gradient furnace, the samples were annealed for 1hour at 500ºC and cooled slowly overnight. The annealing was done to remove internal stresses within the sample. No changes in the melting progress would be expected to occur during annealing. The crucibles were then fixed in an epoxy resin mold and cut in half lengthwise. Six 5-cm segments were made from each sample. Each segment was mounted on a slide, thin-sectioned, and polished for characterization using SEM and EDS (Elliott et al. 1994).

Noble metal particles were detected in all temperature ranges of the HWVP-1 sample. Most of the particles observed were Ru or RuO_2 (oxidation states were not determined; Ru is generally assumed to be present as RuO_2) or Pd. Only one Rh particle was observed. Pd and RuO_2 were seen to exist in particles of varied composition and size. Pd was first seen as irregular 3- µm particles embedded in a Cd-rich cluster at 592°C. In the same temperature neighborhood, Pd was also detected as an alloy with Ag in a spherical dendrite structure of approximately 50 µm. Pd and RuO_2 were seen at 648°C in a 20-µm cluster in which RuO2 was a collection of 3-µm particles in one corner of the cluster. RuO_2 was detected as a component in La-rich particles 10 µm in size at 655°C and 758°C. The Ru distribution in the particles was uniform. Pd appeared again at the temperatures 670°C, 767°C, 826°C, and 834°C as collections of fragmented 1- to 2-µm particles. The collections ranged up to 10 µm in size and had blurred, indistinct edges. Small amounts of Ag and Ru were detected in these particles. Rh was not found in this region. At approximately 898°C, Pd was observed as a chain of three particles, the largest measuring about 6 µm, and the other two measuring about 1 µm. The particles did not have a distinct border but exhibited irregular, cloudy edges. Near one of the Pd particles was a cluster of RuO_2 particles in a Ni-rich area. The Ru/Ni-rich cluster measured about 7 µm across, similar in size to other clusters seen at lower temperatures. Other particles of RuO_2 in nearby areas had indistinct boundaries, appearing as hazy or diffuse clouds. Pd particles in other areas showed a rounded appearance, with no trace of alloying. At 924°C, the only Rh particle found was seen as a single, hazy cloud 10-µm wide. The size of RuO_2 and Pd particles in this hot region varied between 1 and 10 µm, and their distribution within the melt appeared random.

As in the HWVP-1 feed, the HWVP-2 feed contained identifiable noble metal particles in all temperature ranges examined. The vast majority of particles were RuO_2, though Pd and Rh were also found. In the colder end of the sample, RuO_2 was seen as a cluster of 1- to 2- µm needles at 619°C. These needles were very typical of RuO_2 particles seen throughout the sample. Some larger masses were seen, such as one at 600°C, which contained both Ru and Pd. However, most particles in this temperature region were approximately 5 µm, irregularly shaped mixtures of Ru and Pd, and were often found at the

waste/frit interface. Beginning at approximately 650°C, most of the Ru and Pd were seen as single, dense (but irregularly shaped) particles ranging up to 5 μm in size. Some clusters of these smaller particles were seen. The first isolated Rh was detected at 655°C as a 10- μm-long chunk. Beginning at approximately 700°C, Pd was most often found as smaller (1 to 2 μm) and more solid, dense particles. However, at 728°C, a larger (15 μm) particle was seen. The first alloy of all three noble metals was seen at 755°C as a small, almost spherical particle less than 1 μm across. At temperatures beyond approximately 800°C, more large clusters were present; however, small particles were still very common. Rhodium was detected as a 10-μm cluster of solid, dense particles. Pd was generally seen only in particles mixed with Ru, not in a pure state. At the hottest temperature region (879°C - 936°C), most particles were small (<5 μm) and almost all were RuO_2. No Pd particles were found in this region (Elliott et al. 1994).

The DWPF sample differed from the HWVP samples in that no identifiable noble metal particles were found in the cold end (dried feed) of the sample. The lack of detectable particles suggests that they exist as sub-micron particles in the high-Fe waste particles, undetectable by SEM/EDS. Results at higher temperatures confirmed the small noble metal sizes (<1 μm). The first noble metal identified was Ru, found at 735°C as a pair of micron-sized particles bordering an Al-enriched region of several tens of microns. By 789°C, four Pd particles were found within a 5-mm region, all porous, diffuse, of micron size, and located in Fe- and Mn-rich pockets. Rh was first observed in a cluster of sub-micron particles containing high Ru concentrations. At temperatures above 840°C, several such combinations of Ru and Rh were discovered in various 1- to 10-μm shapes, some diffuse and some with higher relative Ru concentrations than others. Only two other noble metal features were observed in the hottest end of the crucible. At 898°C, a 2-μm particle with circular shape and a fuzzy border was identified as a pure composition of all three noble metals. The three metals were indistinguishable from each other in the particle. No other particles with similar circular shape were seen, even at higher temperatures. All three metals were again seen at 924°C, in a particle 10-μm long and several microns wide. Most of the particle had a porous appearance similar to some pure Pd particles seen earlier. However, one micron-sized area was distinctly brighter and without pores, and was higher in Pd. It appeared to be a separate particle that had agglomerated onto the larger particle. Analysis showed the feature to have the same amount of Rh and Ru as the rest of the particle, but a much higher concentration of Pd.

The concentration of noble metals in the KfK feeds is much higher than in the HWVP on DWPF feeds, as was shown in Table 3.17. The number and size of noble metal particles found was also greater in the sample. At the colder end of the sample, a large (1-mm) chunk of RuO_2 was found at 704°C. Some noble metals were found in regions rich in Zr, Fe, and Ni at these low temperatures. A few irregularly shaped 5- to 10- μm RuO_2 or Pd particles were also seen in this region. In the range between 760°C and 817°C, convoluted, folded-looking Ru particles were very common, either on the surface or in the bulk of the sample. These particles were typically up to 30 μm in size. Ru was also found as a thin layer along the surface extending for hundreds of microns. As in the HWVP-2 feed, Ru was detected as spheres or sliver-shaped crystals, approximately 1- to 5- μm long. Pd was most predominant as micron-sized particles, at times in clusters of separate particles or in association with bubbles. Between 874°C and 1039°C, Ru and Pd became common as large (up to 15 μm) diffuse Ru patches surrounded by dense, submicron Pd particles. In some cases, the diffuse mass contained a mixture of Ru and Pd. Large (100-μm and 500- μm) masses of crystalline RuO_2 particles were seen at approximately 878°C. These masses consisted of small, mostly sliver-shaped crystals, with a few larger crystals present. A few Pd particles were found in association with Ce-rich regions (Elliott et al. 1994).

To provide input to the TEMPEST modeling effort, two sections at the hottest end (approximately 924°C and 930°C) of the HWVP-2 sample were examined in detail. The HWVP-2 melt was used because it was representative of the waste flowsheet being used in other melter testing. The

number, size, shape, and approximate composition of the particles or agglomerations were determined. The particles at this temperature are assumed to be representative of particles leaving the cold cap and entering the bulk of the melt. This was considered to be a boundary condition for the modeling. The accuracy of the values determined for the number and size of particles is not known. As stated earlier, only particles larger than approximately 0.2 μm could be counted. However, the amount of noble metals present as particles smaller than this cannot be determined.

All noble metal particles in the sections examined were classified by particle size. Particles were listed in increasing order by size, and then divided into categories. Each particle's size was approximated by a rectangle enclosing the entire particle. The rectangle's smaller and larger dimensions were recorded as well as the total area, which equals the area of the rectangle. The total area in most cases includes area that was not noble metal, but glass, due to the irregular shape of many of the particles and the fact that most particles were not rectangular, but spherical, elliptical, or some other shape. An estimate was made of the portion of the area occupied by noble metal. This estimate was used to calculate an equivalent area (Equivalent Area = Area Fraction x Area). In addition, the ratio of the larger dimension to the smaller dimension is given to provide an estimate of the particle shape. The particles were then classified into three groups. For each group, the average particle area, average area fraction of noble metal, average ratio of larger dimension to smaller dimension, and average equivalent area were determined. The number of particles per melt area and the area fraction of noble metal particles in the bulk of the melt were also determined. The area fraction should approximately equal the volume fraction. The density and electrical conductivity of the particles can be assumed to be equal to that of RuO_2, because over 99 percent of the particles seen were ruthenium dioxide. No palladium particles were detected and less than 1 percent of the particles contained rhodium. The SEM methods used in these analyses would detect noble metals particles larger than 0.2 μm. The fact that no palladium and very little rhodium were observed in the glass indicates that very little agglomeration of these metals occurs in the melter cold cap. This, of course, does not mean that agglomeration or alloying of these metals cannot occur in the melt pool (Elliott et al. 1994).

The first group of particles is small (< 2 μm) particles that appear fairly dense and compact. Their shape in most cases is approximately spherical. The second group of particles consists of those that were larger and much more irregularly shaped ("sponge-like"). The third group actually consists of a single large particle (also "sponge"-shaped). Because of its size it was separated from the second group. A summary of the particle characteristics is shown in Table 3.18. The density of RuO2 is 6.97 g/cm^3. Other properties of the particles (thermal and electrical conductivity) can be assumed to be equal to those of RuO_2.

Table 3.18. Particle Characteristics of HWVP-2 Feed (920°C - 930°C)

	Group 1	Group 2	Group 3
Shape	Solid Sphere	“Sponge”	“Sponge”
Predominant Type	RuO_2	RuO_2	RuO_2
Effective Particle Diameter [(a)]	1.3 μm	3.8 μm	12.4 μm
Ratio of Large/Small Dimension	1.7	1.6	1.9
Particles/Melt Area (number/mm^2)	34	16.3	0.33

(a) The diameter is calculated using total particle area and assuming a spherical shape of the particle or agglomerate.

In all samples, the noble metals had largely separated from the waste by approximately 700°C. In some cases, as discussed in the previous sections, masses of noble metals were present in the dried or sintered feed before melting had begun. This suggested that feed preparation methods might partially determine noble metal particle sizes in the feed before melting. At hotter temperatures (above 800°C), the noble metals either formed particles composed of a single metal or oxide, or formed alloys of two or three noble metals. No alloying with Te was seen; however, the amount of Te in the wastes was small and may not have been detectable. At the hot end of each sample (which simulates the end of the cold cap and the beginning of the bulk of the melt), particles were generally on the order of 1 μm in the DWPF and HWVP-2 melts and closer to 10 μm in the KfK and HWVP-1 melts. This could possibly suggest a relationship between frit size and resulting noble metal particle size since the frit used in the KfK melt was much larger than in the HWVP or DWPF melts. However, other variables such as noble metal concentration, waste preparation procedures, and foaming behavior could also account for the difference in particle sizes.

In all feeds, even though one noble metal particle size or shape may have been more common, there were numerous exceptions. For example, although small particles were predominant in the KfK sample at the hotter end, 100- μm and 500- μm clusters of RuO_2 particles were seen. These agglomerations of particles could have as much effect on melter performance as the more common, but smaller, particles. This unpredictability existed for particle shapes and densities as well as sizes, making it difficult to predict melter performance by modeling using only information from the gradient furnace testing. It is not yet known what happens after the particles intermix in the melter for several hours. The effects from intermixing over time are very dependent on convection and residence time in the melter.

Many mechanisms were proposed for noble metal agglomeration in feeds and glasses. Some of the mechanisms were as follows:

- During precipitation of metals by sodium hydroxide, noble metal oxides and hydroxides are most likely absorbed in amorphous phases, leading to noble metal segregation.

- Noble metals and their oxides, which are both relatively insoluble in glass, became concentrated in the remaining waste particles, leading to potentially agglomeration.

- Metallic particles are not wetted by molten glass and tend to accumulate on frit surfaces after the other components have dissolved (Cobb and Hrma 1990). It was postulated that these metallic particles stay inside bubbles and were lifted to the top surface, on which they floated until they fused with a sufficient number of similar particles and sank to the melter bottom. Ruthenium dioxide was, however, stable and insoluble. It is readily wetted by molten glass. A possible agglomeration mechanism for RuO_2 is shear flocculation. This can occur when clusters of RuO_2 particles are stretched by shear of the melt, which is forced to move by growing and ascending bubbles. This happens around individual bubbles moving through the melt. In the areas of a high bubble density (foam), RuO_2 particles can agglomerate within melt films that separate bubbles. These films are first stretched and then broken, thus subjecting the melt to a substantial amount of shear.

After the molten glass leaves the cold cap of a melter and enters the pool underneath it, it was speculated that RuO_2 agglomeration continues in the convective flow due to shear flocculation. In this way, large agglomerates could form. In a laboratory crucible, in which the melt was vigorously sheared in the meniscus that exists on the crucible wall above the melt, agglomerates grew up to 1 mm size within 16 hours (Cobb and Hrma 1990). The terminal settling velocity of a spherical particle was, by Stokes'

law, proportional to the square of the radius of the particle. The agglomerates consisted of RuO_2 particles and the melt contained within them. Because of their fractal nature, their density decreased approximately linearly with their radius. Hence, the terminal settling velocity of agglomerate increased proportionally to its radius. As a result, some agglomerates would not be discharged from the melter with the melt; they would settle to the bottom and eventually create a conductive layer.

3.3.2. Research Scale Melter Testing

Per the FY 1991 PNL statement of work, the objectives of RSM testing were "to establish operating parameters for ESM tests at KfK and evaluate glass containing noble metals, obtain data that provide an understanding of noble metals behavior in conjunction with feed and glass chemistry to predict melter performance...conduct studies of test parameters, including glass melter temperature, residence time, plenum temperature, and glass redox." (Kruger 1991). To perform this scope of work, a small joule-heated test system was designed in FY 1990 and constructed in FY 1991. Approximately 8 weeks of testing were conducted in the RSM in FY 1992 to obtain process and product data as a function of process variables.

The relevant slurry and process variables were varied through the ranges of the HWVP operating limits. The following variables were investigated:

- Noble metals concentration in the feed - nominal for the HWVP was 0.15 wt percent noble metals in the glass.
- Slurry oxide loading in the feed - nominal for the HWVP is 500 g TO/L. The design range was 400 to 600 g TO/L.
- Redox ($Fe^{+2}/\Sigma Fe$) of the glass - the acceptable range for the HWVP glass was $Fe^{+2}/\Sigma Fe = 0.005$ to 0.23.
- Glass process temperature - the nominal operating temperature for the HWVP was 1,150°C. The limits were 1,050°C and 1,170°C.
- Melter plenum temperature - minimum operating plenum temperature for the HWVP was 650°C.

Process data were used to determine any measurable effects on melter operation, such as glass resistance or process rate. Process data were also used to support continued validation and refinement of the numerical codes. HWVP process limits established for many feed and melter parameters were glass temperature, plenum temperature, glass redox, slurry oxide, and the noble metals concentration. Analytical data were obtained for slurry, glass, and in-melter glass/sludge samples. In addition, post-test examination of the melter was done to measure metal deposits.

The RSM, because of its small size, was chosen to characterize the effects of noble metals on melter performance as a function of melter operating parameters (glass and plenum temperatures) and feed properties (oxide concentration, redox potential, and noble metal concentrations). Because of the short residence time of the RSM, 5 hours, a settled region was not expected to form based on intuition and an estimation of settling velocities. However, the glass exiting the melter was characterized to detect any changes in noble metal properties as a function of the parameters listed above. The test matrix for the RSM testing is shown in Table 3.19. The glass reduction/oxidation potential was measured by the ratio of ferrous (Fe^{+2}) to total iron (ΣFe). A high redox glass was defined as having $Fe^{+2}/\Sigma Fe$ greater than 0.005. Originally, all of the nominal operating conditions chosen for the RSM were those expected for the HWVP. Because of feed rheology problems, the nominal feed oxide loading had to be lowered from 500gTO/L to 400 g TO/L to permit pumping. Initially, two low glass temperature segments had been prescribed. After the first low temperature segment, it was determined that operating the melter at this low temperature was useless; the melter could barely be fed. The plenum temperatures shown in Table

3.19 were the pretest estimates. The plenum temperatures experienced during the run were much different because of the difficulty placing enough plenum heating capacity in this small melter.

Table 3.19. RSM Test Matrix

Segment No.	Description	Noble Metal Concentration	Oxide Loading (g TO/L)	Glass Redox (Fe^{+2}/EFe)	Glass Temperature (EC)	Plenum Temperature (EC)
1-3	Nominal	Nominal	400	0.005	1,150	550
4	Low glass temperature	Nominal	400	0.005	1,050	550
5	High oxide	Nominal	500	0.005	1,150	550
6	High plenum temperature	Nominal	400	0.005	1,150	650
7	High glass temperature	Nominal	400	0.005	1,200	950
8	Reducing glass	Nominal	400	0.23	1,150	800
9	High NM[(a)] concentration	2X	400	0.005	1,150	800
10	High NM, Ag, Te	2X	400	0.005	1,150	800
11	High NM, reducing glass, high glass temperature	2X	400	0.23	1,200	800

(a) NM = Noble metals.

The RSM noble metals test comprised 48 days of melter operation divided into nine segments. The test was divided into segments so that a parametric evaluation of the effects of various operating conditions on noble metals effects could be evaluated. These parameters included melter operating parameters (glass and plenum temperatures) and feed properties (oxide concentration, redox potential, and noble metal concentrations).

Feed samples were drawn from the final fritted material at the beginning of each segment and at intermittent times during each segment. In general, the composition of the feed remained constant over the course of the test and varied only in oxide loading, redox states, and noble metals concentrations as prescribed in the original test design. Two test segments were completed with reducing feed. Segment 8 contained high redox feed at the nominal noble metals concentration and Segment 11 contained high redox feed at 2X noble metals concentration. To determine the amount of reductant (sugar) required to

reduce the feeds to the upper HWVP limit ($Fe^{+2}/\Sigma Fe = 0.23$), feed samples were drawn and vitrified in a crucible at varying sugar concentrations. The resulting glasses were analyzed to assess the redox level. Based on the results of these tests, it was decided to spike the feed for Segment 8 with 6.8 g/L of sugar. The sugar addition in Segment 8 did not significantly affect the measured redox of the glass. In fact, the redox ratio of the high temperature segment (Segment 7) was more reduced than was Segment 8. This was surprising because it was expected that the laboratory tests using a crucible exposed to air would be more oxidizing than the melter cold cap. Just the opposite was observed. The $Fe^{+2}/\Sigma Fe$ for glasses by segment number is presented in Table 3.20.

Table 3.20. $Fe^{+2}/\Sigma Fe$ for Glass by Segment Number

Segment Number	Segment Description	Wt % Fe^{+2}	Wt % ΣFe	Ratio Total $Fe^{+2}/\Sigma Fe$
1	Nominal	0.02	5.322	0.004
4	Low glass temperature	0.021	5.122	0.004
5	High oxide	0.01	4.423	0.002
6	High plenum temperature	0.008	4.968	0.002
7	High glass temperature	0.094	4.88	0.019
8	High redox	0.005	4.944	0.001
9	High NM concentration	0.007	4.994	0.001
10	High NM, Ag, Te	0.012	4.968	0.002
11	High NM, redox, glass temperature	0.094	4.839	0.251

The concentrations of silver and tellurium were increased twofold in Segment 10 to evaluate their effect on noble metals precipitation. Silver and tellurium have been observed to alloy with palladium in HLW glasses. The extra silver and tellurium were added to the 55 gallon drum of unfritted melter feed from which material were taken to make up the melter tank batches for segment 10.

In hindsight, the RSM was more oxidizing than the crucible most likely because the cold cap was very thick during normal operation. This provided a substantial residence time for the dried feed in the melter plenum, which should have been very oxidizing. Because of these observations, the quantity of sugar added to the feed for Segment 11 was increased to 15g/L. This amount, which was based on engineering judgment, was very close to the correct amount. The ferrous-to-total-iron ratio of the glass during Segment 11 was measured to be 0.25. The target was $Fe^{+2}/\Sigma Fe = 0.23$. In run Segment 11, a spike of barium hydroxide was introduced to feed as a tracer to evaluate the mixing in the RSM. Barium was selected because of its low concentration in the nominal glass and its high analytical resolution. Barium was added to the feed as 2.47 g $BaOH \cdot 8H_2O$ per liter of feed at 400gTO/L. This equates to an increase of 0.25 wt percent Ba in the glass.

Figure 3.3 shows the results of these analyses as a function of time after the Ba was added to the melter feed tank. The melter pour rate data from the glass canister scale were used to generate a curve of the theoretical Ba content of the glass product coming from the melter, assuming that the melter was a well-stirred tank and the melter feed rate varied directly with the glass pour rate. The calculation was performed for a cylindrical tank 6 in. in diameter, 3 in. deep and using a glass specific gravity of 2.5 This curve was found to fit the data well if it was assumed there was a 2.5-hour lag time between a change in the melter feed composition and a change in the glass product composition. This curve is also shown on Figure 3.3.

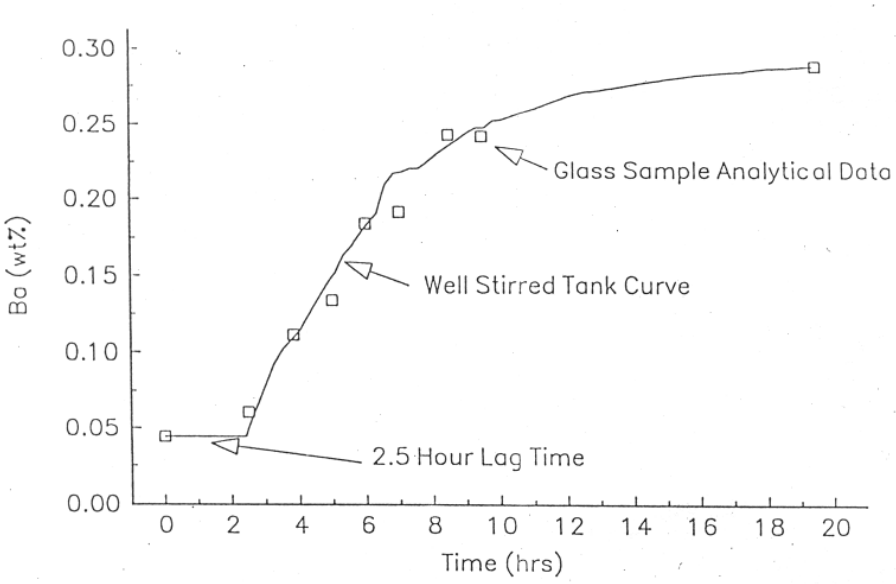

Figure 3.3. Barium Tracer Test for the RSM (Elliott et al. 1994)

The source of this apparent lag time was probably the cold cap in this melter, which was quite thick relative to the glass depth when compared with larger melters. A 2.5-hour lag time would represent about 1.9 kg of glass, 4.7 L of feed, or 1.6 in. of glass depth in the melter at the average processing rates over the period of time the test was performed (1.87 L of feed/h or 0.75 kg/h of glass). Calculations for the lag caused by the length of the feed line from the melter feed tank to the melter indicate that this contribution is small (~0.1 hour). Some of the lag time was probably due to the abnormally large cold cap that was present in the melter. The remainder was probably in the relatively cold portion of the glass just under the cold cap, which was too viscous to mix.

The glass samples were analyzed using SEM-EDX to determine the qualitative composition of the particles. To better characterize the particle morphology and size distribution, optical microscopy analyses were also completed. Using an image analyzer with the optical microscope, the area percent of clusters on a sample slide could be measured as well as the area percent of RuO_2 needles within the clusters. The area percent of needles on a slide can be obtained by multiplying the two percentages. Table 3.21 presents the results of these analyses. The analyses of the samples from the post-test destructive examination of the melter (samples C1 through C4) are also included in the Table 3.21. The samples from the bottom of the tank (samples C1, C2, and C4) all had a continuous, but heterogeneous, metallic layer approximately 2- to 4-mm thick. For all three samples, this layer consisted of metallic particles (10 to 20 μm) of a Ru/Rh alloy surrounded by two separate, continuous phases. One of these continuous phases was an alloy of metallic Pd/Ag/Te with a small amount of Ru metal. The other continuous phase was pure RuO_2. It was not certain that the Ru was an oxide. It was assumed to be nonmetallic because of the darkness of the phase and the absence of other elements that would indicate an

alloy. None of the bottom samples, including the sample C4 directly under the shortened electrode, contained any metallic phases of Inconel constituents. The outer edges did contain Fe/Cr/Ni spinels, but not in the concentrations required to account for the material loss from the electrodes.

The results of the particle size distribution measurements performed using the optical microscope were used as input to the computer models of the RSM. A summary of these data is shown in Table 3.22. For reference, the GFT data is also shown in this table.

Table 3.21. Results of SEM, EDX, and Optical Microscopy Observations

Segment	SEM/EDX Observations	Optical Microscopy Observations
1 - Nominal	Sparse RuO_2 particles, <5 μm diameter	Corresponding micrograph.
4 - Low glass temp	Similar to Segment 1 but particles are slightly larger (<10 μm) and some contain traces of Rh.	5 to 10 μm clusters with some up to 16 μm. 1 area percent clusters with 9 area percent RuO_2 within the clusters.
5 - High oxide	Identical to Segment 1.	5 to 9 μm clusters with many smaller particles. 6 area percent clusters with 14 area percent RuO_2 within the clusters.
6 - High plenum temp	Similar to Segment 4 except larger particles, 10 to 20 μm.	5 to 10 μm clusters. 0.07 area percent clusters with 13 area percent RuO_2 within the clusters.
7 - High glass temp	RuO_2 needles 10 to 20 μm; Pd, Te, Ag spheres <1 μm; 2 to 4 μm Fe, Cr, Ni cubic spinels.	Corresponding micrograph.
8 - High redox	RuO_2 needles only; most are <5 μm with a few 20 μm.	N/A
9 - 2X noble metals	RuO_2 needles (most are <10 μm, a few up to 50 μm); Fe, Cr, Ni spinels (2 to 3 μm).	N/A
10 - 2X noble metals, Ag, Te	RuO_2 needles up to 200 μm. 1 to 2 μm Pd spheres, no alloying.	Average particle of 12 μm with clusters up to 60 μm observed. 2 area percent clusters with 6 area percent RuO_2 within the clusters. Corresponding micrograph.
11 - 2X noble metals, high temp, high redox	Spherical, metallic particles only. Pure Ru, Ag, Pd and alloys of Ru, Ag, Pd, Te, Rh, Cu. Sizes range 1 to 5 μm.	Corresponding micrograph.

Table 3.21. Results of SEM, EDX, and Optical Microscopy Observations (continued)

Segment	SEM/EDX Observations	Optical Microscopy Observations
C2 - Post-test sample, center, bottom of melt cavity	Metallic layer with Ru, Rh alloy particles; Pd, Ag, Te alloy surrounding phase with a small amount of Ru; secondary phase of pure RuO_2. Outer edges of metallic layer have Fe, Cr, Ni spinels.	N/A
C3 - Post-test sample, melt cavity center	Spheres of Ag/Pd with Te. Very sparse Ru metal particles attached to spinels.	N/A
C4 - Post-test sample, under short electrode	Metallic layer with Ru, Rh alloy particles; Pd, Ag, Te alloy surrounding phase with a small amount of Ru; secondary phase of pure RuO_2. Outer edges of metallic layer have Fe, Cr, Ni spinels. Very sparse Ru metal particles attached to spinels.	N/A

Table 3.22. Measured Particle Size Distributions

Diameter Range, μm	Volume Percent		
	GFT Data	Research-Scale Melter Segments 4, 5, and 6	Research-Scale Melter Segment 10
0-1	0.1		
1-3	13.5		
3-5	32.2		
5-7	20.9	11.7	0.1
7-9	0	19.8	0.6
9-11	0	24.3	1.6
11-13	33.4	4.9	2.9
13-15		27.5	2.8
15-17		11.7	2.6
17-19			5.2
19-21			5.7
21-23			1.4
23-25			2.7
25-30			2.7
30-40			16.5
40-50			11.7
50-60			21.4
60-80			22.1

The retention of the noble metals in the feed was estimated as follows: It was assumed that no noble metals were retained during the first segment. This can be justified by the fact that over the length of this segment, no noticeable change in the melt resistance was seen. The XRF analysis for this first segment was then assumed to be the baseline and any difference between the XRF analyses of subsequent segments and this segment were assumed to represent a real change in the data. This method basically assumed that there was a positive bias to the XRF data for all the elements. The XRF data was chosen over the ICP-MS data because it appeared to have less scatter. The difference between segments was therefore assumed to represent a real, absolute change in the amount of noble metals present in the glass and the retention calculated using the target values for the amount of each element in the feed. Using these assumptions a calculation of the percent retained was made for each element and the noble metals as a whole. A sample calculation equation is shown below to demonstrate the method used.

$$\text{Noble Metal Retained}_{seg} = \frac{NM_{XRF\,nominal} - NM_{XRF\,seg}}{NM_{target}} \qquad 3.1$$

where NM_{target} = target noble metal concentration, $NM_{XRFnominal}$ = nominal noble metal concentration, and $NM_{XRFsegment}$ = segment noble metals concentration. Of course, the nominal values and feed values were doubled for the calculations performed in the segments containing double the nominal amounts of the noble metals. This data is shown in Table 3.23.

These data indicate very little retention of noble metals in the melter through test Segment 8 with the exception of Segment 7. These data are reinforced by the data for the resistance of the melt, which

was measured during the run. The resistance data did not indicate any discernable decrease in the melt resistance through Segment 8. The melt resistance data for Segment 7 indicated an increase in resistance, although the data were rather sparse and made it difficult to determine whether the resistance was truly changing or not. This segment was the high glass temperature segment; the data for the redox measurement of the glass indicated that it was somewhat reduced at $Fe^{+2}/\Sigma Fe = 0.019$. This finding was supported by the SEM and optical microscopy data for this segment, which indicated that this segment contained spheres of palladium alloyed with silver and tellurium. This was further supported by the fact that this segment was found to have the highest retention of palladium of any of the segments containing nominal amounts of noble metals.

Table 3.23. Percent of Noble Metals Retained in the Melter (Elliott et al. 1994)

Description	Segment Number								
	1 Nominal	4 Low Glass Temp.	5 High Oxide	6 High Plenum Temp.	7 High Glass Temp.	8 High Redox	9 High NM Conc.	10 High NM, Ag, Te	11 High NM, Redox, Glass Temp.
Pd Retained (percent)	0	3	24	12	35	0	24	35	99
Rh Retained (percent)	0	0	10	10	17	-3	28	35	63
Ru Retained (percent)	0	10	6	8	19	7	40	41	65
Total NM Retained (percent)	0	7	10	9	22	3	34	39	72

Interestingly, the high temperature segment (7) was found to be more reducing than the high redox segment (8) in which the feed had sugar added. A possible explanation for this is that the large amount of time that the feed was found to spend in the cold cap allowed all of the sugar to oxidize using oxygen from the plenum gases. This would mean that by the time the feed reached the point where it was beginning to melt into the glass, none of the reducing sugar was available to reduce the melt. In fact the data for Segment 8 indicated that it had the lowest total noble metal retention of any segment other than the nominal one, which was assumed to have none. The other segments containing the nominal amounts of noble metals indicated about 7 to 10 percent retention of noble metals. It is questionable whether this degree of resolution is possible using this data. There may be some effect from aging of the particles in the melter, causing them to get larger. The RuO_2 particles in the glass coming from the melter appeared to be larger in Segments 4 and 6. Segment 5, however, which had the largest retention of Segments 4 through 6, did not appear to have RuO_2 particles any larger than the nominal segment. When the change was made to twice the nominal amount of noble metals, the retention of noble metals increased

dramatically. This was accompanied by a definite decrease in the melt resistance and a large increase in the size of RuO_2 particles in the glass product. Segment 9 (2X noble metals) had the largest rate of decrease in melt resistance of any of the segments.

Segments 10 and 11 had increasingly higher retention of noble metals. Segment 10 (2X noble metals with high silver and tellurium) had an increase in the amount of palladium and rhodium retained and very little change in the ruthenium retention. This would coincide with the postulated effect of alloying of the palladium with the silver and tellurium to produce larger particles with higher settling velocities. The SEM/EDX data for this segment, however, did show the presence of palladium particles, but unalloyed. It is possible that the palladium is normally dissolved in the glass as a metal and that the combination of extra palladium and extra silver and tellurium attempting to dissolve in the glass caused the palladium to reach its solubility limit in the glass and the extra precipitated. Ruthenium had the same retention in Segment 10 as it did in Segment 9. This would also be consistent with the silver and tellurium only affecting the palladium retention, because the ruthenium is present as RuO_2 and theoretically not affected by the silver and tellurium. A higher retention of rhodium (approximately 7 percent) is difficult to explain. It may simply be beyond the ability of the analytical methods to resolve the change. This segment showed a definite decrease in melt resistance, but at a smaller rate than Segment 9.

Segment 11 (2X noble metals, silver, tellurium and high redox) had the highest overall retention with nearly all of the palladium being retained and around 65 percent of the rhodium and ruthenium being retained. The SEM/EDX data for this segment indicated that all of the visible particles were spherical and, therefore, most likely metallic. The particle compositions ranged from pure ruthenium, silver, or palladium to alloys containing ruthenium, silver, palladium, tellurium, rhodium and copper. No RuO_2 particles were visible anywhere in the glass product. Given the spherical, metallic nature of these particles, it is not surprising that a large fraction of them were retained. Interestingly, the resistance in this segment did not decrease perceptibly during this segment; in fact, it increased slightly. The difference between the retention of noble metals in the nominal and 2X noble metal segments was dramatic. The nominal segments averaged 5 percent calculated retention, while the 2X segments averaged 46 percent. One obvious difference in these segments was the size of the RuO_2 agglomerates. The nominal segments had agglomerates ranging up to 20 μm, while the 2X segments had agglomerates up to 200 μm. It remains to be seen if settling alone can explain the difference in the retention between 1X and 2X segments.

An obvious mechanism for retaining RuO_2 in the melter is the capture of the RuO_2 crystal agglomerates that are commonly seen. In the case of rhodium it is known that it will substitute itself in place of ruthenium in the RuO_2 crystals. In most of the test segments, the calculated retention for rhodium was approximately equal to that of ruthenium. Because the rhodium should have been present in approximately one-third the concentration of ruthenium, that would mean that about 1/3 of the RuO_2 was really RhO_2. The SEM/EDX data showed that in every case in which a RuO_2 crystal was seen, rhodium was present. The peaks generated by the EDX analysis for ruthenium and rhodium were very close together, making it difficult to estimate the amount of ruthenium and rhodium present. Rhodium was certainly present. It is possible that about one-third of the RuO_2 was actually RhO_2; this would account for the rhodium retention.

The palladium retention was more difficult to explain. Calculation of palladium retained in the melter resulted in significant quantities in segments where no metallic palladium was seen. Obviously, when palladium was present in either alloyed or unalloyed spherical particles, the settling of these particles was a mechanism for retention. But in cases where the palladium could not be seen as a separate phase from the glass (SEM should be capable of easily seeing particles less than 0.5 μm), another mechanism for retention must be postulated. Segments 5 and 9 showed 24 percent retention of palladium, though no palladium particles were seen.

Bottom samples were taken from the RSM after the melter was sawn in two. These samples were analyzed by ICP-MS and XRF. Table 3.24 gives the distribution of the noble metals in the three bottom samples C-1, C-2, and C-4. The distribution is given for the two analytical methods as well as that calculated from XRF glass product analyses discussed above. These analyses were in remarkable agreement, considering the possibility for analytical error. The level of agreement between the data for XRF bottom sample analyses and the distribution calculated from the XRF glass product data would tend to reinforce the believability of the mass balance analysis. The form that of the noble metals on the bottom of the melter posed some interesting questions. Three distinct phases were 1) a largely continuous phase of what appeared to be RuO_2, 2) a largely continuous phase of Pd/Ag/Te with small amounts of ruthenium and rhodium in it, and 3) particles of ruthenium and rhodium embedded in the previous phase.

Table 3.24. Noble Metal Distribution in Bottom Samples (Elliott et al. 1994)

Element (% of total noble metal)	ICP-MS (%)	XRF (%)	Calculated from Glass Product Data (%)
Palladium	14	24	23
Rhodium	18	16	15
Ruthenium	68	60	63

All test segments except the last one showed signs of RuO_2, but always as an agglomeration. Yet the RuO_2 found on the bottom of the melter appeared to be in relatively large pieces of continuous RuO_2. Of the two metal phases, it would appear that the Pd/Ag/Te phase was molten prior to the melter being cooled (based on its continuous appearance). The presence of the silver in this alloy may have reduced the melt temperature to the point that this phase was molten at the temperatures near the end of the testing. The rhodium/ruthenium phase might have embedded itself in this molten layer as it settled from the melt above. The melting temperature of this phase would not be low enough for it to be molten. It was also possible that the metals present separated themselves into two phases after they precipitated onto the bottom of the melter and sat there for many days. Because only the last test segment was reduced to the point where all of the noble metals in the glass were found as metals, it is possible that prior to the start of this segment, all the ruthenium on the bottom was present as RuO_2 crystal agglomerates. When the last segment occurred, however, the reducing nature of the glass may have reduced this RuO_2 to ruthenium metal. Then in the several days following the test, when the melter was left to idle, the glass melt would have been reoxidizing and may have been oxidizing the ruthenium metal on the bottom to RuO_2 again. This would explain the appearance of the RuO_2 as a largely continuous phase instead of needle-like crystals.

The resistance measured between the electrodes and the noble metal accumulation in the melter are shown in Figure 3.4 are shown over the entire run. In addition, the points during the run at which the glass samples and feed samples were taken for the analyses presented in this report are shown. This data shows the clear correlation between a decreasing resistance in the melter and the change to 2X noble metals. It also shows that there was no detectable decrease in the melt resistance over the 1X noble metal testing section (Segments 1 through 8). The amount of noble metals retained in the melter by the end of the 1X segments was only about 10 percent of the total noble metals accumulated in the melter by the end of the testing.

The post-test examination of the melter revealed that one of the electrodes had lost nearly one-third of its length. Metal down-drilling and severe corrosion of refractories were also observed. The corrosion data were documented and mechanisms of corrosion were proposed (Cooper et al. 1993).

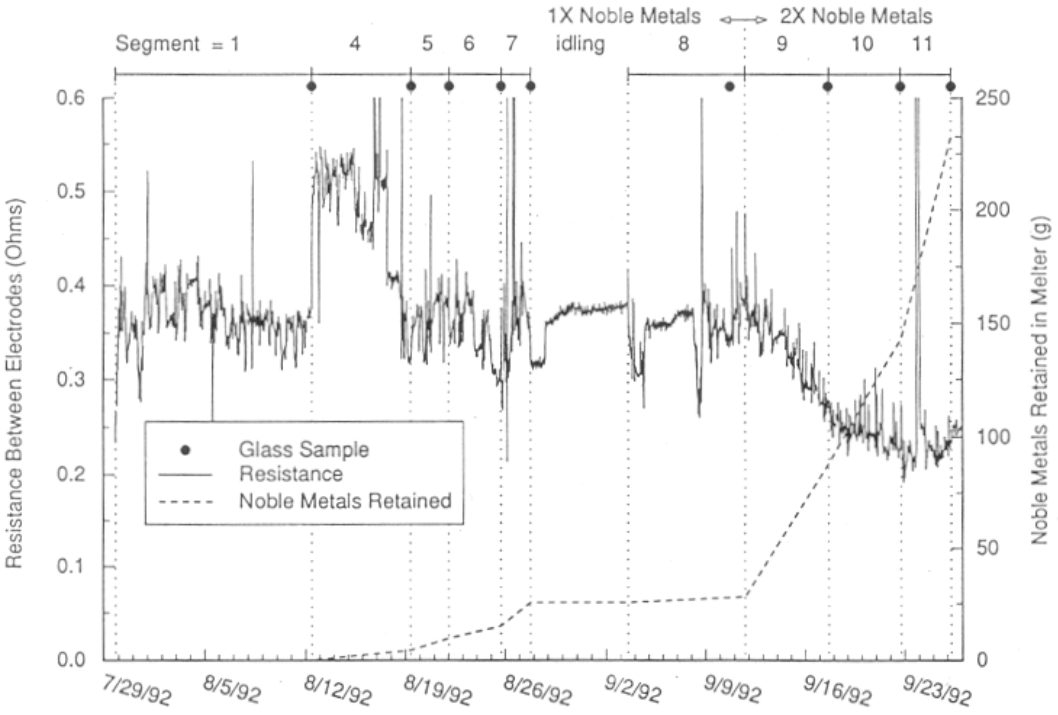

Figure 3.4. Resistance Between Electrodes and Noble Metal Accumulation over Entire Melter Campaign (Elliott et al. 1994)

3.3.3. Engineering Scale Melter Testing

Engineering-scale melter (ESM) testing was conducted in FY 1992 to evaluate noble metals behavior during prolonged melter operation at the projected proposed Hanford plant operating conditions. The overall objective of the ESM test was to operate a 1/10th-scale HWVP melter under anticipated HWVP process conditions over sufficient run time to determine if the noble metals accumulate in the melter as a function of time and feeding conditions. The ESM is a 1/10-scale melter constructed and operated at Kernforschungszentrum Karlsruhe (KfK) in Germany. The ESM operated for 9 days without noble metals for shakedown testing and 49 days with noble metals. The final mass balance concluded that 35 wt percent of the ruthenium, palladium, and rhodium fed to the melter settled to the melter floor. Samples taken from the bottom of the melter at the end of the run had high concentrations of noble metals, 20 to 45 times those of the nominal glass. Near the end of the run, the electrical resistance between the lower set of electrodes decreased by 10 - 15 percent, further indicating a settled layer of noble metals.

The NCAW waste simulant was prepared in the United States and shipped to Germany in drums. Two separate batches of feed, 3 m^3 of feed without noble metals and 14 m^3 of feed with noble metals were prepared. The feed batch without noble metals was to be used for shakedown testing. Once at KfK, the feed without noble metals was transferred into the feed makeup tank and the feed with noble metals was stored in an agitated storage tank. Both batches were low in aluminum, calcium, molybdenum, and

zirconium such that they had to be shimmed before each batch was formulated at KfK. Five individual batches were prepared at KfK, one without noble metals and four with noble metals. Feed preparation included shimming, addition of sodium nitrate and nitrite because this was a variable between batches, formulating, digestion, addition of recycle chemical, and addition of frit. These compositions were the reference NCAW simulant compositions at the time of the run. The concentrations of noble metals were 0.115 wt percent RuO_2, 0.030 wt percent Rh_2O_3, and 0.035 wt percent PdO.

Several aspects of vitrification were investigated in the ESM work including feed preparation, slurry transport, feed rheology, and noble metals behavior. The ESM run consisted of two segments. The first segment was for shakedown testing of the melter and supporting equipment. This segment lasted for 9 days and consumed one feed batch that did not contain noble metals. The second segment of the ESM run lasted 49 days. It consumed 4 batches of feed that did contain noble metals. A summary of the two run segments is presented in Table 3.25.

Glass samples were taken during each pour from the ESM. Each of these samples was analyzed for noble metals concentrations using XRF. During most of the run, there did not appear to be any accumulation of noble metals within the melter because the concentration of noble metals in the exiting glass was the same as in the feed. When the melter was drained a significant layer of noble metals was detected on the floor of the melter. Based on this information, the XRF data was revisited. All of the glass samples (a total of 50) from two different canisters (#6 and #15) were sent for further analysis. These analyses indicated that the XRF measurements were systematically high and were therefore corrected by subtracting an offset from the XRF values. The offsets were 0.041 wt percent for RuO_2, 0.009 wt percent for Rh_2O_3, and 0.026 wt percent for PdO. The data from the two canisters was used to correct the data from the other canisters. To calculate the retention of noble metals in the melter, the mass of each noble metal in each canister was first calculated using the equations:

$$M_{RuO_2} = \int_0^{M_{glass}} C_{RuO_2} dM_{glass}$$

$$M_{Rr_2O_3} = \int_0^{M_{glass}} C_{Rh_2O_3} dM_{glass} \qquad 3.2$$

$$M_{PdO} = \int_0^{M_{glass}} C_{PdO} dM_{glass}$$

where M_{glass} = mass of glass, Mi = mass of species i in the exiting glass and C_i = concentration of species i in the exiting glass.

A summary of the mass balance for each canister is shown in Table 3.26. By monitoring the mass of noble metals discharged from the ESM and comparing the value to the theoretical discharge curve it was determined that approximately 2.13 kg of Ru, 0.54 kg of Rh and 0.80 kg of Pd were retained in the melter. This equated to retention of 35 percent of the Run, 32 percent of the Rh, and 38 percent of the Pd. These values did not include the noble metals that were retained in the bulk glass and did not settle to the bottom of the melter. The nominal holdup of noble metals in the glass pool (550 kg glass average) was 0.480 kg Ru, 0.132 kg of Rh, and 0.162 kg of Pd. At the conclusion of testing the melter contents were drained via the bottom drain. During draining, 450 kg of glass were drained into two canisters. The draining glass was sampled periodically.

Table 3.25. Summary of ESM Run

	Segment Without Noble Metals	Segment With Noble Metals
Date started	July 2, 1992	July 11, 1992
Date completed	July 11, 1992	August 30, 1992
Total time, hr	210	1185
On-line time, hr	186	1118
On-line efficiency, percent	88	94
Feed consumed, m^3	2.6	14.2
Glass produced, kg	1083	6423
Avg. feed rate, L/hr		
Total time	12.4	12
On-line time	14.1	12.7
Avg. glass rate, kg/hr		
Total time	6.2	6
On-line time	7	6.3
Avg. residence time, hr		
Total time	89	92
On-line time	79	87
Noble metals amount, kg		
Ru	--	6.16
Pd	--	2.10
Rh	--	1.68
Glass canisters		
During operation	3	17
During melter discharge	--	2
Pouring operations	14	86
Total glass samples		
Pouring via overflow	73	434
Pouring via bottom drain	--	28
Melter surface	--	2
Melter bottom	--	7
Total power, kW	37	35
Upper electrodes		
Volts	44.4	42.2
Amps	308	316
kW	13.7	13.3
Lower electrodes		
Volts	42.4	37.3
Amps	265	231
kW	11.2	8.6
Plenum heaters		
Volts	133	138
Amps	94	96
kW	12.8	13.0
Avg. Temperatures, ºC		
Glass	1148	1184
Plenum heaters	849	868
Plenum	709	730
Off-gas	169	167

Table 3.26. Mass Balance of Noble Metals by Canister

Date	Run Time (hr)	Total Feed (L)	Theoretical Glass Product (kg)	Canister Number	Canister Weight (kg)	Total Glass (kg)	Total[(a)] Ru Fed (kg)	Ru Drained (kg)	Total Ru Drained (kg)	Total[(a)] Rh Fed (kg)	Rh Drained (kg)	Total Rh Drained (kg)	Total[(a)] Pd Fed (kg)	Pd Drained (kg)	Total Pd Drained (kg)
7/11/92	0	0	0		0	0	0.00	0.000	0.00	0.00	0.000	0.00	0.00	0.000	0.00
7/13/92	41	602	300	U2-1	363	363	0.27	0.034	0.03	0.07	0.004	0.00	0.09	0.001	0.00
7/16/92	106	1367	682	U2-2	389	752	0.60	0.149	0.18	0.16	0.033	0.04	0.21	0.033	0.03
7/19/92	184	2095	1045	U2-3	384	1136	0.92	0.196	0.38	0.25	0.048	0.09	0.31	0.057	0.09
7/22/92	267	3077	1535	U2-4	380	1517	1.35	0.206	0.59	0.37	0.060	0.15	0.46	0.080	0.17
7/25/92	343	3879	1935	U2-5	378	1895	1.71	0.221	0.81	0.47	0.064	0.21	0.58	0.090	0.26
7/28/92	416	4626	2308	U2-6	382	2277	2.04	0.234	1.04	0.56	0.073	0.28	0.69	0.106	0.37
8/1/92	509	5517	2752	U2-7	360	2637	2.43	0.221	1.26	0.66	0.067	0.35	0.83	0.094	0.46
8/4/92	573	6312	3149	U2-8	390	3027	2.78	0.243	1.50	0.76	0.073	0.42	0.95	0.102	0.56
8/7/92	639	7148	3566	U2-9	384	3410	3.15	0.231	1.74	0.86	0.068	0.49	1.07	0.097	0.66
8/10/92	710	8137	4060	U2-10	397	3807	3.58	0.251	1.99	0.98	0.081	0.57	1.22	0.108	0.77
8/13/92	782	9050	4515	U2-11	397	4205	3.98	0.258	2.24	1.09	0.072	0.64	1.36	0.073	0.84
8/16/92	852	9933	4956	U2-12	396	4601	4.37	0.261	2.51	1.19	0.072	0.72	1.49	0.054	0.90
8/18/92	918	10786	5381	U2-13	394	4995	4.75	0.248	2.75	1.29	0.068	0.78	1.62	0.054	0.95
8/21/92	977	11619	5797	U2-14	364	5359	5.11	0.230	2.98	1.39	0.066	0.85	1.74	0.067	1.02
8/23/92	1039	12380	6176	U2-15	374	5733	5.45	0.241	3.22	1.49	0.062	0.91	1.86	0.063	1.08
8/27/92	1117	13411	6691	U2-16	398	6131	5.90	0.263	3.49	1.61	0.070	0.98	2.01	0.064	1.14
8/29/92	1175	14096	7032	U2-17	292	6423	6.20	0.189	3.68	1.69	0.055	1.04	2.11	0.052	1.20
8/30/92	1193	14225	7097	U2-18	350	6773	6.26	0.255	3.93	1.71	0.076	1.11	2.13	0.078	1.27
8/30/92	1196	14225	7097	U2-19	204	6977	6.26	0.096	4.03	1.71	0.026	1.14	2.13	0.024	1.30
Total					6977			4.03			1.14			1.30	

(a) These values differ slightly from the actual ordered and premixed amounts of noble metals because 14.23 m^3 of melter feed was vitrified instead of 14 m^3. The total ordered noble metals amounts were 6.16 kg Ru, 1.6 kg Rh, and 2.10 kg Pd.

In order to close the mass balance, the amount of the glass remaining in the melter was estimated by measuring the thickness of the remaining glass layer on the melter floor after emptying. This layer was about 20-30 mm thick, which leads to a total volume of about 8-10 l of glass. Assuming an average glass density of 2.6 g/cm^3 the residual amount of glass was about 20-26 kg. With the average concentrations of noble metals in the bottom samples, the estimated amount of noble metals in the bottom layer was 0.6-0.8 kg Ru, 0.1 kg Rh, and 0.1 kg Pd. This was far below the values of 2.1 kg Ru, 0.5 kg Rh, and 0.8 kg Pd estimated using the data in Table 3.26. The scrubber solutions were analyzed for volatilized noble metals and found to contain only 40 grams of Ru, 1 gram of Rh, and 1 gram of Pd. The reason for the discrepancy in the mass balance was unclear. This could be attributed to the uncertainty in the thickness and sampling of the sludge layer after the run. Because of these uncertainties, the mass balance presented in Table 3.26 was used for calculating the retention of noble metals.

During most of the ESM run it did not appear that the accumulating noble metals were having an effect on the melter operation. The effect of noble metals on melter operation is monitored by observing the change in electrical resistance between the lower set of electrodes. If a conductive layer is forming, the resistance between the lower set of electrodes will decrease because of short-circuiting from the electrodes to the layer. If this effect becomes substantial, most of the power will be dissipated on the floor of the melter and the glass above it will cool. There was a slight distortion of the electrical field in the ESM at the end of the run. This was difficult to detect because the temperature changed slightly during the run and the power skewing between the sets of the electrodes was changed approximately 550 hours into the run. At the end of the run the settings on the electrodes was changed back to the original settings from the beginning of the run. Even though the bulk glass temperature had decreased slightly since the beginning of the run, the resistance between the lower set of electrodes was lower. The decrease in electrical resistance between the lower set of electrodes was estimated to be 13 percent. Based on the PAMELA experience, a sludge layer of 2-3 cm spread over the melter floor can be enough to influence the electric field. Having processed more than 90 kg of noble metals in the PAMELA melter, the resistance decrease between the lower electrodes was more than 65 percent. The reason that more of an electrical disturbance was not observed in the ESM might be that an even, connected layer of sludge had not formed yet. Two of the sludge samples taken from the bottom of the ESM after draining were analyzed for specific electrical resistance. The electrical resistance of the samples was more than one order of magnitude less than the nominal glass product.

Several glass product samples were thin-sectioned and analyzed using both optical and scanning electron microscopes. The noble metals particles appeared very similar to those observed in the RSM. Large clusters of ruthenium dioxide up to 100 μm were scattered throughout the glass samples. These clusters were made up of needles attached randomly end-to-end such that they resembled hairballs. In some samples the clusters formed streaks within the glass. The cause of this streaking is not clear but could be an important mechanism in noble metals behavior. Spheres of rhodium and palladium alloys were also observed. The noble metals content of the samples ranged from 0.02 volume percent to 0.05 volume percent.

3.3.4. Computer Modeling

Numerical computer modeling was also an integral part of the melter performance assessment, incorporating data from actual tests to develop the TEMPEST computer model (Trent and Eyler 1993). Once confirmed against scaled test data, computer modeling then provided numerically mocked-up results at full scale. This section presents the results of the computer modeling performed at PNNL (Cooper et al. 1993).

The RSM modeling results were preparatory to simulating the ESM (Grünewald et al. 1993). Appendix B describes the TEMPEST model. Pre-RSM test calculations were conducted during the experiment design phase and are reported by Anderson et al. (1992). Additional as-built, pre-test calculations were conducted following preliminary testing. Preliminary post-test calculations were conducted subsequent to the research-scale melter experiment, but before reducing the experiment data, and final post-test calculations were completed following the data reduction step. Conclusions reached during the computer modeling phase follow:

- Predicted operational parameters (power, voltage, current, and resistance) predicted by the computer model agree to within 4 percent to 50 percent of research-scale melter measurements. Measurements exhibited as much as ±18 percent variations.

- Power control to either a bulk-average or a single-point control temperature was demonstrated. The predicted bulk average temperature varied by as much as 70ºC from the predicted single-point temperature control value. Maximum temperature predictions varied by as much as 120ºC from a control temperature.

- Submodels for concentration-dependent electrical conductivity, viscosity, density, and hindered settling have been implemented, tested, and shown to work. Fully coupled calculations had shown expected physical effects of these submodel couplings.

- Gradient furnace testing and research-scale melter particle characterizations from glass sample microscopy are very useful to the computer modeling. Microscopy results had been used to determine effects of particle porosity and sphericity on terminal settling velocities.

- Predicted glass convection patterns are in remarkably good agreement with streak patterns observed in post-test melter examination. This was the first experimental confirmation of a computer prediction of glass convection patterns in an operating melter.

- Using an accelerated analysis methodology, development of a sludge layer containing a very high concentration of noble metals was successfully computed.

- Predictions indicate that an enhanced noble metals sludge layer develops more readily in an idling melter than a feeding melter with or without pouring. This was because without the cold cap, temperatures differences inducing buoyancy-driven flow are less.

- In a combined fully coupled/uncoupled analysis, a retention of 7 percent of simulated RuO_2 noble metals particles was computed in a 3-day simulation. This computation agreed both qualitatively and quantitatively with test data (5 percent retention of noble metals).

Preliminary post-test calculations were conducted in January and February 1993 using estimated glass properties (RSM/Pre data). The research-scale melter experiment was completed in December 1992 and reduced data from the experiment was made available for comparison to the calculations as the calculations were being completed. The final set of calculations was completed at the end of April 1993 when the glass sample data for electrical conductivity (RSM/Alt data) and viscosity became available. A summary of research-scale melter simulations follows:

- Bulk-average-temperature controlled simulations were computed to steady conditions using the RSM/Alt electrical conductivity data. These were done assuming symmetric electrodes, a bulk

average glass temperature of 1150 C, a cold cap boundary condition to the melt, and no glass pouring.

- Several bulk-average-temperature controlled simulations were performed in which the asymmetric electrode condition observed after destructive examination of the research-scale melter was modeled. These simulations were conducted to identify operational features of the asymmetric electrode configuration and the effect of a pure metal layer on the melter floor.

- Cases were computed to a steady condition using temperature control based upon a single temperature approximating the location of the thermocouple measurement that controlled the experiment. These simulations were to investigate the point-temperature controller and to compare differences between control temperature, bulk melt temperature, maximum temperature, and other operational differences occurring from bulk-average versus point-temperature control.

- Cases were simulated that approximated a fully coupled melt pool in which noble metals were being transported. The purpose of these cases was to investigate the transitory nature of fully coupled settling of noble metals particles into an enhanced conductivity sludge layer.

- Cases were simulated that approximated both feeding and pouring simultaneously in a fully coupled melter model.

- Long-time (days to weeks) analysis methodology for analyzing uncoupled noble metals transport was developed and simulations were conducted to approximate actual particle transport conditions in the research-scale melter.

A computer model of the engineering-scale melter was developed and tested. The plan for computer modeling included using this model for pre-test predictions. The pre-test predictions were designed to develop computational approaches and to test submodels. ("Submodels" couple concentration-dependent glass properties and noble metals particle characteristics to the computation of melter operation parameters and other subsequent predictions of the development of an enhanced conductivity, noble metals-enriched sludge layer.) In pre-test computations, target values of the experiment test plan were used to define input.

Following the engineering-scale melter experiment, post-test computer modeling was done using data from the experiment in two ways. Measured property data and glass sample analysis to determine particle characteristics were used as input to post-test analysis and as a basis for improving computer submodels. Predictions with the improved submodels were then compared to measured experimental data from operations. Additional details, especially of the experimental results, are given in Grünewald et al. (1993). Conclusions drawn from the engineering-scale melter predictions include the following:

- Material balances, including retention, for RuO_2, Pd, and Rh were in excellent agreement with corresponding experimental data. This agreement was key to the objective of this work.

- Concentration distributions throughout the melter were typically less than ±2 percent of the average concentration in the melt at any given time (excluding the sludge layer). The melt pool was concluded to be well mixed.

- Sludge layer thickness between 1 and 1.5 cm developed based on an assumed maximum packing of 6 vol percent.

- Power and current were typically overpredicted by 10 percent to 15 percent. Voltage was underpredicted because of discrepancies in electrical conductivity.

- Comparison of predicted rms-resistance across the electrode pairs with rms-resistance computed in the engineering-scale melter test from measured voltage and current were inconclusive.

Predicted resistance across the electrode pairs without the influence of noble metals (at the beginning of test) was greater than that determined in the engineering-scale melter test. As a sludge layer accumulated, predicted resistance across the upper electrode pair remained nearly constant. It was relatively unaffected by the sludge layer. Experimental resistance across the upper electrode pair was also relatively constant. Predicted resistance across the lower electrode pair, however, showed a marked decrease (both the rms-resistance and the true resistance) as the sludge layer accumulates. Experimental data indicated the resistance across the lower pair to be relatively constant, even though a 1- to 3-cm sludge layer has accumulated on the melter floor. Thus, it could be concluded that either 1) the maximum packing factor of 6 vol percent used in the electrical conductivity data correlation is too large, 2) the sludge layer thickness during operation was greater than the 1- to 3-cm layer observed, or 3) the sludge layer was not continuous across the floor. The source of the discrepancy in the comparison of the resistance across the lower pair remains to be resolved.

In post-test analyses, TEMPEST was used to compute noble metals material balance and retention. Analyses were done using continuum species transport to represent each of the three primary components, RuO_2, Pd, and Rh, as settling particulate fields, and assuming that the total amount of noble metals could be lumped into a single representative particle field. The first is referred to as the three species model and the latter is referred to as the total noble metals model.

The time-dependent variation of the predicted RuO_2 balance is presented in Figure 3.5. In the figure, the mass in kg-RuO_2 is plotted as a function of time. Curves were included for the total amount of material fed to the melter, the total amount of material in the melter at a given time, the total amount of material predicted to be on the floor, and the total amount of material contained within the glass in the melter. The total amount of material in the melter was the sum of the material on the floor and the material in the glass. The total amount of material fed to the melter was a linear function which is just mass-source-rate times time, in the absence of operational interruptions. The total amount of material in the glass increased and reached an equilibrium value. For the results presented in Figure 3.5, the amount of material in the glass reached an asymptotic value of 0.426 kg during the feed portion of the cycle and drops to 0.397 kg after a pour cycle. Considering that there was 0.2372 m^3 of glass in the computer model, at an average density of 2170 kg-glass/m^3 as used in the computer modeling, equilibrium mass fraction of RuO_2 varied between 0.083 and 0.077 wt percent. This was comparable to the experimental value of about 0.08 to 0.09 wt percent observed (Grünewald et al. 1993). The amount of material on the floor after an initial period of adjustment as operations begin showed a linear rate of increase, consistent with the deposition rate model in these calculations. The jagged points in the curves for total in the melter and in the glass were not a function of a numerical instability. Rather, the upswing of each jag represented the 9 hours of feeding and the down swing of each represents 1 hour of pouring.

Figure 3.6 presents the same RuO_2 material balance, but plotted as a function of kg of glass discharged (poured) from the melter (Grünewald et al. 1993). Note that the mass of Ru was plotted, not RuO_2, to be consistent with experimental data. The conversion from kg-RuO_2 to kg-Ru was (101.07 kg-Ru/133.07kg-RuO_2). In the figure, the solid symbols were the experimental data. The lines were TEMPEST predictions. The predictions were made only to a time at which 3800 kg of glass was poured. Up to this time, agreement between data and predictions was very good. Close examination of the experimental feed rate indicates that the feed rate was not constant, as was assumed in the calculations.

The predictions indicated that the amount of Ru discharged from the melter was slightly over-predicted, correspondingly resulting in the retention being under-predicted.

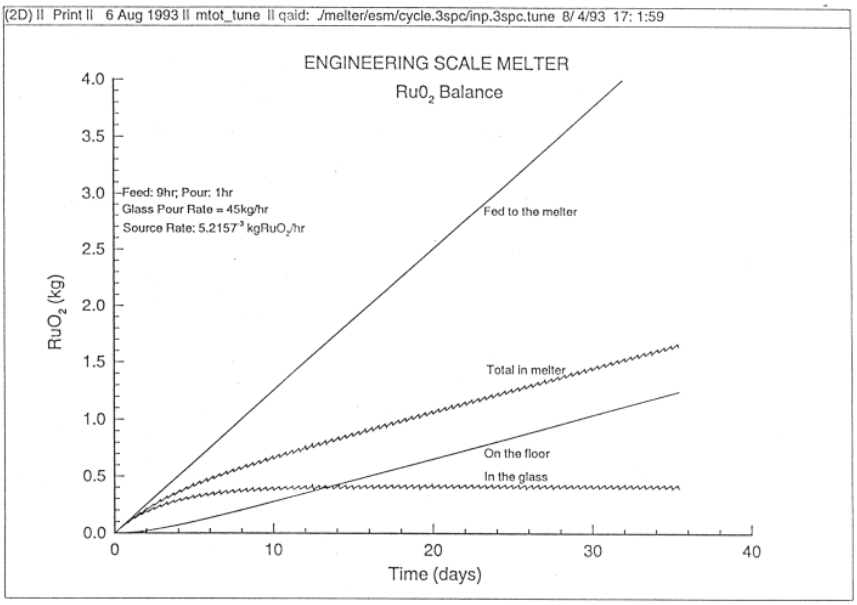

Figure 3.5. Predicted RuO_2 Material Balance at Experimental Conditions in the ESM (Elliott et al. 1994)

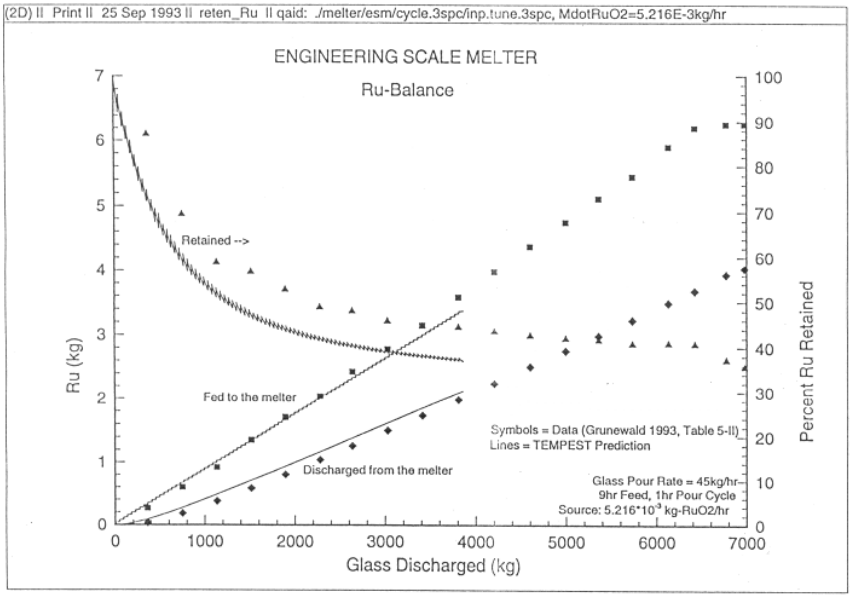

Figure 3.6. Ru Balance Compared to Experimental Results for the ESM (Elliott et al. 1994)

Figure 3.7 presents the same predicted Ru material balance. In Figure 3.8, the asymptotic mass fraction of Pd in the poured glass varied between 0.10 and 0.11 kg-Pd over the feed/pour cycle,

corresponding to mass fractions of 0.019 and 0.021 wt percent, respectively for glass density of 2170 kg/m^3. Experimental values of Pd wt percent were mostly in the range of 0.02 to 0.03 wt percent. In Figure 3.9, the asymptotic retention was approaching 34 percent compared to the experimentally determined value of 38 percent determined by integration. Thus, the agreement between Pd data and predictions was very good.

Corresponding results for Rh in Figure 3.10 show an equilibrium mass of Rh in the discharged glass between 0.086 and 0.093 kg-Rh over the feed/pour cycle. These corresponded to mass fractions of 0.017 and 0.018 wt percent in the discharged glass. Experimental values were near 0.025 wt percent over much of the experiment (Grünewald et al. 1993). In Figure 3.11, the asymptotic predicted retention was approaching 34 percent, a number that was in very good agreement with the experimental value of 32 percent. Thus, the predictions of Rh mass were also in good agreement with data.

These results indicate that the modeling assumptions used in this analysis, and the analysis approach, are quite good and that good agreement with data is obtained for predicting retention of noble metals in the engineering-scale melter.

The time-dependent results for the accumulation of mass on the melter floor can be used to estimate the thickness of a noble metals-enriched sludge layer. Figure 3.12 presents the results for time-dependent RuO_2 mass, showing curves for mass of RuO_2 in the glass and mass on the floor. The amount of mass on the floor could be converted to an equivalent layer thickness by dividing the mass on the floor by the density of RuO_2, area of the floor, and maximum packing factor, or

$$\Delta h = M_{floor} / \left(\rho_{RuO_2} \cdot A_{floor} \cdot C_{v,max} \right)$$

where h = sludge layer thickness
M_{floor} = mass of RuO_2 on the floor, kg-RuO_2
ρ_{RuO2} = density of RuO_2, 6970 kg-RuO_2/m^3
A_{floor} = floor area, 0.28 m^2
$C_{v,max}$ = maximum packing concentration, m^3-RuO_2/m^3.

Results for the assumed maximum packing concentration, $C_{v,max}$, of 0.06 and 0.08 are also presented in Figure 3.12. Extrapolation of these results to the end of the experiment, 1193/24 = 49.7 days-run-time, indicated a sludge layer between 1 and 1.5 cm. Experimental observations indicated that a sludge layer between 1- and 3-cm thick existed after the melter was drained (Grünewald et al. 1993). If a lesser maximum packing concentration were used, the computed thickness would be greater. Samples from the bottom of the melter indicated mass fractions approaching 5 wt percent, corresponding to a volume fraction of about 5·2170 kg-glass/6970 kg-RuO_2 = 1.6 vol percent. If the 5 wt percent really did represent a maximum packed concentration, then the estimated sludge layer would be nearly 5.6-cm thick. The 0.06 maximum-packed concentration was determined by examining micrographs of glass samples and measured sludge concentrations.

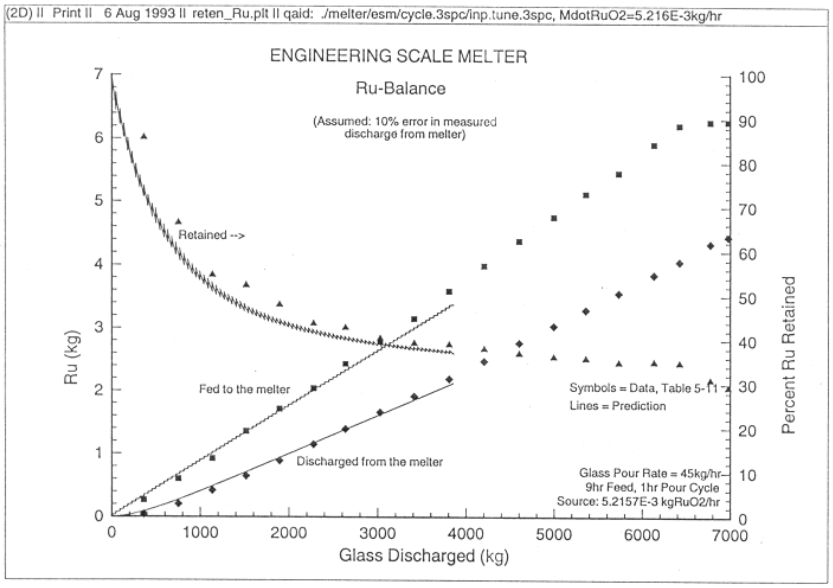

Figure 3.7. Ru Balance Compared to ESM Experimental Results (Elliott et al. 1994)

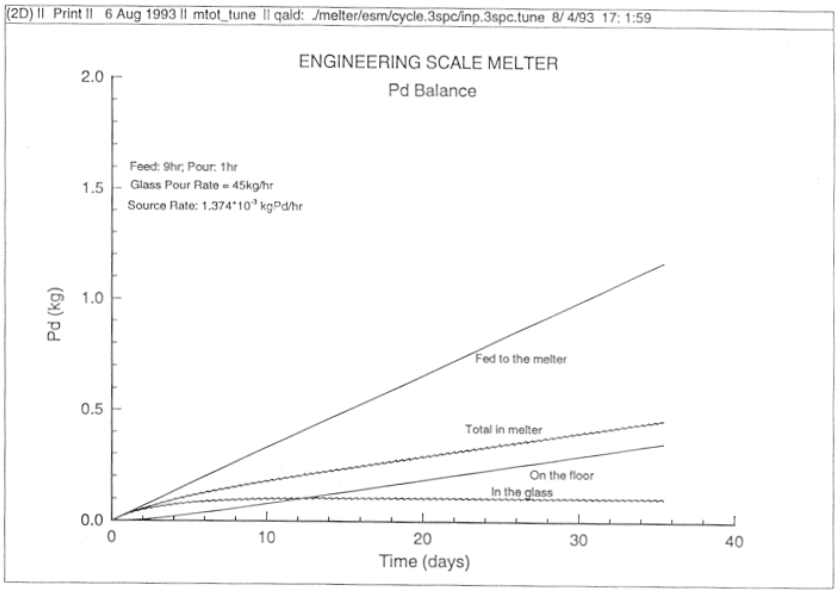

Figure 3.8. Predicted Pd Balance at ESM Experimental Conditions (Elliott et al. 1994)

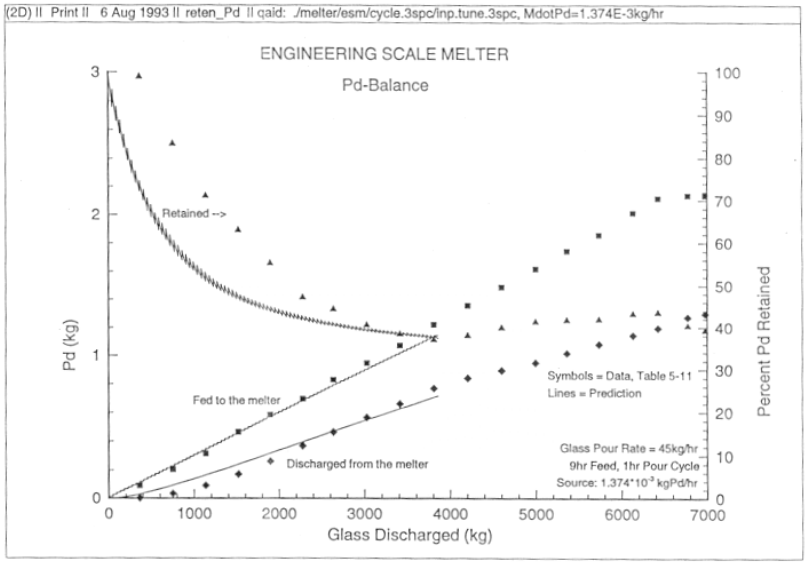

Figure 3.9. Pd Balance Compared to ESM Experimental Results (Elliott et al. 1994)

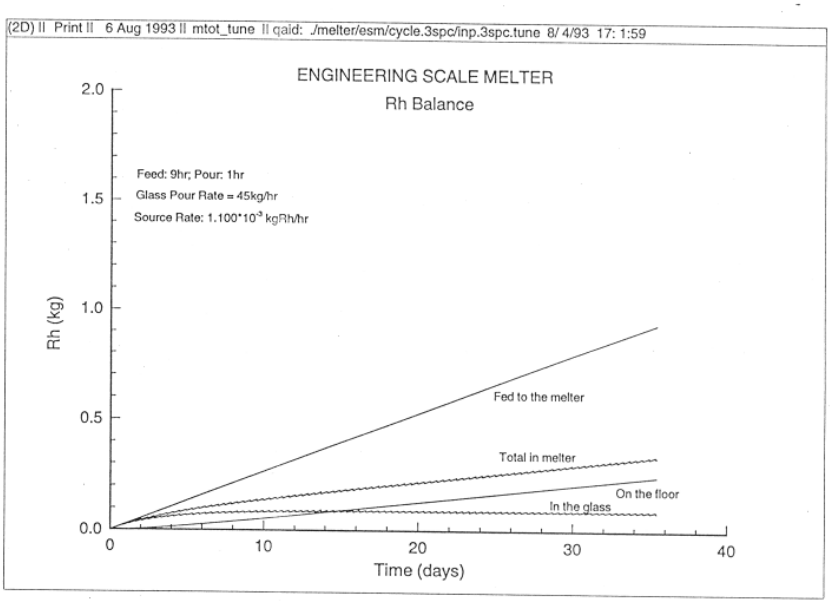

Figure 3.10. Predicted Rh Balance at ESM Experimental Conditions (Elliott et al. 1994)

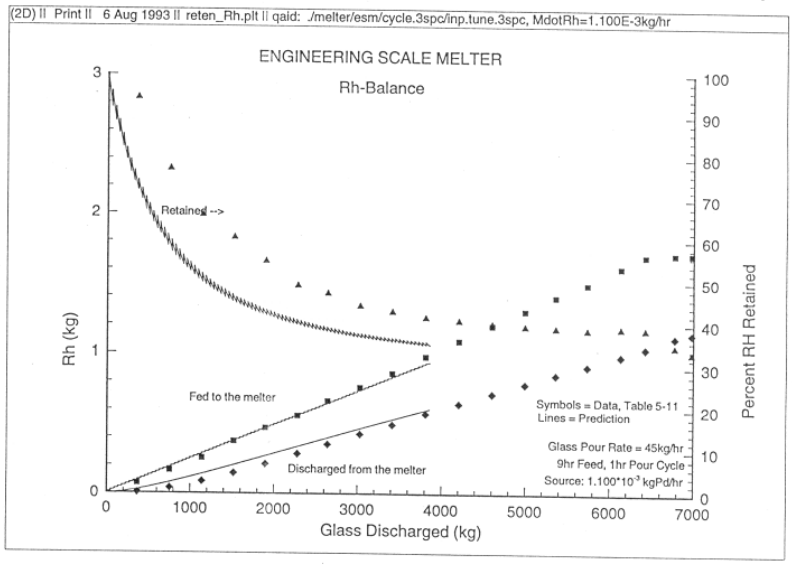

Figure 3.11. Rh Balance Compared to ESM Experimental Results (Elliott et al. 1994)

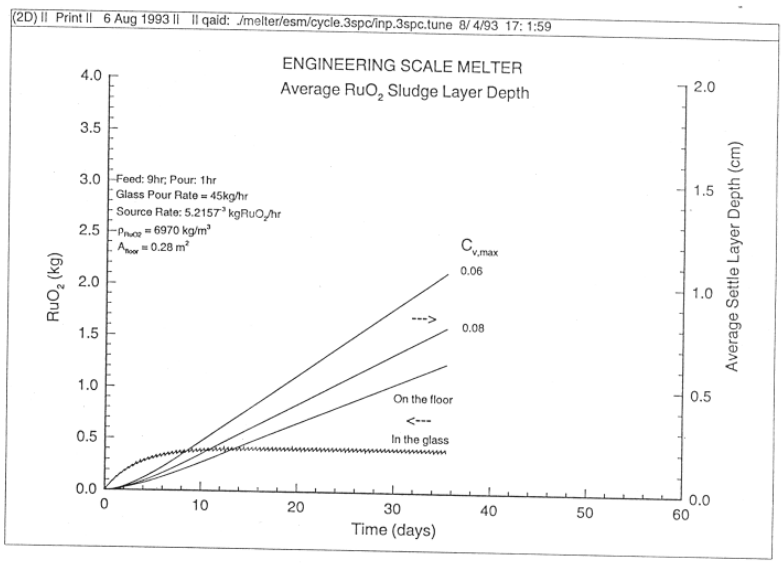

Figure 3.12. Predicted RuO_2 Sludge Layer Depth in the ESM (Elliott et al. 1994)

In addition to the individual species calculation for RuO_2, Pd, and Rh, another calculation was conducted assuming a single particle component with characteristics of RuO_2. This calculation was conducted as an upper bound calculation because RuO_2 particles appear like "hairballs" with a high degree of porosity. The equivalent effective volume of these particles occupied a much greater volume than do the smaller, metallic Pd and Rh particles. Thus, they would create a thicker sludge layer than would small, rounded metal particles. For this calculation, a noble metals (NM) source rate of 0.0178-kg NM/hr was used. This feed rate was approximately a factor of 3 greater than the actual RuO_2 feed rate in the experiment and approximately a factor of 2 greater than the total of RuO_2, Pd, and Rh fed to the melter. Nevertheless, the results were useful because they indicated that in the range of the concentrations of noble metals considered, the retention characteristics were largely independent of the source term magnitude. In an actual melter, this would be true up to the point where a sludge layer became sufficiently thick to affect the melt pool flow, thermal, and electric characteristics. These results also provided a second data set from which interpolations of sludge layer thickness could be made.

Results of the single noble metals component mass balance are presented in Figures 3.13 to 3.15. Figure 3.13 shows the mass balance as a function of time. Comparing this result with that of the RuO_2 results in Figure 3.5 shows a very similar characteristic to the overall material balance. Furthermore, the retention for this case (see Figure 3.14) is also approaching an asymptotic value less than 40 percent. Figure 3.15 shows the computed effective sludge layer depth for assumed maximum packing concentrations of 6 and 10 vol percent. These depths are approaching the 4- to 5-cm-thick range.

Figure 3.16 compares the TEMPEST-predicted results with a lumped-parameter method. The lumped-parameter method is a mathematical description of a well-mixed volume with associated in flow and out flow (see next section). The melt pool is the well-mixed volume and the mass balance is a simple ordinary differential equation solution in time. The TEMPEST results were very consistent with the lumped-parameter results and lay between the two cases of an assumed volume change during pouring and an assumed constant volume melt pool during pouring. This comparison showed that the constant volume melt approximation used in the TEMPEST model adequately models the conditions in the melt pool, even though it differed from the actual situation where the melt surface, and hence melt volume, changes during the pouring and feeding portions of a cycle. Another observation that could be made from the results of Figure 3.16 was that TEMPEST was predicting the melter to be a well-mixed volume. In fully coupled calculations conducted without allowing settling of material to a stationary floor layer, less than a 2 percent variation existed in the concentration distribution in the melt pool. This result supported the use of a lumped-parameter method to estimate retention in the melter and to conduct parametric analysis with the lumped-parameter approach. The more computationally intensive TEMPEST approach could then be used to investigate specific aspects of coupled melter operation resulting from a parametric analysis that defines a range of operational limits. Upon completion of the ESM computer modeling, the HWVP reference melter was also modeled. The results are elaborated in the report by Elliott et al. (1994).

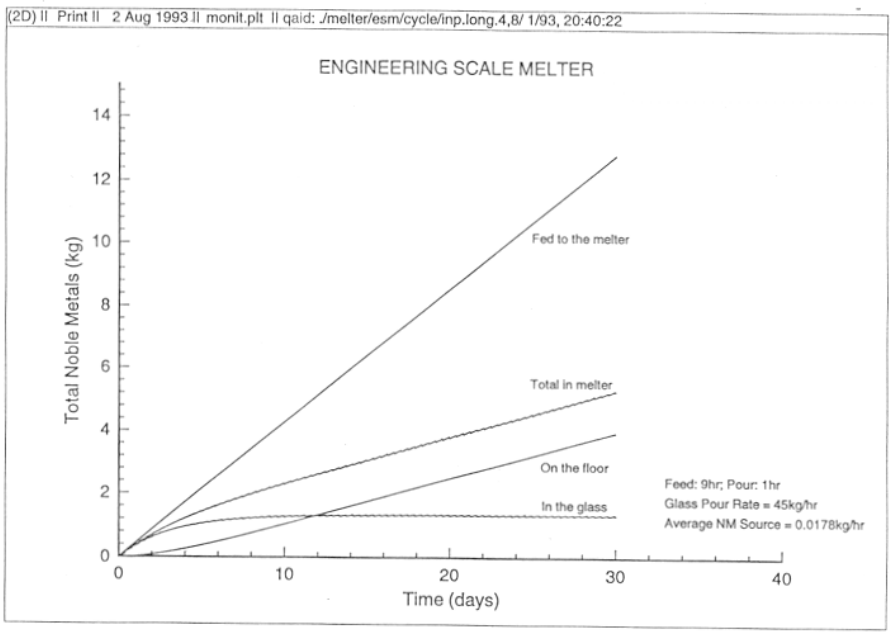

Figure 3.13. Predicted RuO_2 Balance for Assumed 3X Noble Metals Feed Rate in the ESM (Elliott et al. 1994)

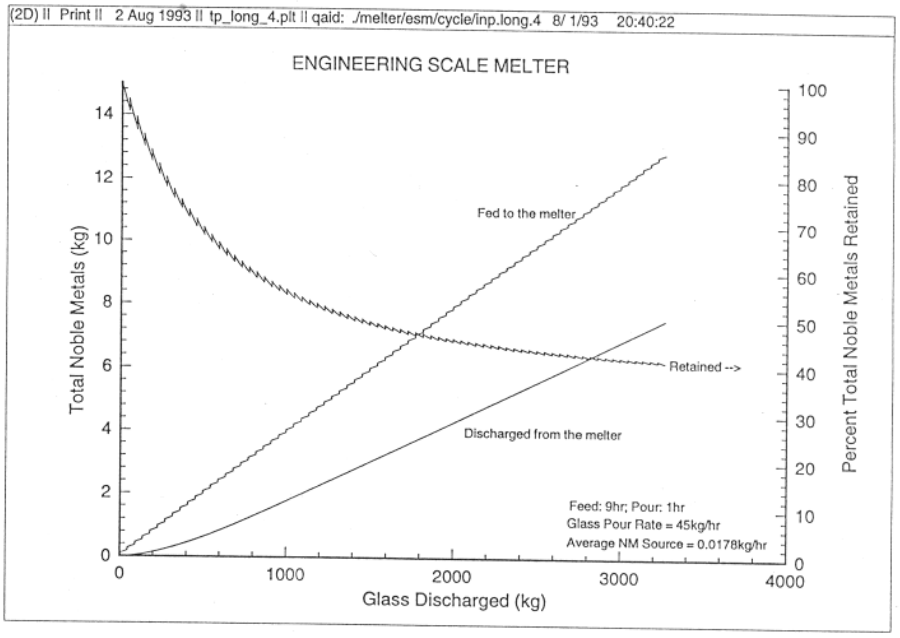

Figure 3.14. RuO_2 Retention for Assumed 3X Noble Metals Rate in the ESM (Elliott et al. 1994)

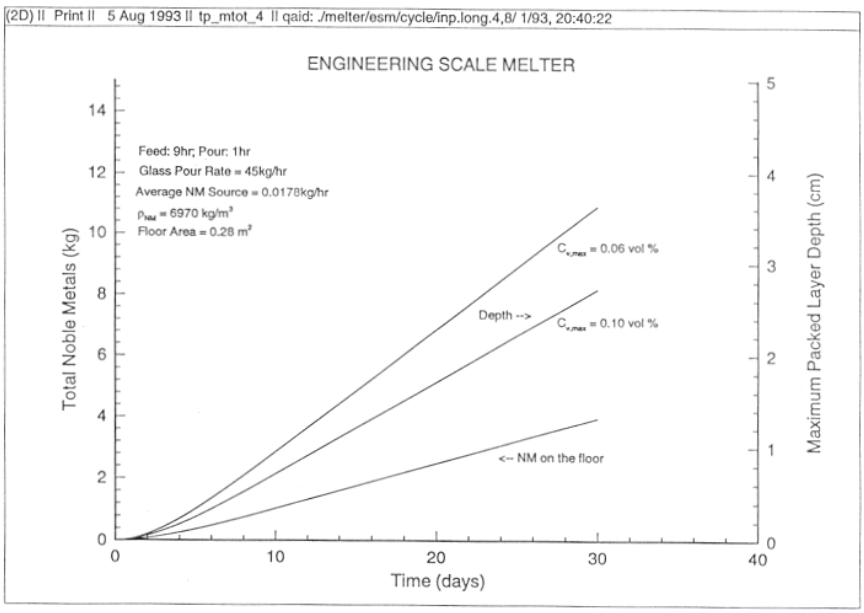

Figure 3.15. RuO_2 Sludge Layer Depth for Assumed 3X Noble Metals Feed Rate in the ESM (Elliott et al. 1994)

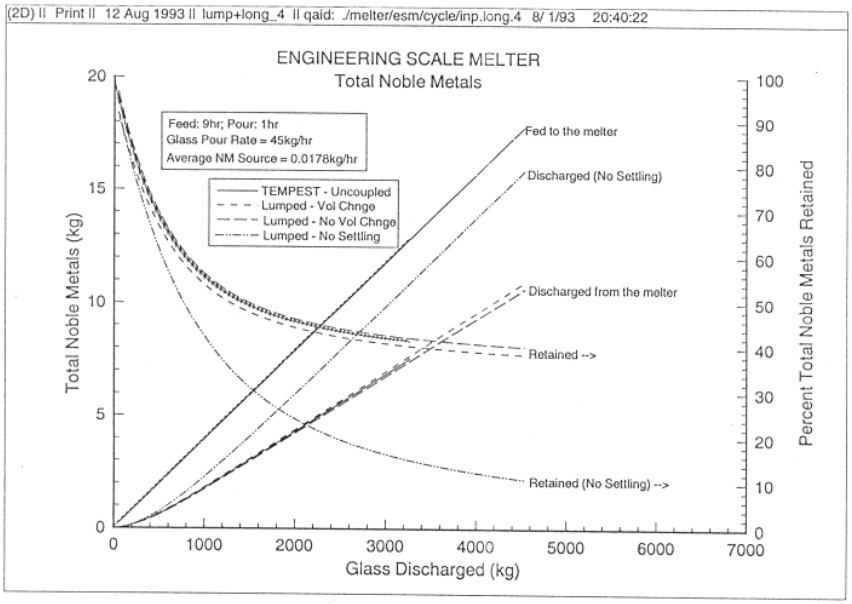

Figure 3.16. Total Nobel Metals Retention Compared to Lumped-Parameter Analysis for the ESM (Elliott et al. 1994)

Based on the above mass balance data, the noble metals settling rates and the sludge buildup rates were determined (Table 3.27). Predicted data (using ESM data input) was used in the determination. It was assumed that the settling rate was constant during the campaign.

Table 3.27. Noble Metals Settling and Sludge Layer Buildup

Element	Noble Metals on the Floor (lb/day)	Sludge Layer Buildup (cm/day)
RuO_2	0.076	0.013
RuO_2 (3X feed rate)	0.294	0.038
Pd	0.019	---
Rh	0.016	---

3.3.5. Engineering Analysis

PNNL used a combination of TEMPEST computer modeling and experimental studies to predict the effects of noble metals on the plant melter life. In parallel to the TEMPEST computer modeling, a separate analysis was conducted to determine the effects of noble metals using engineering approximations. That is, instead of numerically modeling the thermal and convective flows of the glass, the melter was approximated as a well-mixed tank with a given settling rate of noble metals. This provided a model that could predict the melter sludge layer accumulation as a function of time using a hand calculations routine. The advantages of using a simple engineering analysis are: 1) it is much less labor intensive than the TEMPEST modeling, 2) it allows more flexibility such that parametric studies can be conducted to evaluate the relative effect of key operating parameters, and 3) it provides a reality check for the TEMPEST modeling. The disadvantages are that an engineering analysis does not provide insight to the effects of momentum and heat transfer as done by TEMPEST and it cannot predict the results of a sludge layer accumulation such as electrical shorting and overheating. This section contains a description of the engineering analysis conducted as part of the melter performance assessment. The main focus of the engineering analysis was the use of the lumped-parameter model.

The lumped-parameter model was developed as a simplified melter model to be used in parallel to TEMPEST modeling. This simplified model was the main component of the engineering analysis. The LP model is very complementary to the TEMPEST model. The TEMPEST model gives very detailed insight into the physics, taking place in the melter, from flow patterns to temperature gradients. The price paid for such a detailed model is efficiency. It takes 40 to 120 hours of central processing unit (CPU) time on an IBM-580 super workstation to bring the melter model to steady state after a change in melter settings. This does not include preprocessing or post processing tasks. To relate the IBM processing time to other computers, the IBM workstation operates at about 48 percent of the CPU speed of a CrayYMP supercomputer. In real time, the IBM is faster because of on-line inefficiencies on the Cray. Thus, only a limited number of TEMPEST models can be run because of time and budget constraints. Performing parametric studies with the TEMPEST code is difficult. The lumped-parameter model allows for quick estimates of the effects of several variables on noble metals retention within the melter. These variables include noble metals concentration, noble metals settling velocity, feed rate, and different feed/pour/idle cycles. The lumped-parameter model is limited in that it can only predict the accumulation of noble metals; it cannot predict the electrical disturbances resulting from the noble metals accumulation. The model is described in Appendix C.

Two sets of lumped-parameter model runs were completed. One set for the ESM and one set for the plant melter. The runs for the engineering-scale melter were completed for two reasons, we had experimental data to compare with our results and we had TEMPEST data to compare with our results. The runs for the plant melter were completed as a part of a parametric study to determine the changes in noble metals retention as a function of changes in operating parameters. In this section, only ESM results are briefly presented. Detailed analysis of other results is available in the report by Elliott et al. (1994).

In order to investigate the differences in retentions reported for the ESM run and the lumped-parameter, the results were directly compared with respect to ruthenium fed and discharged from the melter. The ruthenium mass balance is plotted with the results of the lumped-parameter model in Figure 3.17. Two sets of lines (one for the ESM results and one for the lumped-parameter model results) are presented in this figure, ruthenium fed to the melter as a function of glass discharged and ruthenium discharged from the melter as a function of glass discharged. As shown in the figure, the lines for the discharge curve were within 0.15 kg Ru that was considered acceptable. The interesting anomaly indicated in the figure was the difference between the two curves for Ru fed to the melter. These two curves should agree nearly exactly because they represented the concentration of Ru in the feed on an oxide basis. But after 2500 kg of glass has been discharged from the melter, the curves began to diverge. At their maximum separation, the difference was 0.5 kg of Ru or nearly 10 percent of the total Ru fed to the melter. The engineering-scale melter data was reviewed further to determine the reason for the difference in these curves.

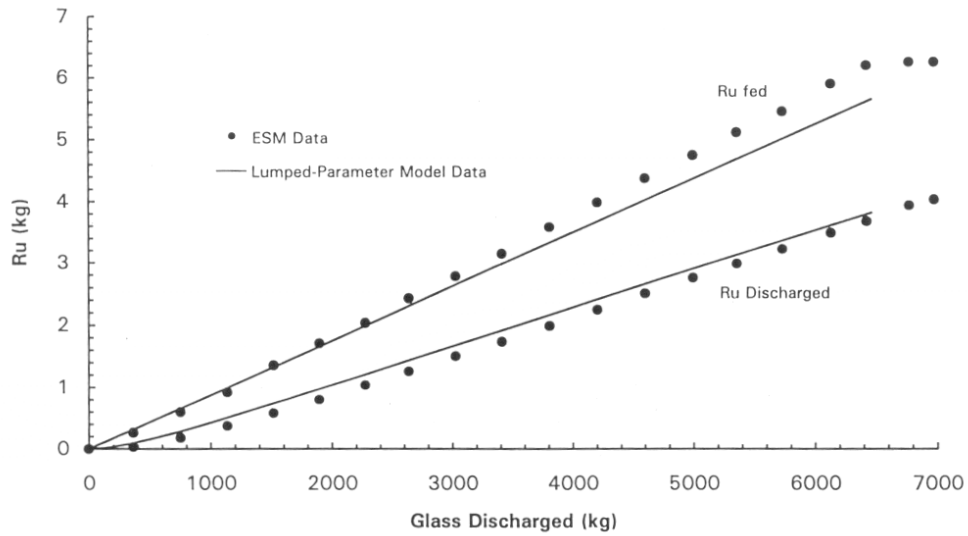

Figure 3.17. Comparison of Lumped-Parameter Model Results with ESM Data (RuO_2 settling velocity = 10^{-6} m/s)

A comparison of the TEMPEST results with the lumped-parameter model results is shown in Figure 3.18. Comparison of the lumped-parameter model results with those of TEMPEST confirmed that they were predicting the similar results given the same input. The lumped-parameter model predicted about 3 percent higher Ru retention after 4000 kg of glass had been discharged. But as the glass produced increased, the TEMPEST results and the lumped-parameter model results converged.

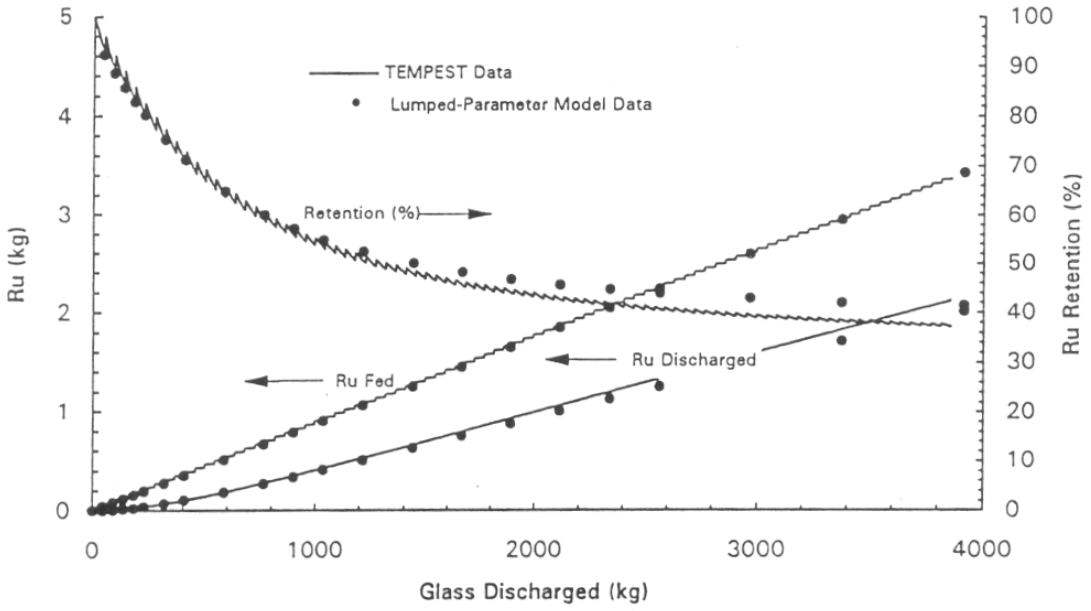

Figure 3.18. Comparison of Lumped-Parameter Model and TEMPEST Model Results (The arrows indicate which y-axis is referenced for each curve.)

The lumped-parameter model was found to be a useful tool based on comparing its results with the engineering-scale melter experimental results as well as the computer modeling results of the TEMPEST code. Once the lumped-parameter model was developed and tuned it was applied to modeling the HWVP plant melter. The results of HWVP plant melter are elaborated in the report by Elliott et al. (1994).

3.4. WVDP Studies

The slurry-fed ceramic melter (SFCM) was in test operation for vitrification of nuclear wastes starting from December 1984 to December 1989 at the WVDP. In this study, deposition of insolubles and crystallized species on the floor of the SFCM during vitrification process were analyzed. The results indicated that the thickness of the sludge layer on the floor of the SFCM was not more than 6 cm deep and consisted mostly of Fe-Cr spinels, and RuO_2 dispersed in a glassy borosilicate matrix. Also, crystalline Cr_2O_3 and undissolved phases consisting primarily of alumina and chromia were present in trace amounts but were inhomogeneously distributed in the glassy matrix on the SFCM floor. Greater than 87 percent of the RuO_2 fed to the melter was flushed out with normal glass pouring. As the SFCM was designed prior to the sloped bottom German and Japanese melters, it had a unique prismoidal shape with sloping walls and a bottom electrodes which was intended to minimize noble metals effects.

Five days of non-radioactive surrogate operations with noble metals were conducted before radioactive operations. No electrical disturbances were noted during the short period, but deposits were found on the melter bottom and at the dihedral angle between melter walls, analogous to the German W-4 campaign experience. A preliminary material balance showed that 95 percent of the Ru had been washed out via. the overflow drain. The WVDP has been operating a radioactive joule heated glass melter since 1996 (Barnes et al. 1986). The expected Ru concentration in the WVDP radioactive glass was 0.08

percent by weight based upon fuel burnup fission products yields. The resistance between the melter electrodes steadily decreased during the first year of radioactive operation. After approximately one year of operation, a dramatic change in the electrical resistance of the melter was found (Fall of 1997) that required adjustment to current control limits to the melter. The downward trend in electrical resistance and the skewing of current towards the bottom electrode were caused by the deposition of noble metals (Rh, Pd, and RuO_2) on the melter floor and sloped walls. A team of experts (assembled by West Valley) was consulted on this topic in 1997. The recommendations given by the team were: 1) assess the adequacy of currently available diagnostic/monitoring capabilities for detecting accumulation of noble metals, 2) develop enhanced melter monitoring and detection capabilities with appropriate action limits, 3) predict future melter power needs and develop work around to meet these needs, 4) continue to collect and evaluate data aimed at characterizing the noble metal deposits in the melter, 5) develop tools to dislodge the deposits of noble metals in situ, 6) develop methods for furnishing and draining the melter to remove deposits, and 7) develop methods for visually inspecting the melter if it is drained and mechanically dislodging the deposits. These recommendations were followed by specific activities.

PNNL was asked to numerically model (using TEMPEST) the WVDP melter to help understand the current conditions in the melter and to explore alternate electrode configurations to extend melter lifetime in the event that the current melter configuration becomes inoperable due to short circuiting through the noble metals sludge layer. Four major simulations were completed: 1) Clean melter (without noble metals), 2) Melter with noble metal sludge layer, 3) Alternate electrode configuration #1 – shorted electrodes driven by single top electrode, and 4) Alternate electrode configuration #1 – shorted electrodes driven by twin top electrodes. The clean melter model was produced as a base to compare with melter electrical data measured prior to the noble layer buildup. With suitable agreement demonstrated for the clean melter simulation, various combinations of noble metal layer geometries and properties were added and simulation results compared with current operating data. Observations of noble metal layers and spinels in experimental melters were used as guidance in this process. Once reasonable agreement was demonstrated for the noble metal layer case, this model was adapted to explore two alternate electrode configurations. The noble metal geometry was important in the simulation because it acted as an extension of the adjacent electrode and thereby influenced the electrical current patterns and glass temperature distributions with the melter. In all cases, electrical parameters were controlled to provide an 1150ºC operating temperature at the R1 and R2 thermowells.

For the clean melter case, the predicted and measured voltages agreed well, but resistances were 10 percent higher, thus resulting in somewhat lower predictions of currents and overall power. Model boundary temperatures were an important factor in this result and a number of different cases were simulated to give expected physical behavior, for example, in radiant losses from the melt surface. The values used in the final model were realistic considering the overall uncertainty in the model and the simulation results were considered to be close enough to serve as a starting point for the remaining models. The temperature contour plots showed a very uniform melter temperature.

Several different models were run to simulate the impact of a deposited layer of noble metals. The objective was to add noble metals to the melter floor until the predicted operating parameters (resistance, current, and temperature) matched the observed conditions in the melter. This required adding an extensive noble metals layer. Initially, two different cases were run to model metals layer with an electrical conductivity of 2000 S/m. The noble metals layer geometry was chosen based on observations made during FACTS testing where a layer of spinels settled on the bottom of the melter and partially on the side electrodes. The spinels also settled on the two shallow sidewalls so that “fingers” formed between the bottom electrode and the side electrodes (Krause and Luckscheiter, 1991). The initial simulation data indicated that, even with the 2000 S/m sludge layer, the circuit resistances were still above those being measured on the WVDP melter. This indicated that the melter probably had more settled sludge than what was being assumed in the model. It was decided to continue modeling using

higher sludge conductivities (4000-8000 S/m) to simulate thicker sludge layers and eventually to add a more extensive noble metals sludge layer to the model. After reviewing the results, a final model was run with a thicker noble metal layer. Noble metal thickness ranged from 3.6 cm over the bottom electrode to 2.5 cm at the top of the channel with a 2 cm gap included between the noble metal sludge layer and the end electrodes. The gap was included to simulate the expected melted region where current was a maximum. The final model used a sludge layer electrical conductivity of 2000 S/m. Electrical parameters for the final model produced good agreement with measured data as shown in Table 3.28.

Table 3.28. Comparisons of Predictions with Measured Data

	VA (volts)	VB (volts)	VC (volts)	IA (amps)	IB (amps)	IC (amps)	RA (m-ohms)	RB (m-ohms)	RC (m-ohms)	P_{tot} (kW)
Clean Melter										
Predicted	105	74	74	400	490	490	263	151	151	92
Measured	113	74	74	442	540	540	256	137	137	105
Noble Metal Layer										
Predicted	74	46	46	800	1120	1120	92	41	41	126
Measured	46	34	40	797	1191	1021	58	28	39	118

Note: These modeling results are not yet published in open literature[3]. Additionally, sludge samples collected from the melter are being analyzed. Currently, settling rate of the noble metals could not be estimated with the available data. With continued effort, this would be possible in the future.

The response of the West Valley Demonstration Project (WVDP) melter to the slow accumulation of high-conductivity noble metals has been successfully modeled ("corner model")[4]. The predicted melter electrical resistance response to these conductive phases, and the actual measured data are shown in Figure 3.19. The WVDP melter has three electrodes, one installed at the bottom center of the melter and two near the glass surface at opposite ends of the system. The electrical power systems are designed to independently control the energy dissipated in each electrode power circuit, from the bottom electrode to each top electrode and between the top electrodes. The predicted responses for these circuits are shown in the figure as squares (bottom-to-top electrode prediction and top-to-top electrode predictions) and the actual data are represented by the triangles and diamond symbols (RIX-2031 is the top electrode circuit and RIX-2032 and RIX-2033 are the bottom to top electrode circuits). This model accurately predicted the melter response and was used to verify that the power supply system designs were sufficient to respond to the expected melter resistance changes.

This resistance model assumed that the melter was continuously fed with a constant noble metal concentration, the noble metal deposition rate in the melter was constant, the principal noble metal sludge accumulations were at the junction of the melter floor and walls and in contact with the electrodes, that the noble metal deposits were a parallel current path to the glass, and glass/noble metal resistance data collected by S. Weisenburger from deposits removed from the K-W2 melter at the Karlsrhue site. The accumulations in the "corners" of the melter were consistent with the observations made during the examination of the WVDP melter following a five-year, non-radioactive, test campaign (Figure 3.20) and

[3] J. A. Fort, D. L. Lessor, T. E. Michener, K. P. Recknagle, and M. L. Elliott, "Model Predictions of he West Valley Demonstration Project Melter with Noble Metals and Alternative Electrode Configurations," WVSP 99-11, December, 1998 (Draft).
[4] Communication with Steve Barnes

the response of the K-W2 melter. The cross sectional area of the noble metal deposits was assumed to increase with a constant rate of mass accumulation and this deposition data was correlated to the melter response using the initial electrical resistance and that measured after 10,000 hours of operation. The glass resistivity was established at 3 ohm-in. Using the starting conditions and the German resistivity data for a ~20 weight percent noble metal/glass sludge (0.04 ohm-in.) was assumed. These data, when combined with the successful melter response model, indicate that less than 10 percent of the noble metals entering the melter were retained in the system.

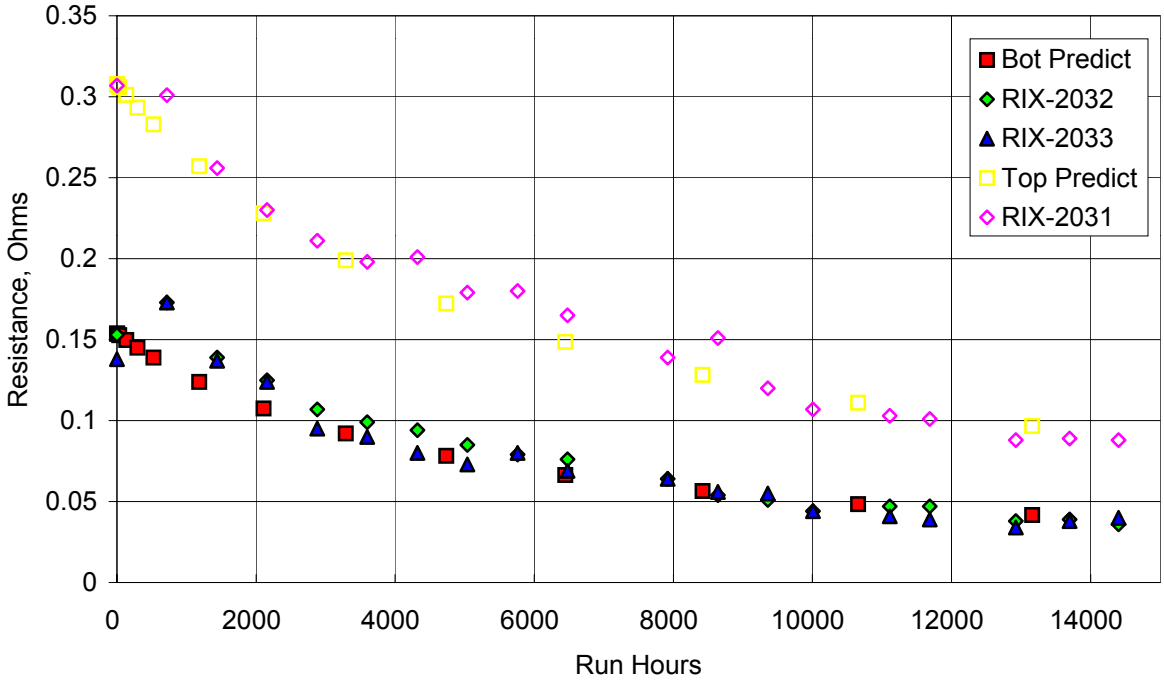

Figure 3.19. "Corner" Model Validation

Figure 3.20. Noble Metals Accumulation in the "Corners" of the Melter

4.0 EMSP Studies on Spinel Settling

The HLW loading has been limited by the perceived risk for glass processing in the currently used electric melters that are equipped with Inconel electrodes and operate at a nominal temperature of 1150°C. To prevent crystalline material from forming in the melter, a situation that is considered undesirable, the liquidus temperature of glass is required to be below 1050°C. This requirement limits the waste loading.

For most waste streams, the crystalline phase that readily precipitates from HLW glass is spinel. Spinel crystals tend to settle and form sludge that would accumulate on the melter bottom. As the sludge layer grows, it may eventually block the flow of glass from the melter. According to the worst-case scenario, the sludge would cause serious melter-operation problems and lead to a premature melter shutdown. Even a few percent increase in waste loading translates into billions of dollars in savings, thus there is strong economic incentive to establish bounds of tolerable spinel formation provided melter performance is not adversely affected. Hrma and coworkers initiated a systematic study (a three years long effort) of spinel settling in FY 1998 under Environmental Management Science Program (EMSP). The team has already made significant progress in the areas of 1) feed to glass conversion, 2) equilibrium, 3) effect of thermal history, 4) effect of minor impurities, 5) crystal dissolution, 6) crystal growth, 7) surface crystallization, 8) redox, 9) settling, 10) spinel sludge rheology, and 11) modeling. This is a continuing effort. In this section, the present status of this effort is briefly reviewed and the progress made in the areas of equilibrium, crystal growth, spinel settling, and modeling of melters are highlighted.

The fundamental issue is the rate of growth of the sludge layer. The kinetics of crystal growth in glass depends on the number density of nuclei (Kalaninia et al. 1980; Zanotto and Galhardi 1988; James 1974; Orlhac et al. 1999). The team measured the effect of minor component addition on the equilibrium concentration of spinel, the rate of crystal growth, and the number density of spinel in an 11-component simluated HLW glass. The results showed that minor components had a profound effect on the size of spinel crystals that precipitate from molten glass, identifying the spinel crystal size as one of the key factors for spinel settling and deposition in the glass melter. Previous composition variation studies (Hrma et al. 1995a; Hrma et al. 1995b) distinguished between major HLW glass components and so-called "Others", a collection of minor waste components. Others had little effect on most of the glass properties, such as viscosity or chemical durability, but some minor glass components had a profound impact on crystal formation (Hrma et al. 1994). For example, spinel contained several minor HLW glass components (NiO and Cr_2O_3), without which it would probably not form at all (Mika et al. 2000). A typical "Others" mix is shown in Table 4.1. The mix contained components that have low solubility (Rh_2O_3, RuO_2) in glass or precipitate from glass in the form of clusters or colloids (SeO_2, P_2O_5, Cr_2O_3, TiO_2, Ag-Cu alloy) that might provide sites for crystal growth (Darab et al. 1996). The team used MS-7 glass, a simplified version of a typical Hanford HLW glass, as a baseline. The glass had a liquidus temperature (T_L) of 1078°C (Izak et al. 2000). 1 to 4.3 mass percent of "Others" was added to the baseline (see Table 4.2).

Table 4.1. Composition of "Others" in Mass Fractions of Components

Oxide	Mass Fraction	Oxide	Mass Fraction	Oxide	Mass Fraction	Oxide	Mass Fraction
Ag_2O	0.022	CuO	0.009	PbO	0.052	SrO	0.009
BaO	0.092	F	0.018	Rh_2O_3	0.009	ZnO	0.012
CdO	0.212	La_2O_3	0.083	RuO_2	0.009	MnO	0.111
CeO_2	0.022	MoO_3	0.003	Sb_2O_3	0.022		
Cl	0.003	Nd_2O_3	0.055	SeO_2	0.028		
Co_2O_3	0.028	P_2O_5	0.142	SO_3	0.058		

Table 4.2. MS-7 Glass with 0 to 4.3 Mass Percent of "Others"
(Compositions in Mass Fractions)

	0 mass percent	1 mass percent	2 mass percent	3 mass percent	4.3 mass percent
Al_2O_3	0.0800	0.0793	0.0786	0.0778	0.0769
B_2O_3	0.0700	0.0694	0.0687	0.0681	0.0673
Cr_2O_3	0.0030	0.0030	0.0029	0.0029	0.0029
Fe_2O_3	0.1150	0.1140	0.1129	0.1119	0.1106
Li_2O	0.0454	0.0450	0.0446	0.0442	0.0437
MgO	0.0060	0.0059	0.0059	0.0058	0.0058
MnO[(a)]	0.0050	0.0039	0.0028	0.0017	0.0000
Na_2O	0.1530	0.1516	0.1503	0.1489	0.1471
NiO	0.0095	0.0094	0.0093	0.0092	0.0091
SiO_2	0.4531	0.4490	0.4450	0.4409	0.4357
Others	0.0000	0.0100	0.0200	0.0301	0.0431
ZrO_2	0.0600	0.0595	0.0589	0.0584	0.0577
T_L[(b)]	1084	1073	1061	1049	1034

(a) MnO is also a component of Others (Table 4.1) (b) Estimated T_L of MS-7 Glass with "Others"[5]

The goal of the team is to determine the effect of "Others" concentration on the number density of spinel crystals in glass and the crystal growth rate. The crystal number density (n_s) is given by the equation

$$n_S = \frac{V_S}{a^3} \qquad 4.1$$

where a is the average crystal size and V_s is the volume fraction of crystalline phase in glass. It is related to the mass fraction (C) (obtained from XRD) as

$$V_S = \frac{1}{(1/C+1)(\rho_s/\rho_g)+1} \approx C\frac{\rho_g}{\rho_s} \qquad 4.2$$

where ρ_s is the crystalline phase density (5.13 mg/mm^3 for spinel) and ρ_g the glass density (2.7 mg/mm^3). The approximation is valid for C << 1. The crystal growth rate was fitted by the Kolmogorov-Johnsom-Mehl-Avrami equation, which relates C to the time (t) of crystallization at constant temperature:

$$C = C_o\left\{1-\exp\left[-(kt)^n\right]\right\} \qquad 4.3$$

where n is the Avrami exponent, k the rate coefficient, which is a function of temperature (T), and C_o the equilibrium mass fraction of crystalline phase in glass. For spinel, C_o can be fitted by the equation:

$$C_o = C_{\max}\left\{1-\exp\left[-B_L\left(\frac{1}{T}-\frac{1}{T_L}\right)\right]\right\} \qquad 4.4$$

[5] Courtesy of J. Crum (unpublished results), 1997.

where, C_{max} and B_L are temperature-independent coefficients, and T_L is the liquidus temperature.

Figures 4.1 and 4.2 show the spinel crystalline phase that precipitates from HLW glasses at temperature (T) > 1050°C is spinel). Figure 4.3 displays spinel composition in MS-7 glass as a function of temperature. Just below liquidus temperature (T_L), spinel contained more Cr_2O_3 (by mass) than NiO. As temperature decreased, trevorite ($NiFe_2O_4$) became the dominant component. Other oxides were either minor components of spinel (MnO, and possibly MgO and Al_2O_3) or inclusions (Na_2O, SiO_2, and ZrO_2). Glass inclusions were likely to be trapped in rapidly growing crystals (Figure 4.2).

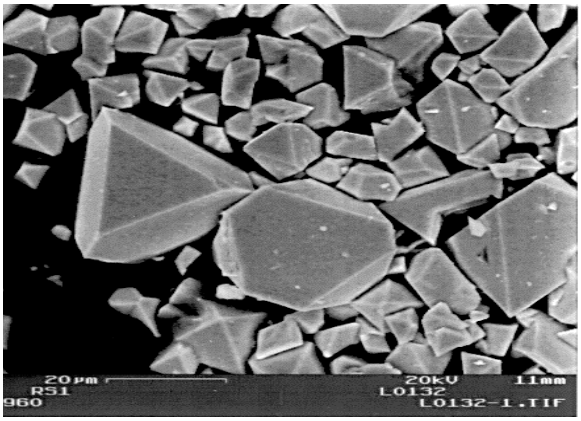

Figure 4.1. Spinel Crystals from a HLW Glass (SEM)

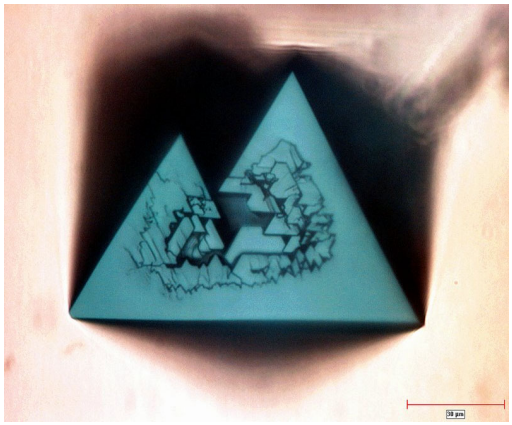

Figure 4.2. A Spinel Crystal Twin from a HLW Glass (optical microscope)

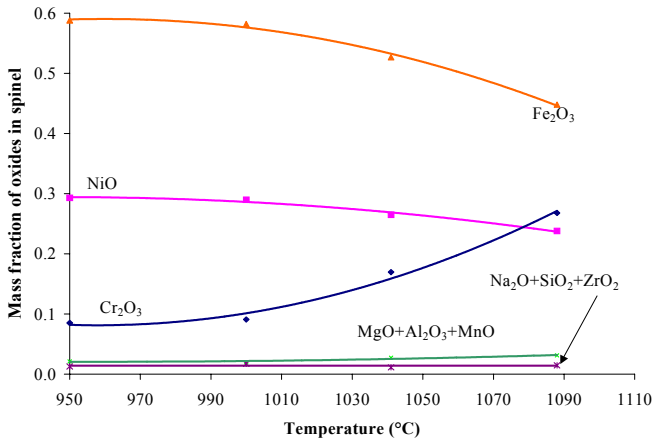

Figure 4.3. Spinel Composition vs. T (SEM/EDS)

The relationship in equation 4.4 is displayed in Figure 4.4 for glasses of varied composition of the MS-7 baseline glass.

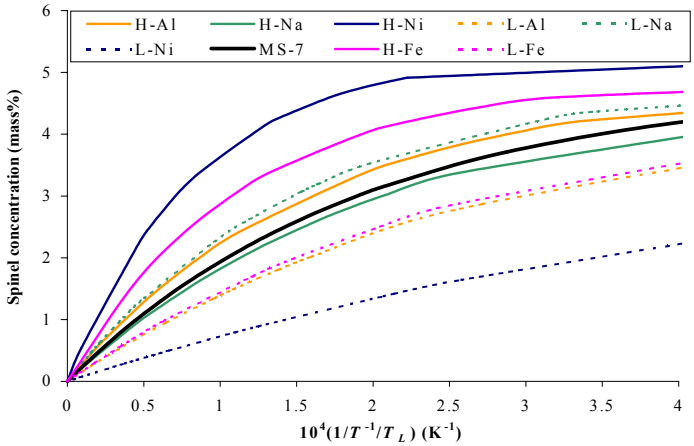

Figure 4.4. Equilibrium Fraction of Spinel in Glasses with Varied Components vs. (1/T-1/T_L)

The difference between T_L and the temperature at which an acceptable $C_o = C_{acc} << 1$ is

$$\Delta T = \frac{T_L^2}{C_{\max} B_L} C_{acc} \qquad 4.5$$

Figure 4.5 shows T_L, C_{max}, B_L, and ΔT (C_{acc} = 0.01) vs. change in glass composition (Δg_i is the i-th component addition to baseline glass).

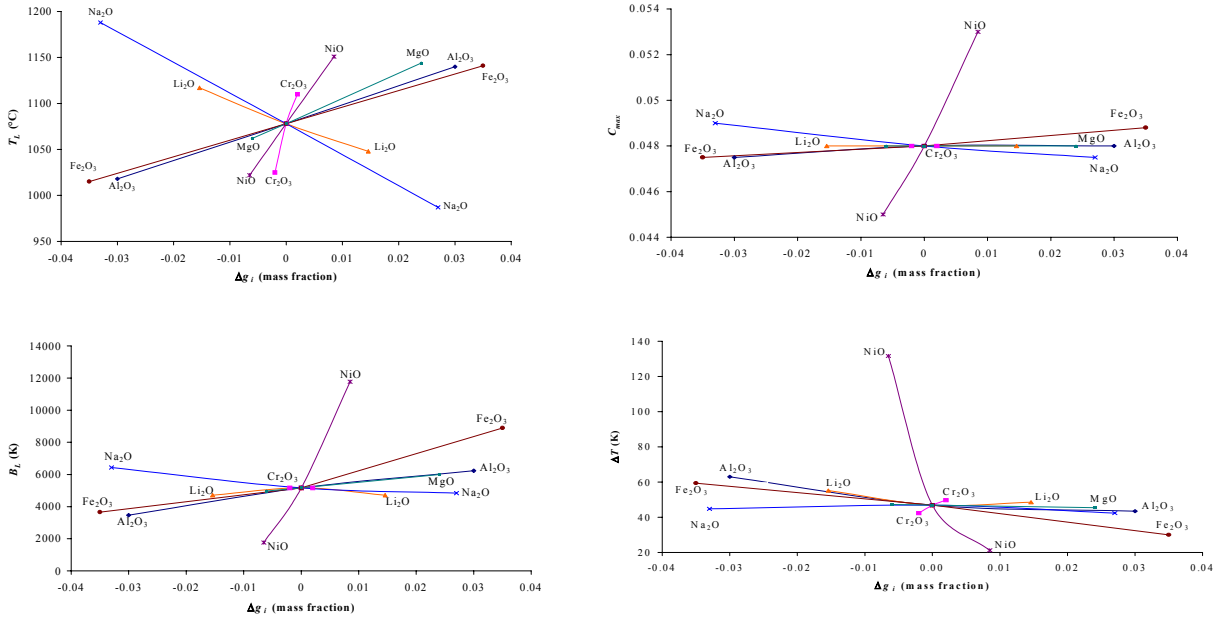

Figure 4.5. Effect of Glass Composition on the Equilibrium Coefficients T_L, C_{max}, B_L, and ΔT (C_{acc} = 0.01) [Equations 4.4 and 4.5]

MS-7 glass was held at 1200°C for 30 minutes and then cooled to the heat-treatment temperature to precipitate spinel. Crystals grew while settling (Figure 4.6). The lines in Figure 4.6 represent the function

$$a = a_0\left(1 - e^{-bt}\right)$$

where a is the crystal size, $a_0 = \beta T$ (with $\beta = 0.0885$ μm/K) is the final crystal size, and $b = b_0 \exp(-B_{growth}/T)$ (with $b_0 = 3.53$ h^{-1} and $B_{growth} = 4018$ K) is the growth rate coefficient.

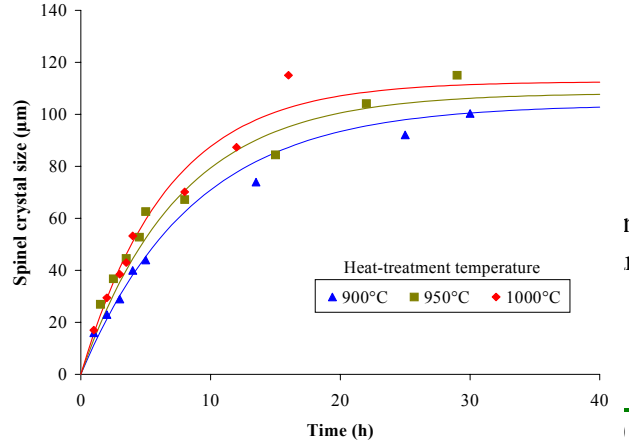

The final crystal size, the C n Table 4.3. If room-temperature glass is isother m) because of the large number of nuclei. These cry

T(°C			
900	104	0.0217	10.1
950	108	0.0163	6.7
1000	113	0.0103	3.7

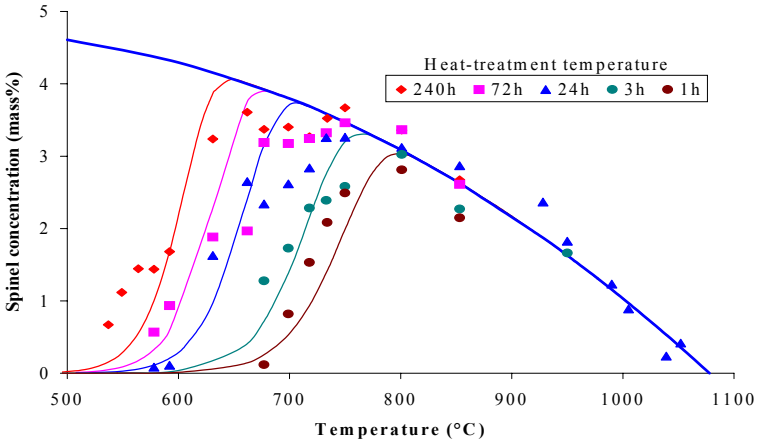

Figure 4.7. Avrami Plot of Spinel Crystallization Kinetics

In a laboratory crucible, spinel settling usually drove a single flow-cell (Figure 4.8). The depth of the settling front (h) increased in accordance with the modified Stokes law if the initial period of crystal growth was considered (Figure 4.9).

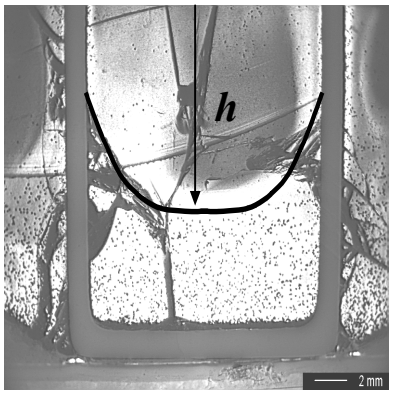

Figure 4.8. Spinel Settling Front in a Crucible

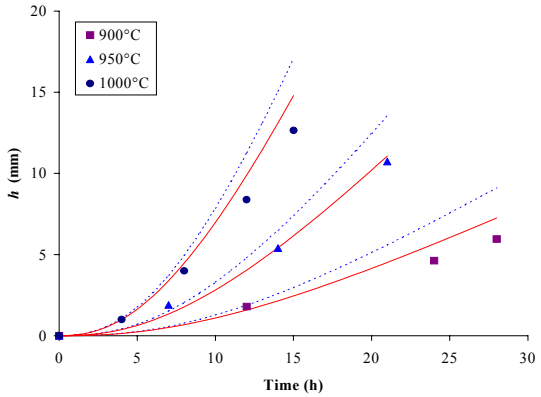

Figure 4.9. Settling Front Depth vs. t and T

Measurements were performed on a special HLW 10-component, RuO_2-free glass with T_L = 1344°C. Spinel sludge from this glass behaved as a rheopectic pseudoplastic liquid. Its shear stress (t_{ef}) was an increasing function of velocity gradient (∇v_{ef}) and time. At constant T and ∇v_{ef}, the changes in sludge structure were causing a higher friction and increasing t_{ef} with time (aging). The aging phenomenon was not observed at T > 1300°C. As ∇v_{ef} and T increased, the apparent viscosity (η_a) decreased as the sludge structure was rearranging. The sludge approached time-independent behavior above 1300°C. At 1094°C, η_a of the sludge from a similar glass with minor components added, including 0.03 mass percent RuO_2, was roughly 20 times higher than that of RuO_2-free glass, but only 2 to 4 times higher at temperatures above 1300°C. Spinel crystals bonded with RuO_2 needles are shown in Figure 4.10.

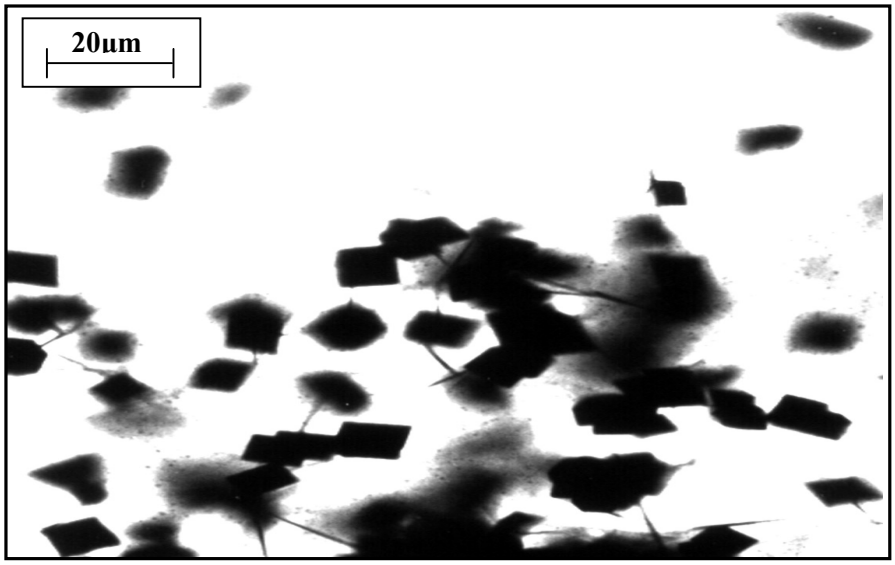

Figure 4.10. Spinel Crystals Bonded with RuO_2 Needles

A HLW glass melter was modeled using the Glass Service Ltd. GS-CAD model code (Figure 4.11). The temperature and flow in both cuts (cross and longitudinal) show the good mixing ability of this type of melter. A spinel settling model is being developed. A preliminary assessment of spinel distribution in the melter is shown in Figure 4.12.

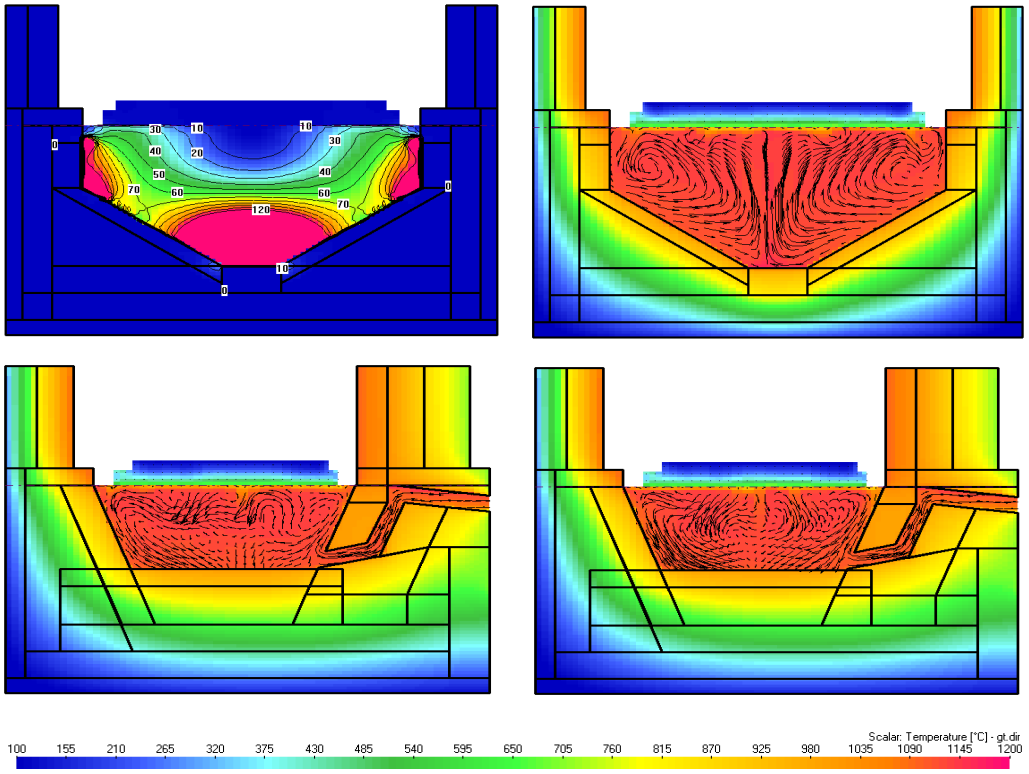

Figure 4.11. Electric (in kW/m^3), Temperature, and Flow Fields in a HLW Glass Melter

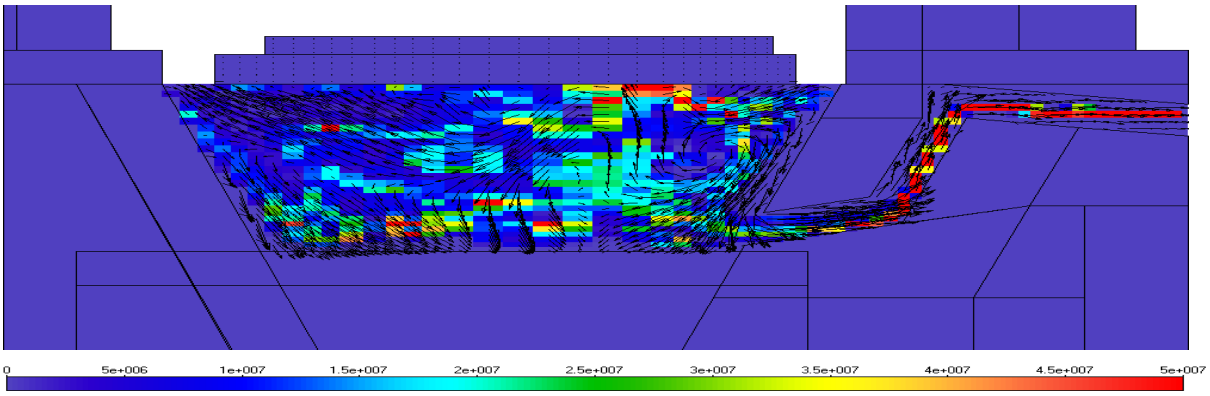

Figure 4.12. Number Density (Spinel Crystals per m^3) in a HLW Glass Melter (Preliminary calculation)

Note: Commercial modeling software by Glass Service, Ltd and Fluent have incorporated features involving bubbling. To the best knowledge of the authors, no published reports are available on modeling of bubbling applied to suspend or resuspend particles from waste glass melters. However, if given specific properties of the particles it would be expected that such an assessment could be performed to some degree of accuracy.

Fluent'e forced bubbling model is briefly described below (http://www.fluent.com/). Forced bubbling is modeled by introducing an additional source term in the momentum equation for the vertical component of the glass melt velocity. The force balance on a single bubble in the glass tank yields the terminal velocity of the bubble as:

$$V_{bub} = \frac{g r_b \rho_g}{3\mu_g}$$

g = gravity, r_b = bubble radius, ρ_g = density, μ_g =viscosity of glass, respectively.

The net force per unit volume due to the bubbles in the glass tank can be written as:

$$F = \frac{CH}{V} 4\pi \, r_b V_{bub}$$

V is the bubbler volume, C is the bubbling frequency and H is the height of the tank. Velocity vectors and temperature contour on the plane through the centers of bubblers in glass tank are shown in Figure 4.13.

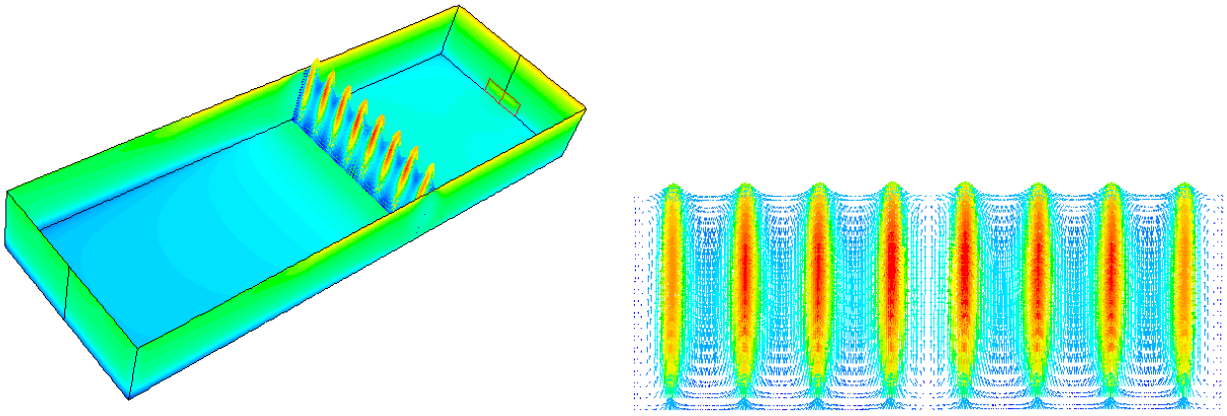

Figure 4.13. Velocity Vectors and Temperature Contour in a Glass Tank
(http://www.fluent.com/)

5.0 Future Work and Recommendations

1. The results indicate effects of both physical and chemical properties of noble metals determine the settling or retention in a nuclear waste glass melt. Physically, smaller the particle size, lower the settling in melters. Chemically, minor components could have significant effect on the crystallization and settling of spinel crystals. This poses new challenge in selecting suitable surrogates for studying and understanding these two aspects. Two separate surrogates may have to be used for testing in FY 2001.

2. Idling increases settling in melters. Two potential techniques of keeping the noble metals suspended in the melt are: 1) Modify the insulation and heaters to introduce more convection currents even during idling (preferential localized heating/cooling may also be attempted) and 2) Physical stirring or bubbling.

3. Slope-bottomed definitely alleviates the problem. But, bottom drain systems have not proven successful. Novel glass and sludge removal methods need to be developed and tested in cold melters to restore the melters to their original electrical capabilities. Additional concern will be corners and high viscosity regions in melters.

4. Environmental Management Science Program (EMSP) study presently in progress at PNNL has already identified several parameters that will significantly affect the spinel settling and are: 1) feed to glass conversion, 2) equilibrium, 3) thermal history, 4) effect of minor impurities, 5) crystal dissolution, 6) nucleation and crystal growth, 7) surface crystallization, and 8) redox. A systematic parametric variation study is recommended to establish good understanding of the science of noble metals issue.

5. Existing data indicate that a combination of physical modeling, crucible study, computer modeling, and limited melter studies will be more useful in planning the surrogate testing in FY 2001.

6. Modeling has proven very valuable in understanding the dynamics of the noble metals issue in melters. PNNL's TEMPEST code and commercial software (Fluent and Glass Service, Ltd) can readily be applied. Since the last detailed modeling work computational tools have improved and should provide an even better capability in assessing the effects of particle and glass properties, melter designs and operating conditions, and mixing options. Any future noble metals studies should also fully utilize these tools.

6.0 References

Allen, P. M. 1989. "Noble Metals Campaign." Presented at the U.S. DOE/BMFT Vitrification and Glass Technology Workshop, Aiken, South Carolina, November 10-14, 1989.

Anderson, L. D., T. Dennis, M. L. Elliott, L. L. Eyler, and P. R. Hrma. 1992. Investigation of Noble Metals Behavior in a Ceramic Melter Cold Cap. Milestone Report PHTD-C91-04.01B, Rev. 0, Pacific Northwest Laboratory, Richland, Washington.

Asano, H., M. Morioka, T. Sugawara, H. Yamaguchi, T. Murakoshi, and A. Sakai. 1986. "Physical Modeling Test of Joule Heated Ceramic Melter System for High Level Waste Vitrification." Spectrum '86, Proceedings of the American Nuclear Society International Topical Meeting, September 14-18, 1986, Waste Management and Decontamination and Decommissioning, Niagara Falls, New York. pp. 942-951.

Bansal, B. 1978. Physical Modeling of All-Electric Furnaces, IEEE Transactions – Industry Applications, Vol. IA, Issue 1, pp. 55-61.

Barnes, S. M., L. L. Petkus, T. F. Murawski, C. C. Chapman, J. M. Pope. 1986. *Reference Vitrification Process and Equipment Description with Results from Checkout Testing*, DOE/NE/44139-32. West Valley Nuclear Serevices, West Valley, New York.

Bickford D. F. and C. M. Jantzen. 1986. "Devitrification of Defense Nuclear Waste Glasses: The Role of Melt Insolubles," *J. of Non-Crystalline Solids*, 84: 299-307.

Cobb, W. T. and P.R. Hrma. 1990. Behavior of RuO_2 In A Glass Melt. Ceramic Transactions, 23:233-237.

Cooper, M. F., M. L. Elliott, L. L. Eyler, C. J. Freeman, J. J. Higginson, L. A. Mahoney, and M. R. Powell. 1993. Research Scale Melter Test Report. Milestone Report PHTD-K902, Pacific Northwest Laboratory, Richland, Washington.

Darab, J. G., H. Li, D.W. Matson, P.A. Smith, and R.K. MacCrone. 1996. "Chemical and Structural Elucidation of Minor Components in Simulated Hanford Low-Level Waste Glasses," in *Synchrotron Radiation Techniques in Industrial, Chemical, and Materials Science* (Editors K.L. D'Amico, L.J. Terminello, D.K. Shuh), Plenum, New York, p. 237.

Dempster, J. 1998. Waste Form Compliance Plan for the WVDP HLW Form, WVDP-185, Rev. 12.

Elliott, M. L., L. L Eyler, L. A. Mahoney, M. F. Cooper, L. D. Whitney, and P. J. Shafer. 1984. Preliminary Melter Performance Assessment Report, PNL-9822, Pacific Northwest Laboratory, Richland, Washington.

Fletcher, J. M., and F. S. Martin. 1955. Chemistry of Ruthenium. Report No. C/M 256, Atomic Energy Research Establishment, Great Britain.

Geldart, R. W., S. O. Bates, and S. J. Jette. 1987. Preliminary Evaluation of Noble Metal Behavior in the Hanford Waste Vitrification Plant Reference Glass, HW-39. Milestone Report HWVP-87-V110202F, Pacific Northwest Laboratory, Richland, Washington.

Grünewald, W, G. Roth, W. Tobie, S. Weisenburger, K. Weiss, M. Elliott, and L. Eyler. 1993. Vitrification of Noble Metals Containing NCAW Simulant with an Engineering Scale Melter (ESM). Milestone Report PHTD-K0967, Rev. 0, Institut für Nukleare Entsorgungstechnik of Kernforschungszentrum Karlsruhe, Karlsruhe, Germany.

Hrma, P., G.F. Piepel, J.D. Vienna, P.E. Redgate, M.J. Schweiger, and D.E. Smith. 1995a. "Prediction of Nuclear Waste Glass Dissolution as a Function of Composition," *Ceramic Transactions* (Editors V. Jain, R. Palmer), Vol. 61, American Ceramic Society, p. 497.

Hrma, P., G.F. Piepel, M.J. Schweiger, D.E. Smith, D.S. Kim, P.E. Redgate, J.D. Vienna, C.A. LoPresti, D.B. Simpson, D.K. Peeler, and M.H. Langowski. 1994. *Property/Composition Relationships for Hanford High-Level Waste Glasses Melting at 1050°C*, PNL-10359, Vol. 1 and 2, Pacific Northwest Laboratory, Richland, Washington.

Hrma, P., G.F. Piepel, P.E. Redgate, D.E. Smith, M.J. Schweiger, J.D. Vienna, and D.-S. Kim. 1995b. "Prediction of Processing Properties for Nuclear Waste Glasses," *Ceramic Transactions* (Editors V. Jain, R. Palmer), Vol. 61, American Ceramic Society, p. 505.

Hutson, N. D. 1992. Integrated DWPF Melter System (IDMS) Campaign Report: Hanford Waste Vitrification Plant (HWVP) Process Demonstration (U). WSRC-TR-92-0403, Rev. 1, Westinghouse Savannah River Company, Savannah River Technology Center, Aiken, South Carolina; Hutson, N. D., and M. E. Smith. 1992. "The Behavior and Effects of the Noble Metals in the DWPF Melter System." Proceedings of the High Level Radioactive Waste Management Conference, American Nuclear Society, La Grange Park, Illinois. 1:541-548.

Hutson, N. D. 1993. IDMS Task Summary Report Part 1: The Behavior and Effects of the Noble Metals in the DWPF Melter System. WSRC-TR-93-0458, Savannah River Technology Center, Aiken, South Carolina.

Hutson, N. D., J. R. Zamecnik, M. E. Smith, D. H. Miller, and J.A. Ritter. 1991. Integrated DWPF Melter System (IDMS) Campaign Report: The First Two Noble Metals Operations (U). WSRC-TR-91-400, Defense Waste Processing Technology, Savannah River Laboratory, Aiken, South Carolina.

Igarashi, H. and T. Takahashi. 1991. "The Draining of Noble Metals in Vitrified Nuclear Waste by a Melter With a Sloping Floor." Glass Technology 32(2):46-50.

Igarashi. H. 1992. "Melter and Process Operational Experiences with Noble Metal Elements." Prepared for the PNC/DOE Specialists Meeting on High-Level Waste Vitrification, Tokai-mura, Japan, November 18-19, 1992.

Izak, P., P. Hrma, B.K. Wilson, and J.D. Vienna. 2000 "The Effect of Oxygen Partial Pressure on Liquidus Temperature of a High-Level Waste Glass with Spinel as the Primary Phase," American Ceramic Society Proceedings, St. Louis, MO.

James, P. F. 1974. "Kinetics of Crystal Nucleation in Lithium Silicate Glasses," *Physics and Chemistry of Glasses*, 15 95-105.

Jensen, G. A., A. M. Platt, G. B. Mellinger, and W. J. Bjorklund. 1984. "Recovery of Noble Metals from Fission Products." *Nuclear Technology* 65:305-324.

Kalaninia, A. M., V.N. Filipovich, and V.M Fokin. 1980 "Stationary and Non-Stationary Crystal Nucleation Rate in Glass of $2Na_2O{\cdot}CaO{\cdot}3SiO_2$ Stoichiometric Composition," *Journal of Non-Crystalline Solids*, 38 & 39 723–728.

Krause, Ch., and B. Luckscheiter. 1991. "Properties and Behavior of the Platinum Group Metals in the Glass Resulting from the Vitrification of Simulated Nuclear Fuel Reprocessing Waste," *J. Material Research*, 6(12): 2535-2546.

Kruger, O. L. 1991. Fiscal Year 1991 *Statement of Work for Applied Technology Tasks to be Performed by Pacific Northwest Laboratory in Support of the Hanford Waste Vitrification Plant Project*. WHC-SP-0638, Rev. 0, Westinghouse Hanford Company, Richland, Washington.

Mendel, J. E., W. A. Ross, F. P. Roberts, Y. B. Katayama, J. H. Westsik, Jr., R. P. Turcotte, J. W. Wald, and D. J. Bradley. 1977. *Annual Report on the Characteristics of High-Level Waste Glasses*. BNWL-2252, Pacific Northwest Laboratory, Richland, Washington.

Mika, M., P. Hrma, and M.J. Schweiger. 2000., "Rheology of Spinel Sludge in Molten Glass," *Ceramics-Silikaty* (accepted).

Morris, J. B. 1985. *Solidification of Highly Active Liquid Waste*, Annual Progress Report April 1982-March 1983. AERE-G 2960, Program on Radioactive Waste Management for the UK Department of the Environment, United Kingdom.

Morris, J. B., D. Walmsley, A. Hollinrake, and G. Horsley. 1986a. *The Dismantling of the One-Third-Scale Joule Ceramic Melter and Preliminary Investigation of Electrode Corrosion*. AERE-R 12056, UKAEA Atomic Energy Research Establishment, Harwell, England.

Morris, J. B., J. T. Dalton, J. P. Evans, A. Hollinrake, G. Horsley, E. L. Paige, P. W. Sutcliffe, and D. Walmsley. 1986b. "Electrode Corrosion and Ruthenium Behavior in a Small Joule Ceramic Melter." Spectrum '86, *Proceedings of the American Nuclear Society International Topical Meeting*, Waste Management and Decontamination and Decommissioning, September 14-18, 1986, Niagara Falls, New York. pp. 961-971. CONF-860905-Vol. 1, National Technical Information Service, Springfield, Virginia.

Nakaoka, R. K. and D. M. Strachan. June 1990. Draft: *Melter Performance Evaluation Report*. HWVP-90-1.2.2.04.08B, Pacific Northwest Laboratory, Richland, Washington.

Orlhac, X., C. Fillet, and J. Phalippou. 1999. "Study of Crystallization Mechanisms in the French Nuclear Waste Glass," *Scientific Basis for Nuclear Waste Management XXII* (Editors D.J. Wronkiewicz, J.H. Lee), Vol. 556, Material Research Society, p. 263.

Peters, R. D. 1990. *Physical Modeling Studies of the HWVP Melter and An Alternate Design*, HWVP-90-1.2.204.08A, Pacific Northwest Laboratory, Richland, Washington.

Quigley, M. S. and D. K. Kreid. 1979. *Physical Modeling of Joule Heated Ceramic Glass Melters for High Level Waste Immobilization*, PNL-2809, Pacific Northwest Laboratory, Richland, Washington.

Ross, W. A., D. J. Bradley, L. R. Bunnell, W. J. Gray, Y. B. Katayama, G. B. Mellinger, J. E. Mendel, F. P. Roberts, R. P. Turcotte, J. W. Wald, W. E. Weber, and J. H. Westsik, Jr. 1978. *Annual Report on the Characterization of High-Level Waste Glasses*. PNL-2625, Pacific Northwest Laboratory, Richland, Washington.

Routt, K. R. 1983. "Physical Modeling of a Glass Melter Designed for Vitrification of Defense Waste," *Proc. of Am. Cer. Soc.*, Annual Meeting, Chicago, Illinois, April 23-27, 1983.

Schreiber, H. D., M. Riethmiller and T. Duggan. 1991. "Solution Chemistry of Noble Metals in a Model Nuclear Waste Glass," To be published in *Proceedings of the 5th International Symposium on Ceramics in Nuclear and Hazardous Waste Management*, Cincinnati, Ohio.

Schreiber, H. D., T.R. Harville, and G.N. Damron. 1990. "Redox-Controlled Solubility of Palladium in a Borosilicate Glass Melt," *J. Am. Ceram. Soc.*, 73:1435-1437.

Skarda, R. J. et al. 1985. *Preliminary Evaluation of PSCM and BIPP Melter Design and Operating Conditions Using Physical Modeling*, PNL-5498, Pacific Northwest Laboratory, Richland, Washington.

Smith, M, E., and B. F. Bickford. 1997. *The Behavior and Effects of the Noble Metals in the DWPF Melter System*, WSRC-TR-97-00370, Westinghouse Savannah River Company, Savannah River Technology Center, Aiken, South Carolina.

Trent, D. S. and L. L. Eyler. 1993. TEMPEST: A Computer Program for Three-Dimensional Yime-Dependent Computational Fluid Dynamics, PNL-8857, Pacific Northwest Laboratory, Richland, Washington.

Tsuboya, T., and N. Tsunoda. 1988. "The Japanese Vitrification Program." *Proceedings of the Symposium on Waste Management*, Waste Management '88, March 2-6, 1988, Tucson Arizona. 2:181-188.

Zanotto, E. D. and A. Galhardi 1988. "Experimental Test of the General Theory of Transformation Kinetics: Homogeneous Nucleation in a $Na_2O{\cdot}2CaO{\cdot}3SiO_2$ Glass," *Journal of Non-Crystalline Solids*, 104, 73–80.

.